Application of Two-Dimensional NMR to Kinetics of Chemical Exchange

CHARLES L. PERRIN* and TAMMY J. DWYER

Department of Chemistry, University of California, San Diego, La Jolla, California 92093

Received May 17, 1989 (Revised Manuscript Received March 26, 1990)

Contents

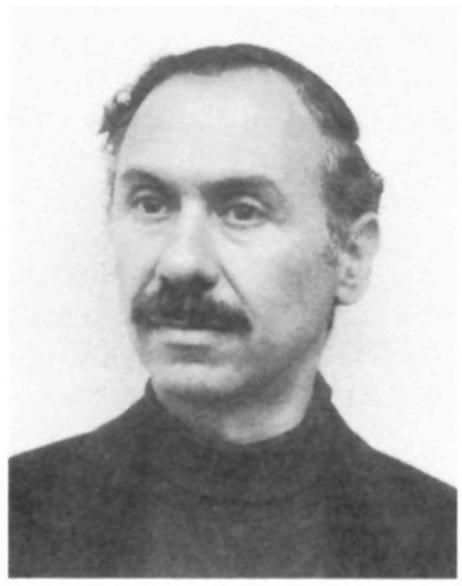

Originally from Pittsburgh, Charles L. Perrin graduated from Harvard College in 1959 and received his Ph.D. in 1963 from Harvard University, under the direction of F. H. Westheimer. Following postdoctoral research at the University of California at Berkeley, he joined the founders of the new campus at the University of California at San Diego. He has been a Special NIH Research Fellow at Gothenburg University and a NATO Visiting Professor at the University of Padua. His research interests span a broad range of physical–organic chemistry.

Tammy J. Dwyer, a native San Diegan, received her B.S. in Chemistry in 1983 from California Polytechnic State University, San Luis Obispo. At Cal Poly she did research under the supervision of Dr. Dane Jones and received the 1983 Undergraduate Research Award. Under the direction of Dr. Charles Perrin, she received her Ph.D. in 1988 at the University of California, San Diego. Her research there included NMR studies of proton exchange in amides, amidinium ions, and ammonium ion. She is currently a lecturer in the Chemistry Department at UCSD.

I. Introduction

Nuclear magnetic resonance (NMR) is an important technique for investigation of the kinetics of chemical-exchange processes. The unique ability to resolve and assign the separate signals due to nuclei in different chemical environments makes NMR especially powerful for kinetic studies. NMR is obviously applicable as a selective but insensitive method for following the time course of concentrations during a chemical reaction. However, there are additional NMR spectral changes due to kinetic processes. These arise under conditions of dynamic equilibrium, where the exchange reaction is proceeding at a detectable rate even though there is no net reaction. Indeed, the reaction product may even be identical with the reactant, as is the case in a degenerate isomerization, or topomerization, which only permutes atoms or groups of atoms among sites on a molecular framework. The application of the resultant spectral changes to the study of kinetics is often called dynamic NMR (DNMR).[1] Several DNMR techniques have been developed that evaluate rates or chemical fluxes associated with chemically exchanging systems. Most commonly used are the classic line-shape analysis and the more recent magnetization-transfer methods.

Line-shape analysis[2] (more properly called total band-shape analysis) makes use of the fact that exchange processes are manifested as characteristic

0009-2665/90/0790-0935$09.50/0

changes in the shape of the NMR signal—broadening, coalescence, and resharpening. If there are only two chemical environments, or sites, the method is particularly attractive. For multisite systems, however, the analysis becomes quite complex. In these instances, computer simulations may be necessary to unravel the kinetics but the spectra may not be good enough to determine all rate constants accurately.

Magnetization transfer (saturation transfer, inversion transfer)[3,4] is an alternative method that has been used to study a variety of dynamic processes. Selective irradiation—saturation or inversion—of one or more resonances of an exchanging system, followed by examination of the effect of that perturbation on the remaining sites, allows determination of the pathways and rate constants of chemical exchange. The magnetization-transfer technique becomes increasingly difficult as the resonances of interest increase in number or decrease in chemical shift separation.

Recently two-dimensional (2D) NMR has been gaining in popularity. This method is also called EXCTSY,[5] for exchange-correlated spectroscopy, and 2D EXSY,[6] for exchange spectroscopy, although it has also been called NOESY, which is a misnomer. We shall use the term 2D EXSY. It is an especially powerful method, often applicable to multisite systems not amenable to study by conventional methods. An additional feature of quantitative 2D EXSY, and one that will be stressed throughout this review, is that it gives site to site rate constants. These often carry information about mechanism, whereas line-shape methods are sensitive only to lifetimes and are less informative.

The purpose of this review is to show how 2D EXSY can be applied to problems in chemical-exchange kinetics. The underlying theory is a necessary prelude, and we have tried to gear that presentation to the practicing chemist experienced in NMR but inexperienced in 2D NMR. Further information on 2D NMR can be found in authoritative books and reviews by Derome,[7] Sanders and Hunter,[8] Ernst, Bodenhausen, and Wokaun,[9] Croasmun and Carlson,[10] Benn and Gunther,[11] Bax and Lerner,[12] and Kessler, Gehrke, and Griesinger.[13] However, these stress the physical and instrumental principles or the applications of 2D NMR to problems of molecular structure, rather than the applications to chemical kinetics. Orrell and Sik[14] have presented a review of dynamic NMR studies of inorganic and organometallic systems, including examples of 2D applications (to 1985). Willem[15] has published a detailed review of 2D NMR applied to the study of dynamic stereochemical problems, including a survey of early applications (to 1986), along with a group-theoretical analysis of chemical exchange processes that can be studied by 2D NMR. Our own approach is to emphasize the chemical, kinetic, and mechanistic information that can be obtained from 2D NMR.

II. Theory

A. 1D NMR

We begin with a discussion of conventional one-dimensional (1D) Fourier transform (FT) NMR. The z axis is along the applied static field B_0 (Figure 1). The magnetic moments of all the nuclei sum vectorially to a (bulk) magnetization M. At equilibrium, the magnetization vector is M^0, lying along the magnetic field, as depicted in Figure 1a. Perturbation of the magnetization away from its equilibrium position can be accomplished by applying a pulse of radiofrequency (RF) irradiation. This is equivalent to an oscillating magnetic field B_1 perpendicular to the static B_0 field (Figure 1b). If any transverse (horizontal) component of M is created, it will precess about B_0 at a characteristic frequency called the Larmor frequency ω. We shall use frequencies with dimension radians/second, and the chemically more familiar frequency, in hertz, is given by $\nu = \omega/2\pi$.

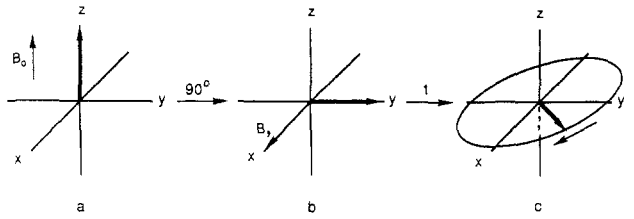

Figure 1. Vector picture of NMR: (a) At equilibrium, the magnetization vector is aligned along the static magnetic field B_0. (b) A 90° pulse rotates the magnetization into the xy plane where it (c) precesses about B_0.

The consideration of precessing magnetizations is unwieldy in the laboratory coordinate system. It is convenient to use a coordinate system rotating at the frequency of the oscillating field B_1. In this rotating frame, B_1 appears fixed and its effect is simply to rotate M about B_1 (Figure 1b). The duration of the pulse can be chosen so that M is rotated by $\pi/2$ rad. Such a pulse is called a 90° pulse. If B_1 is along the x axis in the rotating system, the magnetization vector is rotated to the y axis (Figure 1b). When the B_1 field is removed, the sample magnetization precesses about the static B_0 (Figure 1c). In a frame rotating with the nuclei at the Larmor frequency, the magnetization appears to precess at a frequency equal to the difference between the Larmor frequency and the frequency of coordinate rotation. Nuclei in different environments, or sites, have slightly different Larmor frequencies, so that the total precessing magnetization of a multisite sample is a complicated superposition of the individual oscillations, each with its apparent (difference) frequency ω_j. This magnetization in the xy plane then induces a voltage in the receiver coils. That voltage, as a complicated function of time, is the signal that the spectrometer acquires and accumulates in its computer. This transient signal is called the free induction decay (FID).

The FID is detected as a function of the acquisition time t. Although time is a continuous variable, measurements are made at regularly spaced, discrete values of t. For the purpose of quadrature phase detection, two receiver coils are used. One detects the x component, M_x, and the other detects M_y. These are given by eqs 1 and 2, where the sum is over all sites, each with

$$M_y(t) = \sum_j M_j^0 \cos(\omega_j t + \delta_j) e^{-t/T_{2j}} \quad (1)$$

$$M_x(t) = \sum_j M_j^0 \sin(\omega_j t + \delta_j) e^{-t/T_{2j}} \quad (2)$$

its apparent precession frequency ω_j and spin–spin relaxation time T_{2j}, which accounts for the decay of the magnetization. The phase angles δ_j arise because there is precession during the 90° pulse and because there is an unavoidable delay between the 90° pulse and the

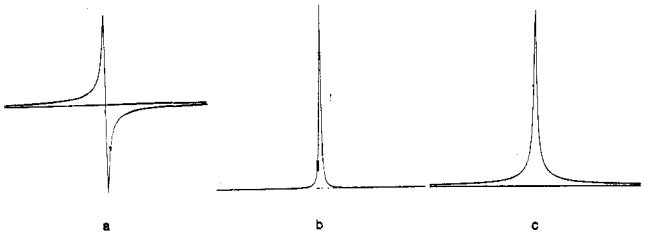

Figure 2. Lorentzian line shapes: (a) dispersion mode; (b) absorption mode; (c) absolute value mode.

beginning of the acquisition. Mathematically it is convenient to combine these into a complex (real plus imaginary) magnetization, given by eq 3. To analyze

$$M_{xy}(t) = M_y(t) + iM_x(t) = \sum_j M_j^0 e^{i(\omega_j t + \delta_j)} e^{-t/T_{2j}} \quad (3)$$

this complicated time-dependent behavior, Fourier transformation converts it to an NMR spectrum, which is a function of frequency (eq 4, where a conversion

$$S(\omega) = \int e^{-i\omega t} M_{xy}(t)\, dt \quad (4)$$

factor dependent on instrument sensitivity has been omitted and where the sum over discrete values of t is written as an integral). Substitution of eq 3 into eq 4 then leads to eq 5. Each term in the second sum rep-

$$S(\omega) = \sum_j M_j^0 \frac{T_{2j}^{-1}}{(\omega - \omega_j)^2 + T_{2j}^{-2}} e^{i\delta_j} + \sum_j M_j^0 \frac{-i(\omega - \omega_j)}{(\omega - \omega_j)^2 - T_{2j}^{-2}} e^{i\delta_j} \quad (5)$$

resents a dispersion mode spectrum (Figure 2a), which is not wanted. The familiar NMR spectrum is the first sum, whose jth term represents one absorption mode peak (Figure 2b) centered at frequency ω_j and of width $(\pi T_{2j})^{-1}$ Hz and intensity I_j given by eq 6. If the phase

$$I_j = M_j^0 \quad (6)$$

factor $\exp(i\delta_j)$ were removed, the two terms could be distinguished as the real and imaginary parts of $S(\omega)$. However, both δ_j and the relationship between the oscillating B_1 field and the two receiver coils are arbitrary. Therefore, both components of $S(\omega)$ are a mixture of absorption and dispersion components. To separate these, the phasing is best adjusted empirically. An alternative is to convert to the absolute value mode (eq 7), but this creates broad peaks with long tails (Figure

$$|S(\omega)| = \sum_j M_j^0 \frac{1}{[(\omega - \omega_j)^2 + T_{2j}^{-2}]^{1/2}} \quad (7)$$

2c) that lead to peak overlap. Another possibility is to display the power mode $|S(\omega)|^2$, but this distorts intensities.

Armed with an understanding of the behavior of the sample magnetization in the time domain and its translation into the frequency domain, one can design NMR experiments (in the form of pulse sequences and phase cycling) to reveal specific information about the particular spin system. A pulse sequence consists of a series of RF pulses separated by time delays during which relaxation, magnetization transfer, or other time-dependent processes can occur. Phase cycling involves alternating the relationship between the phases of the B_1 pulse and the two receivers; this can be used

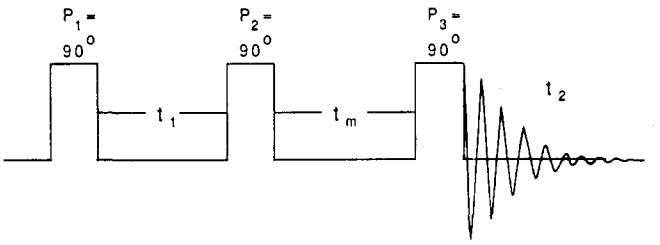

Figure 3. Pulse sequence used in a 2D EXSY experiment. This sequence is repeated for a number of incremented t_1 periods and constant t_m.

to select particular features of the response and to cancel undesirable ones. In the next section we extend these ideas into two dimensions.

B. 2D Exchange Spectroscopy (EXSY)

1. Pulse Sequence

The use of 2D NMR for chemical kinetics was first proposed by Jeener, Meier, Bachmann, and Ernst.[16] The pulse sequence is shown in Figure 3. The acquisition time t_2 is the same as the acquisition time t in 1D NMR. The transverse magnetization M (subscript xy now omitted) is measured as a function of t_2. Although time is a continuous variable, measurements are made at regularly spaced, discrete values of t_2. The labeling time t_1 (sometimes called the evolution time) is also variable. By regularly incrementing t_1 at each successive pulse sequence, t_1 becomes a second discrete variable just like t_2. The mixing time t_m is the time during which chemical exchange occurs and is monitored by the 2D experiment. In principle, it too should be variable. However, the necessity of repeating the pulse sequence for every t_1 makes 2D NMR very time-consuming, so that a single t_m often must suffice. The measured magnetization is then a function of both t_1 and t_2 (eq 8). Double Fourier transformation of this

$$M = M(t_1, t_2) \quad (8)$$

time domain function then converts this to a 2D spectrum (eq 9, where the sums over discrete times are written as integrals) that is a function of the two frequency variables ω_1 and ω_2.

$$S(\omega_1, \omega_2) = \int\int M(t_1, t_2) e^{-i\omega_1 t_1} e^{-i\omega_2 t_2}\, dt_1\, dt_2 \quad (9)$$

To demonstrate how the magnetization behaves during the experiment,[16] we first consider a simple one-spin system in the rotating-coordinate system (Figure 4). The first 90° pulse P_1 is applied along the $-x$ axis and rotates the magnetization from its equilibrium position (Figure 4a) along the static magnetic field B_0 (z axis) to the $-y$ axis (Figure 4b). During the labeling period t_1, the transverse magnetization precesses about B_0 (Figure 4c). Application of a second 90° pulse P_2 along the $-x$ axis rotates the magnetization into the xz plane (Figure 4d), of which only the z component is of interest. The unwanted x component of the magnetization can be eliminated by the use of a field gradient, or homospoil, pulse (HS) during the mixing time (Figure 4e). During the mixing time t_m, the magnetization suffers spin–lattice relaxation (and chemical exchange, whose effects we neglect with only one site) (Figure 4f). Finally, the remaining z magnetization is rotated to the y axis (Figure 4g) by a third

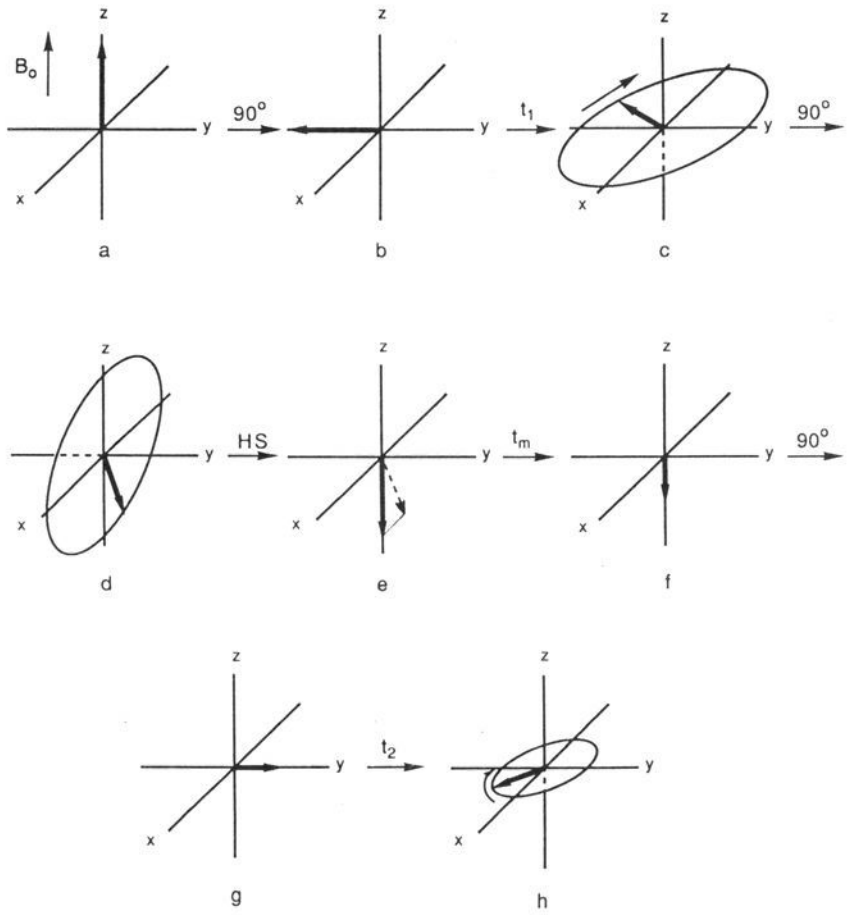

Figure 4. Vector picture of the 2D NMR experiment: (a) The magnetization is initially aligned along B_0. (b) A 90° pulse rotates the magnetization into the transverse plane where it (c) evolves for a time t_1. (d) A second 90° pulse rotates the magnetization into the xz plane. Following a homospoil pulse (e), only the z component is obtained. During the mixing time this z magnetization undergoes relaxation and exchange (f). Following a third 90° pulse (g) the net magnetization (h) is detected during t_2.

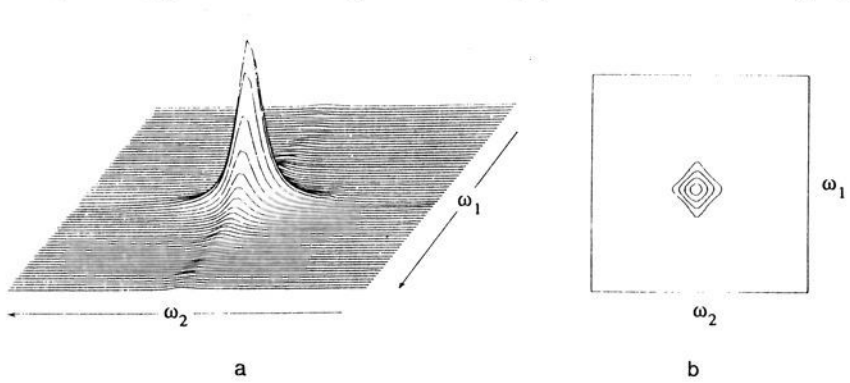

Figure 5. (a) 2D absorption peak. (b) Alternative representation as a contour plot. Reprinted from ref 7. Copyright 1987 Pergamon Press.

90° pulse P_3. During the acquisition period t_2, magnetization in the xy plane (Figure 4h) is measured and stored in a computer.

What is the spectrum $S(\omega_1,\omega_2)$ corresponding to this magnetization $M(t_1,t_2)$? During the labeling period, the magnetization precesses through an angle ωt_1, where ω is the angular frequency of precession for nuclei in that chemical environment. The magnetization that the second 90° pulse rotates into the xz plane has a component cos (ωt_1) or, more generally, $\exp(i\omega t_1)$, to allow for phase indeterminacy. Therefore, $M(t_1,t_2)$ contains a factor $\exp(i\omega t_1)$. Likewise, during the acquisition period, the magnetization precesses through an angle ωt_2. This contributes a factor $\exp(i\omega t_2)$ to $M(t_1,t_2)$. Double Fourier transformation, with proper phasing, produces an absorption peak at $\omega_1 = \omega$ along the first frequency coordinate and at $\omega_2 = \omega$ along the second. This can be displayed either as a two-dimensional peak (Figure 5a) or as a contour plot showing level surfaces (Figure 5b).

The extension to more than one site is trivial. Each site produces a two-dimensional peak at its own frequency along both axes, i.e., along the diagonal of the 2D spectrum.

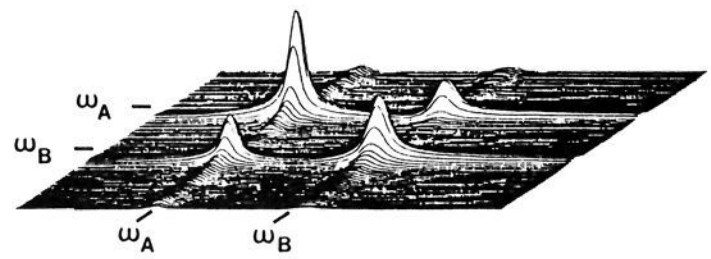

Figure 6. 2D exchange spectrum of *N*,*N*-dimethylacetamide at 30 °C. Diagonal runs from top left to bottom right. Reprinted from ref 16. Copyright 1979 American Institute of Physics.

What if there is chemical exchange between two sites, A and B, characterized by precession frequencies ω_A and ω_B, respectively? During the labeling period, nuclei that are in site A will contribute a component $\exp(i\omega_A t_1)$ to $M(t_1,t_2)$. If during the mixing period t_m some of those nuclei exchange to site B, they will precess at frequency ω_B during the acquisition period and they will contribute a component $\exp(i\omega_B t_2)$ to $M(t_1,t_2)$. Double Fourier transformation will produce a peak at $\omega_1 = \omega_A$ along the first frequency coordinate and at $\omega_2 = \omega_B$ along the second. Those nuclei that do not exchange during t_m contribute $\exp(i\omega_A t_1)$ $\exp(i\omega_A t_2)$ to the magnetization, so they produce a peak at $\omega_1 = \omega_A$, $\omega_2 = \omega_A$. Likewise, nuclei that start in site B and remain there or exchange to site A during t_m produce peaks at $\omega_1 = \omega_B$, $\omega_2 = \omega_B$ or at $\omega_1 = \omega_B$, $\omega_2 = \omega_A$, respectively. Thus, there are not only peaks along the diagonal but also cross-peaks. Figure 6 shows the 2D exchange spectrum of *N*,*N*-dimethylacetamide,[16] with cross-peaks due to exchange of the *N*-methyl groups. The cross-peaks therefore correspond to chemical exchange from one site to another.

It should be noted that there is a variant called SECSY.[17] This places the mixing time t_m in the middle of the labeling time t_1 and leads to a display with diagonal peaks at fixed ω_2 and with paired cross-peaks related by a line of slope −1. This variant has been superseded by the above EXSY method.

2. 2D Spectral Intensities

The 2D NMR cross-peaks provide a clear picture of the exchange process. Especially in multisite systems they map out the exchange pathways by showing which NMR peaks exchange with which other peaks. They are a graphic display of the exchange process. The exact connection between the cross-peak intensities and the exchange kinetics is the goal of the following derivation.

The essential feature of a quantitative 2D EXSY experiment is the relationship between the intensity of a cross-peak and the rate constants for chemical exchange. To understand this relationship, a detailed consideration of a multisite experiment is presented. This is adapted from Macura and Ernst.[18] A more detailed development has been presented by Willem.[15]

The initial, equilibrium z magnetization of nuclei in site j is M_j^0. After the first 90° pulse and labeling time t_1 this magnetization becomes precessing and decaying transverse magnetization (eq 10, where ω_j is the precession frequency for site j and T_{2j} is the spin–spin relaxation time). To allow for phase indeterminacy, eq

$$M_j = -M_j^0 e^{i\omega_j t_1} e^{-t_1/T_{2j}} \qquad (10)$$

10 includes both real and imaginary terms corresponding to y and x components of the magnetization. The second 90° pulse, plus homospoil, then converts transverse magnetization into z magnetization (eq 11). The negative sign arises because two 90° pulses invert the magnetization.

$$M_{z,j} = -M_j^0 e^{i\omega_j t_1} e^{-t_1/T_{2,j}} \tag{11}$$

Next we must consider how chemical exchange and spin–lattice relaxation affect this z magnetization during the mixing period. Let m_j be the deviation of $M_{z,j}$ from its equilibrium value (eq 12). The coupled

$$m_j = M_{z,j} - M_j^0 \tag{12}$$

differential equations that describe the time dependence of these deviations are given as eq 13, where $T_{1,i}$

$$\begin{aligned} dm_1/dt &= -(T_{1,1}^{-1} + \sum_l k_{1l})m_1 + k_{21}m_2 + \ldots + k_{N1}m_N \\ dm_2/dt &= k_{12}m_1 - (T_{1,2}^{-1} + \sum_l k_{2l})m_2 + \ldots + k_{N2}m_N \\ dm_N/dt &= k_{1N}m_1 + k_{2N}m_2 + \ldots - (T_{1,N}^{-1} + \sum_l k_{Nl})m_N \end{aligned} \tag{13}$$

is the spin–lattice relaxation time of nuclei in site i and k_{ij} is the (pseudo-first-order) rate constant for exchange from site i to site j. The term $k_{ij}m_i$, which appears twice, once in the sum over l and once more elsewhere, accounts for the transfer of nonequilibrium magnetization from site i to site j. These equations may be written concisely in matrix form as eq 14, where $\mathbf{m}$ is

$$\dot{\mathbf{m}} = -\mathbf{R}\mathbf{m} \tag{14}$$

a column matrix whose components are m_1, m_2, ..., m_N, $\dot{\mathbf{m}}$ contains the time derivatives of the components of $\mathbf{m}$, and $\mathbf{R}$ is a square $N \times N$ matrix whose off-diagonal elements are $R_{ij} = -k_{ji}$ (BEWARE of the reversal!) and whose diagonal elements are $R_{ii} = T_{1,i}^{-1} + \sum_l k_{il}$.

This $\mathbf{R}$ matrix is the key to the chemical process, since it contains all the site to site rate constants. The point of this derivation is to relate the elements of $\mathbf{R}$ to the intensities in the 2D NMR spectrum. The formal solution to eq 13 or 14, at $t = t_m$, is given by eq 15 or 16, where $m_j(0)$ is the initial deviation, at the beginning

$$m_i(t_m) = \sum_j (e^{-\mathbf{R}t_m})_{ij} m_j(0) \tag{15}$$

$$\mathbf{m}(t_m) = e^{-\mathbf{R}t_m}\mathbf{m}(0) \tag{16}$$

of the mixing period, and $\mathbf{m}(0)$ is a column matrix of these deviations. (The exponential of a matrix is not trivial. It is defined as in eq 17, where $\mathbf{R}^0 = \mathbf{1}$, the

$$e^{-\mathbf{R}t_m} = \sum_{n=0}^{\infty} (-1)^n \mathbf{R}^n t_m^n / n! \tag{17}$$

matrix whose only nonzero elements are ones along the diagonal.) The initial deviation of magnetization from its equilibrium value is given by substituting eq 11 into eq 12. This can be substituted into eq 15, to produce eq 18. Equation 12 can be applied again to solve for

$$m_i(t_m) = -\sum_j M_j^0 (e^{-\mathbf{R}t_m})_{ij}[1 + e^{i\omega_j t_1} e^{-t_1/T_{2,j}}] \tag{18}$$

the z magnetization of site i at the end of the mixing period (eq 19, where δ_{ij} is 1 if $i = j$ and is 0 if $i \neq j$).

$$\begin{aligned} M_{z,i}(t_m) &= M_i^0 - \sum_j M_j^0 (e^{-\mathbf{R}t_m})_{ij}[1 + e^{i\omega_j t_1} e^{-t_1/T_{2,j}}] = \\ &\quad -\sum_j M_j^0 \{(e^{-\mathbf{R}t_m})_{ij}[1 + e^{i\omega_j t_1} e^{-t_1/T_{2,j}}] - \delta_{ij}\} \end{aligned} \tag{19}$$

The third and final 90° pulse converts this z magnetization into transverse magnetization necessary for signal detection (eq 20). During the acquisition

$$M_{y,i}(t_2{=}0) = -M_{z,i}(t_m) \tag{20}$$

time this magnetization precesses and decays (eq 21).

$$M_{y,i} = -e^{i\omega_i t_2} e^{-t_2/T_{2,i}} M_{z,i}(t_m) \tag{21}$$

The total magnetization detected is then the sum over all sites (eq 22). The contributions from the 1 within the brackets and from the δ_{ij} would lead to additional peaks, called axial peaks. Fortunately these can be removed by proper phase cycling.

$$M_y(t_1,t_2,t_m) = \sum_{i,j} e^{i\omega_i t_2} e^{-t_2/T_{2,i}} M_j^0 \{(e^{-\mathbf{R}t_m})_{ij}[1 + e^{i\omega_j t_1} e^{-t_1/T_{2,j}}] - \delta_{ij}\} \tag{22}$$

Double Fourier transformation of the accumulated signal yields a 2D spectrum (eq 23). Each term in eq 23 represents a complex two-dimensional peak. The first or third factor of each term corresponds to a real

$$S(\omega_1,\omega_2,t_m) = \sum_{i,j} \frac{T_{2,i}^{-1} - i(\omega_2 - \omega_i)}{(\omega_2 - \omega_1)^2 + T_{2,i}^{-2}} M_j^0 (e^{-\mathbf{R}t_m})_{ij} \frac{T_{2,j}^{-1} - i(\omega_1 - \omega_j)}{(\omega_1 - \omega_j)^2 + T_{2,j}^{-2}} \tag{23}$$

absorption mode peak of width $(\pi T_{2,i})^{-1}$ or $(\pi T_{2,j})^{-1}$ Hz at frequency ω_i along ω_2 or at frequency ω_j along ω_1, as well as an imaginary dispersion mode signal. There are both diagonal peaks and cross-peaks. The integrated intensity I_{ij} of the two-dimensional absorption peak at ω_i along frequency coordinate ω_2 and at ω_j along ω_1 is given by eq 24, where δ_{ij} is 1 if $i = j$ and is 0 if $i \neq j$.

$$I_{ij}(t_m) = M_j^0 (e^{-\mathbf{R}t_m})_{ij} = [\delta_{ij} - t_m R_{ij} + \tfrac{1}{2} t_m^2 \sum_k R_{ik}R_{kj} - \ldots] M_j^0 \tag{24}$$

It was asserted[19] and subsequently proved[15] that $I_{ij} = I_{ji}$ even if $R_{ij} \neq R_{ji}$. Therefore, the 2D EXSY spectrum must be symmetric across its main diagonal, despite an earlier assertion[20] that unequal populations could lead to asymmetry.

3. Evaluation of Rate Constants

Equation 24 shows that the 2D EXSY spectrum is a graphic display of the exchange pathways. Cross-peaks in the spectrum correspond to nuclei that exchange from one site to another. The intensities of those peaks do not correspond directly to the exchange matrix $\mathbf{R}$, but to its exponential. It should further be noted that conventionally the diagonal of a matrix runs from top left to bottom right, whereas the diagonal of a 2D NMR spectrum customarily runs from bottom left to top right, except in Figure 6.

Equation 24 gives the peak intensities in terms of the rate constants. Instead, it is necessary to express the rate constants in terms of peak intensities, which can be measured experimentally. Several approaches have been developed.

One possibility is to use the initial rate approximation.[21] At short mixing times the exponential of eq 24 simplifies to produce eq 25, valid for the off-diagonal elements. Now the 2D spectrum becomes a graphic

$$I_{ij}(t_m) \sim -t_m R_{ij} M_j^0 = k_{ji} t_m M_j^0 \qquad i \neq j \tag{25}$$

display directly proportional to the exchange matrix **R**. The complexity of the exact equation (eq 24) arises because cross-peaks between i and j can arise indirectly, by exchange from i to k and then from k to j before the mixing period has expired. However, at very short t_m these indirect cross-peaks vanish, so that the equations simplify. Equation 25 thus permits solving for the rate constants, but it is inherently inaccurate, since all cross-peak intensities are low at short t_m. At practical t_m there is a risk that indirect cross-peaks will be mistaken as evidence of a direct exchange process.

One solution is to use several short t_m values and determine k_{ij} as the slope of a plot of $I_{ij}(t_m)$ vs $M_j^0 t_m$. This does distinguish direct cross-peaks, which show nonzero slope, from the indirect ones, which show zero slope. However, the use of multiple t_m values requires considerable instrument time. Rather than accept the inaccuracies of an initial rate method, with its low intensities, the multiple t_m values would be more effective if distributed across the course of the exchange. Therefore, it is recommended to use the general solution, eq 24, especially if limited instrument time restricts the experiment to a single t_m.

A primitive method[22] for using eq 24 was to choose initial guesses for the k_{ij}s, calculate $I_{ij}(t_m)$, and compare with the experimental values of $I_{ij}(t_m)$. Either trial and error or iteration can then converge to the k_{ij}s that best reproduce the experimental spectrum. However, this method is tedious, and it is preferable to solve eq 24.

A matrix method for inverting eq 24 was first presented by Perrin and Gipe[19] (and in a different context by Keepers and James[23]) and subsequently by Bremer, Mendz, and Moore[24a] and by Olejniczak, Gampe, and Fesik.[24b] The solution is given by eq 26, where $A_{ij} = I_{ij}(t_m)/M_j^0$ and **X** is the square matrix of eigenvectors of **A**, such that $\mathbf{X}^{-1}\mathbf{A}\mathbf{X} = \Lambda = \mathrm{diag}(\lambda_i)$ and $\ln \Lambda = \mathrm{diag}(\ln \lambda_i)$, with λ_i the ith eigenvalue of **A**. The equilibrium magnetization, M_j^0, necessary for the computation can be evaluated by one of two methods. One method involves acquiring the 2D spectrum with mixing time zero, since $I_{ij}(0) = M_j^0$. A second method involves simply replacing each M_j^0 by p_j, the relative population of each site, but at the cost of losing the relaxation information contained in the diagonal elements of **R**. (It can be shown that the logarithm of the arbitrary constant of proportionality, which relates p_j to M_j^0, appears as an additive constant on the diagonal of **R**.)

$$\mathbf{R} = -\frac{\ln \mathbf{A}}{t_m} = -\frac{\mathbf{X}(\ln \Lambda)\mathbf{X}^{-1}}{t_m} \tag{26}$$

It is easy to solve eq 24 or 26 explicitly for the simplest two-site case.[16] For an uncoupled system of spins A and B, with the simplifications of equal populations and equal spin–lattice relaxation times, $T_{1,A} = T_{1,B} = T_1$, and with exchange rate constant, $k = k_{AB} + k_{BA}$, the intensities of the diagonal peaks and cross-peaks reduce to eqs 27 and 28. Solving for k then gives eq 29, where $r = (I_{AA} + I_{BB})/(I_{AB} + I_{BA})$. Even if populations are unequal, with mole fractions X_A and X_B, eq 29 still holds, but with $r = 4X_AX_B(I_{AA} + I_{BB})/(I_{AB} + I_{BA}) - (X_A - X_B)^2$. Therefore, simply by knowing the cross-peak to diagonal peak intensity ratio, the rate constant for chemical exchange can be calculated.

$$I_{AA}(t_m) = I_{BB}(t_m) = \tfrac{1}{4}e^{-t_m/T_1}[1 + e^{-kt_m}]M^0 \tag{27}$$

$$I_{AB}(t_m) = I_{BA}(t_m) = \tfrac{1}{4}e^{-t_m/T_1}[1 - e^{-kt_m}]M^0 \tag{28}$$

$$k = \frac{1}{t_m} \ln \frac{r+1}{r-1} \tag{29}$$

For a two-site system the ability to solve the above equations explicitly is of no special utility. In such systems line-shape analysis or magnetization-transfer techniques are preferable to 2D EXSY. The 2D method is an advantage only in multisite systems, and those require using the general solution, eq 26. Equation 26 provides all the site to site rate constants as the off-diagonal elements of **R**. Moreover, it gives both forward and reverse rate constants independently. This permits a check on the results, since forward and reverse rates must be equal (eq 30, where p_i is the relative population of the ith site).

$$k_{ij}p_i = k_{ji}p_j \tag{30}$$

Although eq 26 looks formidable, it is quite easy on a computer. All that is required is to input the experimental intensities and populations, solve for the eigenvalues and eigenvectors of **A**, and perform matrix multiplications. However, in general **A** is not symmetric, so that the usual algorithm for eigenvalues and eigenvectors of a symmetric matrix is not applicable. (In the worst case, experimental errors may even be so large as to lead to complex eigenvalues and eigenvectors.) A remedy is to symmetrize the matrix by replacing each I_{ij} by $^1/_2(I_{ij} + I_{ji})$ and then diagonalize the symmetric matrix whose elements are $^1/_2(I_{ij} + I_{ji})/(M_i^0M_j^0)^{1/2}$. Then, eq 26 becomes $\mathbf{R} = -(M_i^0/M_j^0)^{1/2}\mathbf{X}' \ln \Lambda\, \mathbf{X}'^{-1}/t_m$, where $\mathbf{X}'$ is the matrix of eigenvectors of the symmetric matrix. However, this procedure loses the independent determination of forward and reverse rate constants.

By such procedures it is possible to evaluate each site to site rate constant $k_{ij} = R_{ji}$. By the nature of NMR these are pseudo-first-order rate constants, with dimensions of reciprocal seconds. If the reaction is of higher order, it is necessary to divide k_{ij} by the equilibrium concentrations of the other reactants that react with species i.

Error analysis is not so easy. If the mixing time t_m were variable, the rate constant could be obtained as the slope of a linear plot of an appropriate experimental quantity vs t_m. Also, the error in the rate constant could be obtained from the scatter of points about that line. However, often only one t_m is available, and it is still desirable to estimate σ_k, the error in the rate constant k.

The formula for propagation of errors becomes eq 31, where the sum is over all independent 2D intensities I_{kl}. Each partial derivative can be approximated by finite difference (eq 32), where $k_{ij}(I_{kl})$ equals $-R_{ji}$, calculated according to eq 26 from the experimental intensities, and $k_{ij}(1.0001I_{kl})$ is also calculated from the experimental intensities, except with one I_{kl} augmented by 0.01%. This is a great deal of computation, but it is easy insofar as the computer has already been pro-

$$\sigma_{k_{ij}}^2 = \sum \left(\frac{\partial k_{ij}}{\partial I_{kl}}\right)^2 \sigma_{I_{kl}}^2 \tag{31}$$

$$\frac{\partial k_{ij}}{\partial I_{kl}} \sim \frac{k_{ij}(1.0001I_{kl}) - k_{ij}(I_{kl})}{0.0001I_{kl}} \tag{32}$$

grammed to solve eq 26. The intensity variances, $\sigma_{I_{kl}}^2$ have been estimated by two methods: One possibility[25] is to assume a constant noise level equal to 1% of one of the diagonal intensities, plus 2% of each individual intensity, and then correct for the $T^{-3/2}$ dependence of signal to noise on temperature and for any exchange broadening. Another possibility[26] is to use an automated procedure in the spectrometer software to evaluate the signal to noise in each one-dimensional slice of each peak and then convert these to noise levels. By any such process it is possible to use eq 31 to estimate the error in each rate constant, although this has rarely been done.

C. Intensities

The input for eq 26 includes the intensities of all diagonal peaks and cross-peaks from the 2D spectrum. To extract rate information, one must be able to measure intensities accurately. The most accurate measure is the integrated volume under a peak. This requires integrations (actually summations) in both dimensions. Integration along ω_2 is routine, just as in 1D NMR, but integration along ω_1 is often inconvenient unless the software permits the necessary manipulations. Integrals are always somewhat uncertain, owing to peak overlap, base-line distortions, and arbitrariness of peak boundaries. An alternative is to use peak heights, evaluated by fitting each peak to a Lorentzian shape. If peak widths are variable, they must also be fit, or the equilibrium magnetizations can be measured from peak heights at $t_m = 0$.

A further problem is that conventional methods of displaying 2D NMR spectra employ either the absolute value mode (cf. eq 7 and Figure 2c) or the power mode to obtain suitable line shapes. An absolute value transform cannot be integrated, since the integral does not converge, except with distortions to the line shape. Besides, as in 1D NMR, these transforms can also introduce undesirable intensity distortions as well as peak broadening and overlap. Therefore, it is necessary to select pure absorption mode spectra in both dimensions, free of dispersion components.

Various methods exist for obtaining phase-sensitive spectra in four quadrants.[27,28] These methods are technically quite complex and also instrument-dependent. Now they are being included in 2D software and are becoming routine. The casual reader may wish only to realize that it can be done and to skip the details of this section. The general problem can be seen on inspection of the ijth term (eq 33) from the double sum

$$S_{ij}(\omega_1,\omega_2,t_m) = \frac{T_{2,i}^{-1} - i(\omega_2 - \omega_i)}{(\omega_2 - \omega_i)^2 + T_{2,i}^{-2}} M_j^0(e^{-\mathbf{R}t_m})_{ij} \frac{T_{2,j}^{-1} - i(\omega_1 - \omega_j)}{(\omega_1 - \omega_j)^2 + T_{2,j}^{-2}} \quad (33)$$

of eq 23. Each such term is one peak in a 2D NMR spectrum. Although that term can be separated into real and imaginary parts, these do not represent absorption and dispersion. Instead each of the two factors, one containing ω_2 and the other containing ω_1, must be individually separated into absorption and dispersion components. The separation of the ω_2 factor can be accomplished by the usual quadrature-phase detection. The separation of the ω_1 factor requires proper phase cycling, to accumulate the real and imaginary parts separately. Two ingenious methods have been devised for doing so. Either way, combining the real parts of each dimension then affords eq 34. The resulting absorption peak is Lorentzian in both dimensions.

TABLE 1. **Phase Cycling Used To Accumulate Pure Absorption Mode 2D NMR Spectra via States, Haberkorn, and Ruben[27]**

pulse phase			
P_1	P_2	P_3	receiver
X	X	X	X
Y	Y	X	X
$\bar{X}$	$\bar{X}$	X	X
$\bar{Y}$	$\bar{Y}$	X	X
$\bar{X}$	X	X	$\bar{X}$
$\bar{Y}$	Y	X	$\bar{X}$
X	$\bar{X}$	X	$\bar{X}$
Y	$\bar{Y}$	X	$\bar{X}$
X	Y	X	Y
Y	$\bar{X}$	X	Y
$\bar{X}$	$\bar{Y}$	X	Y
$\bar{Y}$	X	X	Y
$\bar{X}$	Y	X	$\bar{Y}$
$\bar{Y}$	$\bar{X}$	X	$\bar{Y}$
X	$\bar{Y}$	X	$\bar{Y}$
Y	X	X	$\bar{Y}$

$$S_{ij}^{abs}(\omega_1,\omega_2,t_m) = \sum_{i,j} \frac{T_{2,i}^{-1}}{(\omega_2 - \omega_i)^2 + T_{2,i}^{-2}} M_j^0(e^{-\mathbf{R}t_m})_{ij} \frac{T_{2,j}^{-1}}{(\omega_1 - \omega_j)^2 + T_{2,j}^{-2}} \quad (34)$$

The method of States, Haberkorn, and Ruben[27] for obtaining pure absorption mode spectra in both dimensions requires acquiring two separate signals whose pulses are phase shifted by 90°. Taking the difference between FIDs acquired with the phase of P_2 (see Figure 3) at 0° and 180° with respect to P_1 affords the real part of the t_1 dimension. Acquisition of FIDs with P_2 at ±90° with respect to P_1 affords the imaginary part of the t_1 dimension. Each pair of FIDs accumulated for each t_1 value is stored in a different memory block, and their Fourier transformations are carried out separately. All FIDs are Fourier-transformed with the phase correction found to be appropriate for the $t_1 = 0$ spectrum. The data sets are transformed in the t_2 dimension, after which the real parts of the resultant data are extracted and combined for each t_1 value. Transposition of this complex matrix, followed by a second Fourier transformation, yields the final phased 2D NMR spectrum. The 16-cycle phase-cycling routine used in this method is given in Table 1.

A second method of obtaining pure absorption mode spectra in two dimensions is time-proportional phase incrementation (TPPI).[28] Originally proposed and implemented by Redfield[28a] as a means of achieving quadrature detection in one dimension, TPPI was extended to the two-dimensional realm by Wüthrich.[28b] The TPPI method involves incrementing the phase of the first pulse in 90° intervals in coordination with the incrementation of t_1. The phase-cycling sequence used for implementing TPPI in a 2D experiment is shown in Table 2.

TPPI in two dimensions essentially samples t_1 at twice the rate of the States, Haberkorn, and Ruben method. However, only one experiment is stored per

TABLE 2. Phase Cycling Used To Accumulate Pure Absorption Mode 2D NMR Spectra via TPPI

pulse phase			
P_1	P_2	P_3	receiver
X + TPPI	X	X	X
X + TPPI	$\bar{X}$	$\bar{X}$	X
X + TPPI	$\bar{X}$	X	$\bar{X}$
X + TPPI	X	$\bar{X}$	$\bar{X}$
X + TPPI	X	Y	Y
X + TPPI	$\bar{X}$	$\bar{Y}$	Y
X + TPPI	$\bar{X}$	Y	$\bar{Y}$
X + TPPI	X	$\bar{Y}$	$\bar{Y}$

t_1 value, so that the time requirements are the same. The principles behind the phase cycling required for the two methods are sufficiently similar that the choice between the two becomes simply a matter of instrumental capability, and a combination of the two methods is also possible.[29] TPPI is necessary if there is only one analog to digital converter or if the computer software is restricted to real Fourier transforms.

Whichever method one chooses to use to obtain pure absorption mode spectra in both dimensions, it is also necessary to eliminate the undesirable axial peaks. Axial peaks arise as a result of spin–lattice relaxation during t_m, which creates t_1-independent z magnetization that is converted to a signal by the final 90° pulse. This signal manifests itself as peaks along $\omega_1 = 0$ in the final 2D spectrum. With TPPI these are at the edge of the spectrum, but with the method of States, Haberkorn, and Ruben they appear as a ridge in the center. These peaks carry no information about chemical exchange, and they interfere with those that do. Fortunately, the unwanted axial peaks can be removed by additional phase cycling,[7,27,28] included in Tables 1 and 2.

D. Time Considerations

1. Time Required

The experimental time required to obtain kinetic data is a prime consideration when choosing a method of study. 2D EXSY certainly does require a great deal of expensive instrument time. However, it can be competitive with magnetization-transfer techniques, where the time required increases as the number of sites increases. The time required for 2D EXSY is essentially independent of the number of sites, provided that chemical shift differences between the sites are not small.

Most of the time required is experiment time, rather than the computations. Each pulse sequence of Figure 3 requires a total time equal to $t_1 + t_m + t_2 + t_{delay}$, where t_{delay} is any additional delay to allow the equilibrium magnetization to be restored before repetition. If reliable intensities are desired for quantitative calculations, a simple rule is to arrange for $t_2 + t_{delay}$ to be at least $4T_1$, where T_1 is the longest spin–lattice relaxation time of the nuclei of interest. Of course, a long delay is wasted time, and it may be preferable to lengthen t_1 and t_2. The total experiment time depends on several parameters. A key parameter is the spectral resolution, $\delta\nu$, in hertz, that is desired. If peaks are well-separated or inherently broad, high resolution (small $\delta\nu$) is not necessary, but it must be sufficient to permit the extraction of the individual 2D intensities. Just as in 1D NMR, the spectral resolution determines the acquisition time t_2 through eq 35. To match the resolution in the two dimensions, it is sufficient to take the longest t_1 value as half of this t_2, so that the average t_1 is $1/4\delta\nu$.

$$t_2 = 1/\delta\nu \tag{35}$$

The pulse sequence must be executed for each t_1. The number of t_1 values $N(t_1)$ should be equal to half the number of data points acquired during t_2. As in 1D NMR, this latter number is equal to $2\Delta\nu/\delta\nu$, where $\Delta\nu$ is the spectral width needed to include all the peaks of interest. (Irrelevant portions of the spectrum may be excluded, provided there is no foldover into the region of interest.) Therefore, $N(t_1) = \Delta\nu/\delta\nu$. To utilize the computer's algorithm for Fourier transforms, it is necessary to round this number up to the nearest power of 2. To reduce experiment time, fewer t_1 values can be used, at the expense of poorer resolution along ω_1. Prior to the Fourier transformation, it is recommended to zero-fill the t_1 data so as to have the same number of data points in both dimensions.

Further repetition increases signal to noise. The number of acquisitions for each t_1, N_a, must be chosen as an integer multiple of the number of steps in the phase-cycling sequence. The sequences given in Tables 1 and 2 require a minimum of 16 and 8 acquisitions per t_1 value.

The total experiment time is thus given by eq 36. With realistic values, $\delta\nu = 1$ Hz, $\Delta\nu = 512$ Hz, $T_1 = 0.3$ s, $t_m = 0.3$ s, $N_a = 16$, and the total time is 4 h. Even if T_1 is longer or if N_a must be increased, the total time remains reasonable, especially since the experiment can be automated so that it does not require operator attention.

$$t_{total} = N_a N(t_1)(t_{1,av} + t_m + t_2 + t_{delay}) \tag{36}$$

As for computation time, a typical data set, with 512 t_1 values, zero-filled to 1024 and with 1024-point acquisition in t_2, the current Varian software at the University of California, San Diego, will do all the Fourier transforms in both dimensions in <2 min. With 2K blocks the time would quadruple, but this is still short compared to total experiment time.

2. Time Scale of Reactions

The rates of reactions that are amenable to study by dynamic one- and two-dimensional NMR methods vary considerably. Each method has its own range of applicability. Line-shape analysis is applicable to the study of processes occurring with rate constants between 1 and 10^4 s^{-1}. The governing factors in this technique are the inherent line width $\delta\omega$ and the chemical shift separation of the exchanging sites A and B. The guideline condition is $k \approx \delta\omega$ or $k \approx \omega_A - \omega_B$ or $k \approx \delta\omega^2/(\omega_A - \omega_B)$. The saturation-transfer technique, on the other hand, is applicable to slower processes, with rate constants on the order of 10^{-1}–10^2 s^{-1}. The saturation-transfer method is governed by the spin–lattice relaxation times T_1 of the exchanging sites and, in general, requires that $k \approx 1/T_1$, so that the range of applicability may be narrow.

2D EXSY can measure a range of reaction rates as well, the upper limit being governed by $k \approx \delta\omega$ or $k \ll \omega_A - \omega_B$. Too high a rate will broaden and coalesce the relevant signals, obscuring the kinetics. The lower limit

of the range is dictated by $k \approx 1/T_1$. Too low a rate will not allow for significant magnetization transfer during the mixing time before the spins are fully relaxed. Kinetic measurements by 2D NMR are, therefore, applicable for rate constants between 10^{-2} and 10^2 s^{-1}.

Although this is the full range, maximum precision in evaluating a rate constant k by quantitative 2D EXSY is achieved when $k \geq 1/T_1$. Generally for protons and ^{13}C this corresponds to $k \approx 10\ s^{-1}$. It may be possible to adjust the temperature or the concentration of a coreactant or catalyst to bring the rate constant into this range.

Since 2D EXSY (and magnetization transfer) operate on a slightly longer time scale than line-shape analysis, they are useful at lower temperatures. This is often an advantage with sensitive or unstable substances. A further advantage over line-shape analysis is that it is not necessary to make chemical shift or line width measurements in the slow-exchange limit, which is often inaccessible.

For any particular reaction 2D EXSY is limited to a rather narrow range of rate constants and a corresponding narrow range of temperatures. Consequently, the accuracy of activation parameters $\Delta H^\ddagger$ and $\Delta S^\ddagger$ cannot be high. One remedy is to combine 2D EXSY with line-shape analysis at higher temperature.[25] Even though line-shape analysis may be incapable of fitting the multitude of rate constants in a multisite system, the relative rate constants can be determined or extrapolated from the 2D results, so that line-shape analysis becomes only a one-parameter fit.

3. Optimum Mixing Time

Since a 2D EXSY experiment requires so much instrument time, it is not often feasible to repeat the experiment with a series of mixing times t_m. Even if the time is available, long-term instrument instabilities may create systematic errors. Therefore, a single mixing time often must suffice. This corresponds to one-point kinetics, where the rate constant is evaluated from a single time point (plus time zero and time infinity). Such a method is obviously fraught with danger. A multiplicity of time points would improve the precision of the rate constant. One-point kinetics does not even provide statistics to evaluate that precision.

If only one t_m must suffice, it must be chosen carefully. If it is too short, kinetic effects on the cross-peak intensities will be too small to measure accurately. If it is too long, relaxation will dominate or else the kinetic effects will be so large as to be insensitive to the rate parameters. For a system with two sites A and B of equal relaxation time T_1, the optimum t_m can be calculated. It had been claimed[16] that the optimum is $\ln [1 + (k_{AB} + k_{BA})T_1]/(k_{AB} + k_{BA})$, chosen to maximize the cross-peak intensities. Instead, it is proper to minimize the relative error in the rate constant. Then statistical analysis leads to eq 37 as an adequate approximation, and more exact expressions are available.[30] Use of this formula requires an initial estimate of the rate constant that is to be determined, but this is the case for any kinetic study. For multisite systems there is no t_m that is optimum for all rate constants unless all are equal. If they are nearly equal, an average of their mixing times, calculated according to eq 37, will be suitable. If they differ widely, multiple mixing times are advised.

$$t_{m,opt} \sim \frac{1}{T_1^{-1} + k_{AB} + k_{BA}} \tag{37}$$

A clever method called accordion spectroscopy permits the variation of t_m without increasing the total instrument time.[31] Instead of a fixed mixing time, t_m is incremented as a fixed multiple of the labeling time t_1. Typically, t_m is $10–100t_1$, depending on exchange rate and spectral resolution. However, this leads to peak distortions, such that the rate constant is evaluated from peak widths rather than from intensities. To recover the multiplicity of t_m values, it is necessary to select each peak from the 2D spectrum and Fourier transform it back to $I_{ij}(t_m)$.[32] Unfortunately this is not practical in multisite systems or when peaks overlap, which is the realm of applicability of 2D EXSY.

4. Simplified Variants

Since 2D EXSY is so time-consuming, it is worth considering some simplified variants, to see how they are related. Much of the time requirement in 2D NMR comes from the need to scan the range of t_1 values. Yet nearly all of the spectrum along the ω_1 axis is not peaks but instead merely base line. It is not possible to omit those base-line regions simply by omitting some of the t_1 values, since ω_1 and t_1 are connected through the Fourier transform, so that each t_1 contributes to every ω_1. However, it is possible to make judicious choices of t_1 values so as to obtain most of the information of the 2D spectrum.

In these methods it is often convenient to express the magnetizations or intensities as deviations from equilibrium, as in eq 38, where I_j^0 is the equilibrium intensity of the jth site (as in eq 6, where the superscript was omitted). Those deviations are readily obtained experimentally as difference spectra.

$$m_j = I_j - I_j^0 \tag{38}$$

With only two sites, separated by a chemical shift difference $\Delta\omega$ (radians, or $2\pi\Delta\nu$ Hz), and with the spectrometer's reference frequency set on one of the sites, a single t_1 value chosen equal to $\pi/\Delta\omega$, or $1/2\Delta\nu$, can suffice. The second 90° pulse then produces a selective inversion of that site. After the mixing time t_m, during which magnetization transfer occurs, a third 90° pulse creates transverse magnetization, which is acquired and Fourier transformed with respect to t_2 only. If B is the peak that is inverted, the intensities of the two peaks, relative to equilibrium intensities, are given by eqs 39 and 40,[33] where $R_A = k_{AB} + T_{1,A}^{-1}$, $R_B = k_{BA} + T_{1,B}^{-1}$, and $\lambda_\pm = (R_A + R_B \pm [(R_A - R_B)^2 + 4k_Ak_B]^{1/2})/2$. By successively inverting each of the two peaks and measuring both intensities, there result four equations in the four unknowns—k_{AB}, k_{BA}, $T_{1,A}$, and $T_{1,B}$—or four time dependences in the four unknowns, so that it is possible to solve numerically for k_{AB} and k_{BA}.

$$m_A(t_m) = -I_A^0 \frac{2k_{BA}}{\lambda_+ - \lambda_-}[e^{-\lambda_- t_m} - e^{-\lambda_+ t_m}] \tag{39}$$

$$m_B(t_m) = -I_B^0 \frac{1}{\lambda_+ - \lambda_-}[(\lambda_+ - R_A)e^{-\lambda_+ t_m} - (\lambda_- - R_A)e^{-\lambda_- t_m}] \tag{40}$$

Another possibility is to achieve selective inversion of one of the sites by a "soft" (low-power) 180° pulse at that particular frequency. Instrumentally it may be easier to accomplish this with a DANTE pulse.[33] If the inversion is not complete, the equations must be modified to allow for this.[34]

This latter method is readily generalized to N sites. Each of the sites is selectively inverted by a soft pulse or by a DANTE pulse. After a mixing time t_m, a 90° pulse creates transverse magnetization, which is acquired and Fourier transformed. The resulting intensities still obey eq 15, expressed in terms of deviations from equilibrium intensities (eq 38). In the experiment where the ith site is selectively inverted, $m_j(0) = -2M_i^0\delta_{ij}$ and eq 15 reduces to eqs 39 and 40. Alternatively, the deviations m_j can be formed into a column matrix m, which satisfies eq 16. Then, if those column matrices **m** are set side by side to form an $N \times N$ square matrix **M**, eq 16 becomes eq 41, where $\mathbf{M}_0$ is the square matrix

$$\mathbf{M}(t_m) = e^{-\mathbf{R}t_m}\mathbf{M}_0 \qquad (41)$$

of initial deviations of magnetizations from their equilibrium value. This matrix is diagonal if every inversion is absolutely selective, but it can also account for incomplete selectivity or incomplete inversion. Gesmar and Led[35] have used a nonlinear least-squares method to fit all the time courses of all the experimental magnetizations in $\mathbf{M}(t_m)$ so as to determine all the site to site rate constants. It is further possible to include additional constraints in the curve-fitting procedure.[36] However, this approach is subject to the difficulty of fitting the experimental magnetizations to the sum of exponentials implied by eq 41.

A simpler method[37] is to invert eq 41, just as eq 26 inverts eq 24. This leads to eq 42, where $\mathbf{M}_0^{-1}$ must be evaluated from the initial magnetizations immediately following the selective (or semiselective) inversions and

$$\mathbf{R}t_m = -\ln [\mathbf{M}(t_m)\mathbf{M}_0^{-1}] = -\mathbf{X}(\ln \Lambda)\mathbf{X}^{-1} \qquad (42)$$

where **X** is the square matrix that diagonalizes $\mathbf{M}(t_m)\mathbf{M}_0^{-1}$ to Λ, so that $\ln \Lambda$ is a diagonal matrix whose elements are the logarithms of the eigenvalues of $\mathbf{M}(t_m)\mathbf{M}_0^{-1}$. This method was initially applied to a two-site system, with a single t_m and with the simplifying assumption of selective inversion. Then $\mathbf{M}_0$ is diagonal, and it is easy to solve for the elements of **R**. Even in the general case $\mathbf{M}_0$ can be measured experimentally and $\mathbf{M}_0^{-1}$ is readily calculated. The matrix diagonalization can be carried out for each t_m, and a plot vs t_m of the ij off-diagonal element of the matrix on the right-hand side is then linear, with slope equal to R_{ij}, or $-k_{ji}$.[38]

Another variant is the classical saturation-transfer method,[3] generalized to N sites. The steady-state magnetizations at every site j can be measured under conditions where each site in succession is held saturated. Saturation of the ith site means that the magnetization M_i is zero, so that m_i, the deviation from equilibrium, is $-M_i^0$. Under these steady-state conditions, the time derivatives of eq 13 or 14 are all zero, so that the m_j, the deviations of magnetization from equilibrium, must satisfy eq 43, where $\mathbf{M}_{ss}$ is an $N \times$

$$-\mathbf{R}\mathbf{M}_{ss} = 0 \qquad (43)$$

N matrix whose ith column contains steady-state deviations of magnetization when site i is saturated. Equation 43 is a set of N^2 simultaneous homogeneous (right-hand side identically zero) linear equations in the N^2 unknown elements of **R**. Such a set cannot be solved for all the unknowns. However, it is possible to solve for all ratios of rate constants, which is often adequate. To evaluate absolute rate constants, it is also necessary to measure the N T_1 values, each under conditions where all other sites are saturated. This is impractical, but there are some simplifying approximations applicable to the three-site case[3c] and readily generalized to $N > 3$.

A clever simplification of the 2D method for N sites involves N judiciously chosen t_1 values.[39] Following the pulse sequence of Figure 3, Fourier transformation with respect only to t_2 produces spectra from which each m_i, the deviation of ith site magnetization from its equilibrium value, can be obtained by difference spectroscopy. These again satisfy eq 15. These values for the various sites can be constructed into a column matrix **m**, which satisfies eq 16. The column matrices **m** for the N t_1 values can be set side by side to form a square matrix **M**, which satisfies eq 41. The matrix $\mathbf{M}_0$ can be evaluated by repeating the N experiments but with $t_m = 0$. Equation 42 then provides the elements of **R** and all the site to site rate constants. This derivation is general, regardless of the choice of t_1 values. However, to reduce errors, the N t_1 values should be chosen so that the determinant of the matrix $\mathbf{M}_0$ is as large as possible. In the selective inversion method above, $\mathbf{M}_0$ is diagonal, or nearly so. In the alternative "2D" method $\mathbf{M}_0$ is optimally constructed so that its diagonal elements are zero, or nearly so. This can be accomplished by choosing the ith t_1 value according to eq 44, where $\Delta\nu_i$ is the chemical shift of the ith site, relative to the reference frequency ω_0.

$$t_1 = \pi/|\omega_i - \omega_0| = 1/2\Delta\nu_i \qquad (44)$$

All of these methods work because each one creates an initial perturbation of the magnetizations from their equilibrium values. Equation 13 or 14 describes the time course of the restoration of equilibrium, influenced by chemical exchange. That restoration can be followed by NMR and the exchange parameters determined. These simplified variants of the 2D method represent different initial perturbations. Each requires several experiments, since each of the sites must be perturbed in turn. The advantage of the full 2D method is that it perturbs all sites simultaneously, just as FT NMR observes all sites or all frequencies simultaneously.

E. Other Considerations

1. Signal Assignments

Signal assignment is a topic beyond the scope of this review. The 2D NMR method is said to provide site to site rate constants for chemical exchange. Actually it provides rate constants for exchange among NMR signals, and it is necessary to assign these signals to the various sites in the molecule. Often this task can be accomplished easily through well-known empirical correlations between chemical shift and environment. Sometimes coupling constants and/or nuclear Overhauser enhancements provide information regarding through-bond or through-space proximity. In complicated molecules, powerful 2D methods called COSY[7,40] and NOESY[9,11] can dissect this information. Alterna-

SCHEME 1. Rearrangement of Bullvalene

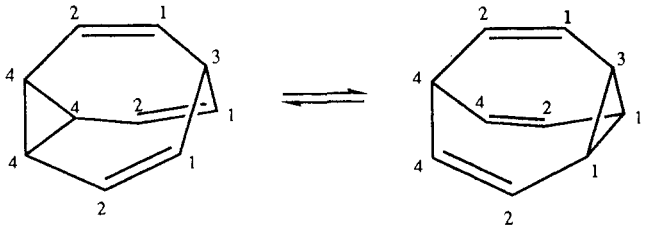

tively, the exchange mechanism may be securely known, and the pattern of 2D EXSY cross-peaks can assist in peak assignments.

2. Mechanistic Considerations

It is still necessary to relate the site to site rate constants, measured by 2D NMR, to mechanistic rate constants, perhaps for several proposed mechanisms. Often this can be done by inspection, especially if there is only one first-order rate constant k in the mechanism. The site to site rate constant k_{ij} is then given by eq 45,

$$k_{ij} = P_{ij}k \tag{45}$$

where P_{ij} is the probability that one passage through the exchange process will transfer a nucleus from site i to site j. This P_{ij} is always very simple—a fraction composed of small integers—0 or 1 or $^1/_2$, etc. For example, in the rearrangement of bullvalene (Scheme 1), the matrix of P_{ij} is given in eq 46. In more com-

$$P_{ij} = \begin{bmatrix} 0 & 1/3 & 0 & 2/3 \\ 1/3 & 0 & 0 & 0 \\ 0 & 0 & 0 & 1/3 \\ 2/3 & 0 & 1 & 0 \end{bmatrix} \tag{46}$$

plicated cases, especially with symmetry, a systematic method using permutation group theory can relate the rate constants and can also construct all the NMR-distinguishable exchange processes that might be considered.[15,41]

When there is more than one rate constant in the mechanism, it is generally necessary to use the steady-state approximation to calculate the probability factors. For example, in the N-protonation mechanism for acid-catalyzed proton exchange in amidinium ions (Scheme 2), the site to site rate constants are given by eqs 47 and 48.[42] Another commonly encountered as-

$$k_{EZ} = k_{ZE} = k_{ZS} = k_p[H^+]k_r/(3k_r + 2k_d) \tag{47}$$

$$k_{ES} = k_p[H^+](k_r + k_d)/(3k_r + 2k_d) \tag{48}$$

pect of this example is that the measured site to site rate constants are always pseudo-first-order, and these must be related to higher order mechanistic rate constants by multiplying these latter by appropriate equilibrium concentrations. Such problems are not unique to 2D NMR but always arise in mechanistic studies,[43] where it is necessary to relate the mechanistic (hypothetical, microscopic) rate constants to the empirical (phenomenological, observable, macroscopic) rate constants.

Often it is possible to measure several site to site rate constants, even though the kinetics are described by a single rate constant, or a very small number of rate constants. For example, three pairs of nonzero site to site rate constants can be measured, in principle, for the

SCHEME 2. Acid-Catalyzed Proton Exchange in Amidinium Ions

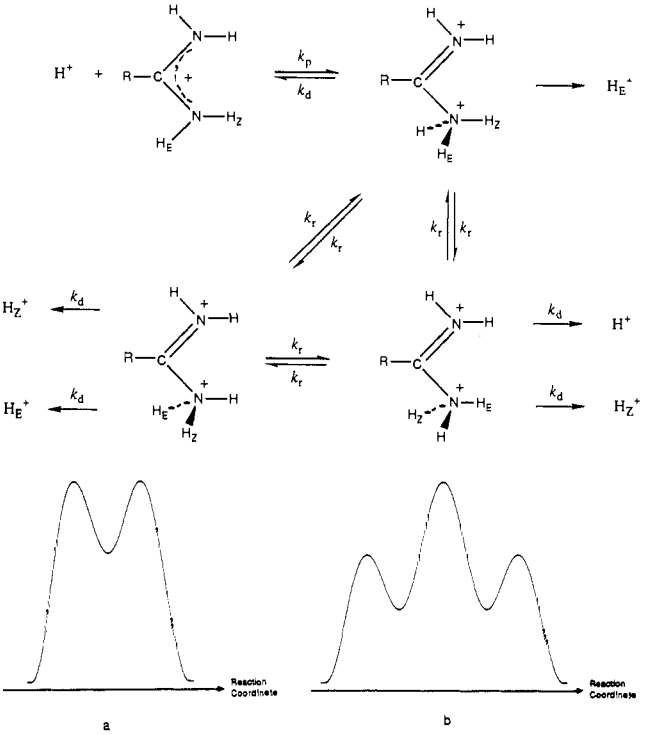

Figure 7. Energy diagram for an exchange process occurring (a) via a symmetric intermediate or (b) via a symmetric transition state.

rearrangement of bullvalene (Scheme 1), but only one macroscopic rate constant is needed to describe the reaction. These rate constants are related through eqs 45 and 46. The independent measurements of the site to site rate constants can be averaged to obtain a more reliable value for that macroscopic rate constant.

Finally, it is worth pointing out explicitly that the mechanism of any exchange reaction must be symmetric.[44] This is a consequence of the principle of microscopic reversibility. The path of a reverse reaction must always be the reverse of the path of the forward reaction, via the same intermediates and transition states. Since forward and reverse reactions are identical (or paired, which is a possible complication that we ignore), an exchange reaction must proceed via a symmetric intermediate (Figure 7a) or via a symmetric transition state (Figure 7b).[44] This holds strictly for a topomerization reaction, where reactants and products are identical, but it can also be extended to a diastereomerization if the substituents are viewed merely as labels that weakly perturb the energetics.[45] (Such a reaction has been called a pseudodegenerate rearrangement.[15] The labels may be needed to desymmetrize the molecule and make the process detectable by NMR.) It then becomes necessary to realize any exchange mechanism to completion and to identify the symmetric intermediate or transition state. This is especially important in organometallic chemistry, where ligand-substitution steps have their own stereochemical requirements.

3. NMR Complications

Scalar coupling interferes with 2D exchange spectroscopy.[46] It creates cross-peaks called J cross-peaks even without chemical exchange. Indeed the 2D COSY

method utilizes this feature, although the pulse sequence is different. Heteronuclear coupling can be removed simply by decoupling. Of course ^1H decoupling is customary in ^{13}C and ^{31}P NMR, etc. The contribution from homonuclear coupling can be reduced by appropriate phase cycling.[46] Further suppression can be achieved by introducing a random variation δt_m into the mixing time t_m or by incrementing each mixing time by a small fraction of the labeling time t_1.[47] However, the simplest remedy is to seek uncoupled systems, such as ^{13}C nuclei and methoxy or arylmethyl hydrogens.

Cross-relaxation also interferes. In 1D NMR this leads to nuclear Overhauser enhancements. In 2D NMR this leads to cross-peaks between nuclei that are near each other in space. Indeed, another 2D NMR method, called NOESY,[9,11] uses this feature to probe proximity, with a pulse sequence identical with the EXSY sequence of Figure 3. To the relaxation–exchange matrix **R** of eq 14 et seq. must be added the contribution from cross-relaxation, given in eq 49,[48]

$$R_{ij} = \frac{\gamma^4\hbar^2}{10r_{ij}^6}\left[\frac{6\tau_c}{1 + 4\omega^2\tau_c^2} - \tau_c\right] \qquad (49)$$

where γ is the magnetogyric ratio, $\hbar$ is Planck's constant/2π, r_{ij} is the distance between nuclei i and j, ω is the Larmor frequency, and τ_c is the rotational correlation time, or the average time required for the molecule to rotate by 34° about any axis. It is the r^{-6} dependence that provides proximity information, both qualitative and quantitative, which has been immensely effective in determining structures and conformations, especially of macromolecules.[48,49] The disadvantage is that this term in **R** can also lead to cross-peaks in the 2D exchange spectrum. According to the initial rate approximation, the cross-peak intensity due to cross-relaxation is again given by eq 25, but with R_{ij} as in eq 49. For small molecules, τ_c is short, so that (with the usual phasing, which produces positive peaks) the direct cross-peaks are negative in pure absorption mode spectra. For large molecules, τ_c is long and the cross-peaks are positive. In the latter case, or in the former without absorption mode spectra, the cross-peaks may be mistakenly attributed to chemical exchange. In either case, the cross-peak intensity may not reflect exchange alone.

Fortunately it is possible to separate cross-relaxation from chemical exchange. Of course cross-relaxation can be excluded if the nuclei are far apart. This is generally the case for intermolecular exchange reactions. Moreover, the rate of chemical exchange is strongly dependent on temperature and also on the concentration of coreactants or catalysts. In contrast, τ_c and R_{ij} are nearly constant. Therefore, it is possible to evaluate independently the contribution of cross-relaxation by repeating the experiments at low temperature or in the absence of coreactants or catalysts. Another possibility is spin-locking, which is applicable even to macromolecules.[50,51] Still other possibilities, applicable when there is scalar coupling, are a modified pulse sequence called zz-EXSY[52] and a 2D heteronuclear correlated method,[53] but analysis is quite complicated.

Many other NMR techniques may be applied in concert with 2D exchange spectroscopy. There are many difficulties that may be encountered in NMR studies, and these may yield to the broad repertory of modern techniques. Among these may be mentioned heteronuclear decoupling, solvent suppression,[54] cross-polarization and magic-angle spinning (CP/MAS) for NMR of solids,[55] spin-locking,[50,51] and a combined COSY-exchange technique called COCONOSY.[56] The details of these methods are beyond the scope of this review.

SCHEME 3. 1,2 Methyl Shifts in Heptamethylbenzenium Ion

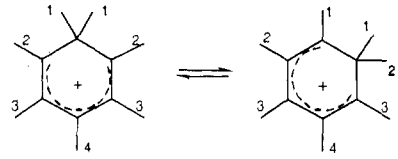

III. Qualitative Applications

The key feature of a 2D EXSY spectrum is the presence of cross-peaks that correspond to site to site exchange. A nonkinetic application of this feature is for simplification of complicated spectra. All 2D NMR methods offer this powerful possibility, since peaks that overlap in a 1D spectrum can be dispersed into two dimensions. In contrast to other 2D methods, which select for scalar coupling or for spatial proximity, 2D EXSY selects those signals that are undergoing chemical exchange. However, we know of no examples where this method has been used for spectral simplification.

The obvious area of applicability is to kinetics. Qualitative 2D EXSY methods have been widely used to map out the chemical exchange pathways of a host of interesting chemical reactions. The applications can be categorized as follows: (A) organic systems, (B) inorganic and organometallic systems, and (C) biochemical systems. We present first an overview of the variety of chemical reactions that have been investigated by qualitative 2D EXSY. We follow the above classification and then repeat it in presenting the applications of quantitative 2D EXSY. Within each section topics are arranged approximately in order of increasing complexity.

A. Organic Systems

1. Solution Studies

The first application[16] was to the classic example of *N*,*N*-dimethylacetamide, $CH_3CON(CH_3)_2$. At 30 °C rotation about the amide C–N bond is fast enough to produce cross-peaks between the two *N*-methyls (Figure 6). More spectacular applications include the rearrangement mechanisms of heptamethylbenzenium ion and bullvalene by ^{13}C NMR.

In the case of heptamethylbenzenium ion[57] (Scheme 3), the methyl region of the 2D EXSY spectrum shows cross-peaks between C_1 and C_2, between C_2 and C_3, and between C_3 and C_4, and no others. Therefore, the rearrangement does not proceed intermolecularly or by random methyl migration to any position. Instead the rearrangement occurs only via 1,2 methyl shifts.

The Cope rearrangement (Scheme 1) of bullvalene[58] is evidenced by cross-peaks between C_1 and C_4 and between C_3 and C_4 in the 2D EXSY spectrum at room temperature. (The expected cross-peak between C_1 and C_2 could not be resolved.) The cross-peak between C_1

and C_4 is more intense than the one between C_3 and C_4, as required by the statistics (eq 46), but no quantitative study has verified the 2:1 ratio.

A mixture of $AlCl_3$ and $HCON(CH_3)_2$ in D_2O shows exchange effects in ^{13}C 2D EXSY spectra that depend on temperature.[58] At 313 K separate signals are seen for $HCON(CH_3)_2$ bound to Al(III) and free in solution, with cross-peaks between them. No cross-peaks are seen between the cis and trans *N*-methyls of either bound or free amide. Therefore, the $HCON(CH_3)_2$ is exchanging between Al-bound and aqueous environments, but amide C–N rotation is slow. At 349 K exchange between bound and free environments is so fast that the peaks are coalesced, and C–N rotation is manifested by cross-peaks between cis and trans *N*-methyls. The spectrum is complicated by the presence of $(CH_3)_2NH$ formed by hydrolysis, but the selectivity of NMR prevents any interference.

A ^1H 2D EXSY study of two trimesitylethylene derivatives **1** shows an interesting comparison.[59] At 330 K each ortho methyl on each of the three rings of **1a** shows cross-peaks with the other ortho methyl on that ring. This corresponds to an exchange process in which

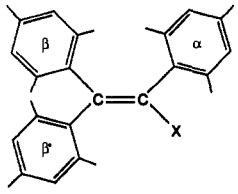

1a, X = OH
1b, X = H

all three rings flip by simultaneously rotating perpendicular to the plane of the double bond. In contrast, **1b** at 290 K shows cross-peaks only between the ortho methyls of the rings labeled α and β. This corresponds to an exchange process in which these two rings flip, while the ring labeled β' rotates through the plane of the double bond. From 1D NMR, $\Delta G^{\ddagger}$ for this process is 16.8 kcal/mol, and $\Delta G^{\ddagger}$ is 20.5 kcal/mol for the three-ring flip, seen only at higher temperature. The change of mechanism is attributed to the steric bulk of the OH, which hinders the β' ring from rotating past it.

An elegant 2D EXSY study of tetra-*o*-tolylcyclopentadienone (**2**) stereoisomers[60] mapped out the exchange network and assisted in signal assignment. In

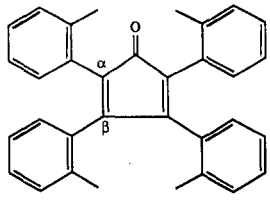

2

$CDCl_3$ ^1H NMR at 500 MHz resolves nearly all eight α-tolyl methyls and nearly all eight β-tolyl methyls of the two achiral and four chiral rotamers (stereoisomers differing in the orientations of the *o*-tolyl rings). These rotamers interconvert by rotations about the *C*-tolyl single bonds. In the 2D spectrum at −43 °C each methyl shows cross-peaks with two others, as required for a mechanism where each tolyl ring rotates independently of the other three. From the connectivity pattern and a quantitative estimate of steric repulsions in each rotamer, it was possible to assign all 16 methyl peaks.

SCHEME 4. Intramolecular Proton Exchange in Tropolone

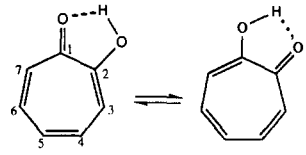

A unique application of 2D NMR is to irreversible photochemical reactions.[61] During the mixing time, a laser pulse causes a photochemical reaction. Since the mixing time can be very short, the second and third 90° pulses of the 2D sequence (Figure 3) are not necessary. A flow system is needed to maintain constant reaction conditions for each t_1 value. The ^1H 2D spectrum then shows crosspeaks at (ω_i,ω_j) corresponding to nuclei that were at chemical shift ω_i in reactant and at ω_j in product. Since the reaction is irreversible, the spectrum is asymmetric, without the paired peak at (ω_j,ω_i). The photocyclization of **3** to **4** was followed by this 2D NMR method, and the cross-peak pattern of the methyl region was used to reassign the product peaks.

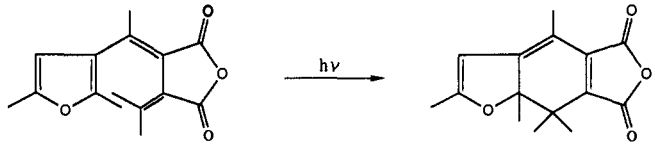

3 **4**

A related study involves the application of 2D NMR to quadrupolar relaxation.[62] Just as chemical exchange can transfer magnetization from one site to another, so also can spin–lattice relaxation transfer magnetization from one site of a spin-coupled nucleus to another. In particular, the ^{13}C NMR spectrum of benzene-d_6 shows a 1:1:1 triplet due to spin–spin coupling to deuterium with spin $I = 1$. The 2D NMR spectrum shows cross-peaks between each pair of components, due to quadrupolar relaxation of the deuterium. The cross-peaks between $I = +1$ and $I = -1$ are most intense because that corresponds to the most efficient relaxation. Similar behavior due to ^{14}N relaxation has been seen in the ^1H 2D NMR spectrum of aqueous NH_4^+,[63] but no quantitative applications to determination of quadrupolar relaxation rates have been made. It should be noted that this contribution to cross-peak intensity must be taken into account in quantitative 2D EXSY.

2. Solid-State and Liquid-Crystal Studies

Proton transfer in crystalline tropolone has been investigated by solid-state ^{13}C CP/MAS NMR.[64] Evidence for an unsymmetrical hydrogen bond and hence the equilibrium shown in Scheme 4 had been determined by gas-phase studies,[65] but the solution-phase reaction is too fast to measure. The ^{13}C 2D EXSY spectrum of tropolone shows cross-peak intensity between C_1 and C_2, reflecting exchange between these two sites. Similarly, cross-peaks are seen between other carbon pairs (C_3 with C_7 and C_4 with C_6), but none with C_5. Rate constants and activation energies were evaluated by inversion transfer.

Proton exchange in phthalocyanine[66] has also been studied by 2D EXSY. In the solid state, the 1D ^{13}C

SCHEME 5. Intramolecular Proton Exchange in Phthalocyanine

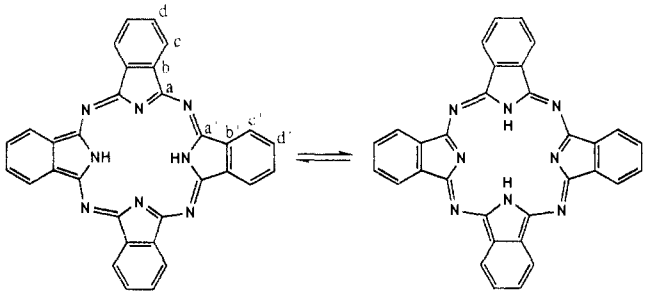

CP/MAS spectrum shows evidence of some sort of temperature-dependent dynamic behavior. However, owing to significant overlap of the pertinent resonances, assignments are difficult and it is not possible to know exactly what processes contribute to the kinetics. The 2D ^{13}C CP/MAS spectrum, on the other hand, clearly displays two sets of cross-peaks connecting the four diagonal resonances assigned as a,a′ and b,b′ (Scheme 5). This spectrum confirmed the two-site exchange process shown and allowed a reexamination of the 1D spectrum for additional structure information.

The ^2H 2D EXSY spectra of polycrystalline dimethyl-d_6 sulfone, $CD_3SO_2CD_3$, and hexamethylbenzene-d_{18} show evidence of molecular reorientation.[67] The spectra were obtained with a modified pulse sequence and without CP/MAS. The diagonal shows a (continuous) powder pattern, with each frequency corresponding to a possible orientation of a S–CD_3 or C–CD_3 bond relative to the applied magnetic field. Instead of cross-peaks there are continuous ridges off the diagonal. These correspond to nuclei that exchange from one orientation to another during the mixing period. Analysis of the frequency dependence of those ridges showed that the jump angle in dimethyl sulfone is 106°, which agrees with the known CSC angle of 103°. For hexamethylbenzene the jump angle is 61°, as expected for rotation about the molecular axis in the solid.

Similar evidence for molecular motion in the solid state was obtained for poly(oxymethylene), $(CH_2O)_x$.[68] ^{13}C NMR with CP/MAS at low speed detects only the polycrystalline material. The low speed preserves the chemical shift anisotropy, which creates a frequency spectrum dependent on the orientation of a CH_2 group relative to the applied field. Cross-peaks are seen in the 2D spectrum, corresponding to reorientation of the CH_2 groups, especially at higher temperature, but details about the reorientation process were not obtained.

In the 2D ^{13}C CP/MAS spectrum of crystalline L-tyrosyl-L-phenylalanine (**5**), cross-peaks are seen between C_2 and C_6 and between C_3 and C_5 of the phenyl ring, which is rotating in the solid.[69] There are no such

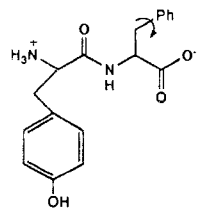

5

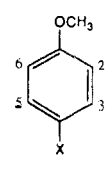

6

cross-peaks for the tyrosine ring, reflecting its relative immobility. A model is crystalline *p*-nitroanisole (**6**, X = NO_2) or *p*-methoxyacetanilide (**6**, X = $NHCOCH_3$),

SCHEME 6. Fluxional Processes in (η^4-Cycloheptatriene)(η^5-cyclopentadienyl)cobalt

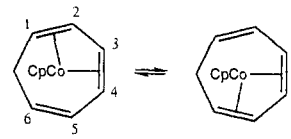

where the occurrence of cross-peaks between C_2 and C_6 (and between C_3 and C_5 of the latter) implies mobility of the aromatic ring, even in the solid.

Deuterium 2D EXSY was applied[70] to examine the dynamics of ring inversion in cyclohexane-d_{12} and 1,4-dioxane-d_8 in various liquid crystalline solvents. The spectra are complicated by the presence of quadrupolar doublets. They could be simplified by using a combination of Zeeman and quadrupole order experiments to eliminate cross-peaks due to quadrupolar relaxation. The resulting pure exchange spectrum of cyclohexane-d_{12} at −27 °C displays cross-peak connectivities that reflect exchange between axial and equatorial deuterons. At −43 °C similar spectra were obtained for the corresponding ring inversion process in dioxane-d_8.

B. Inorganic and Organometallic Systems

Organometallic systems probably offer the greatest opportunity for 2D EXSY. There is a wide variety of NMR-observable nuclei available. The large number of stereoisomers possible for organometallic complexes produces a multitude of NMR sites. Chemical shifts can vary greatly with environment, so that the spectrum is well-dispersed. The diversity of organometallic rearrangement mechanisms leads to a rich field for study.

A simple organometallic example is the fluxional behavior of (η^4-cycloheptatriene)(η^5-cyclopentadienyl)cobalt (Scheme 6).[71] The ^{13}C 2D EXSY spectrum shows cross-peaks between C_1 and C_6, between C_2 and C_5, and between C_3 and C_4, corresponding to the stereoisomerization shown.

Another simple example is ligand exchange in the platinum(II)–8-(dibromomethyl)quinoline complex **7**.[72] The proton 2D EXSY spectrum shows three pairs of cross-peaks between free ligand and that coordinated to the metal.

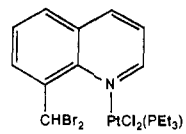

7

The ^1H NMR spectrum of the triply bonded complex $(Me_2N)_2(ArO)Mo{\equiv}Mo(OAr)(NMe_2)_2$ shows four *N*-methyl peaks. This means that the complex exists as a gauche conformer, with hindered rotation about the Mo–Mo and Mo–N bonds. The 2D EXSY spectrum shows only one cross-peak for each *N*-methyl,[73] showing that rotation about the Mo–N bond does occur but that rotation about the Mo–Mo triple bond is slow. The rate constants for bond rotations were determined by saturation transfer.

^6Li 2D EXSY was used to observe the exchange equilibrium between dilithio monomer **8** and dimer **9** in THF solution (Scheme 7).[74] At −20 °C, the 2D exchange spectrum displays cross-peaks between the

SCHEME 7. Monomer–Dimer Equilibrium in Dilithio Products from *n*-Butyllithium plus Diphenylacetylene (Additional Ligands on Lithiums Omitted)

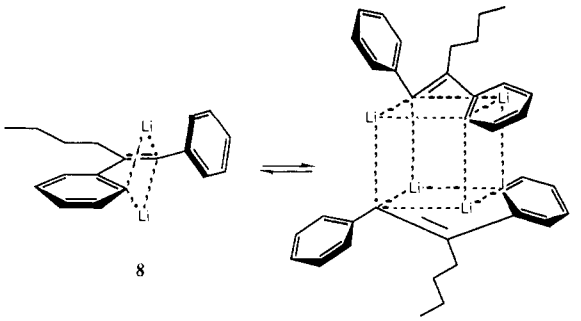

8 9

SCHEME 8. Stereoisomerization of a Binuclear Tin Complex

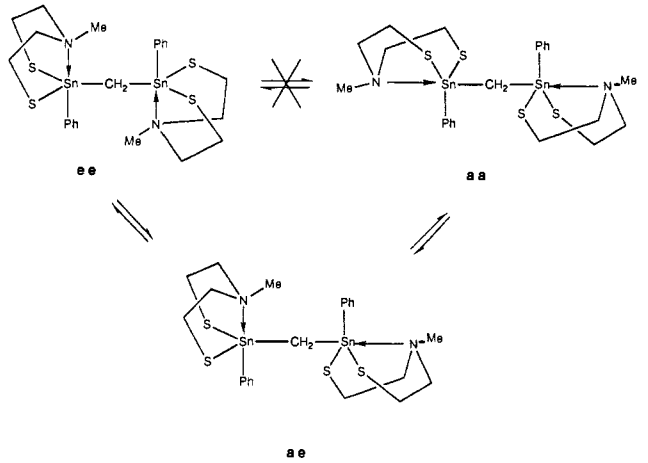

ee aa ae

inequivalent lithium atoms in the dimer, implying intramolecular exchange is occurring. Additional cross-peaks are observed between monomer and dimer signals, reflecting the occurrence of the dimerization/dissociation process shown in Scheme 7.

From a ^{119}Sn 2D EXSY study of the three stereoisomers of a binuclear complex it was concluded that interconversion proceeds as shown in Scheme 8, by independent isomerization of the two tin centers.[6] The NMR spectrum shows separate peaks for the ee and aa isomers, and two peaks for the inequivalent Sn nuclei of the ae isomer. With a long t_m of 50 ms, 2D cross-peaks are seen between all pairs of signals, but a spectrum with t_m 5 ms shows that some of these arise indirectly. With this shorter t_m the only cross-peaks are between aa and ae. The expected cross-peaks between ae and ee are too weak to see because the proportion of ee is low. However, the absence of cross-peaks between the two Sn nuclei of the ae isomer is sufficient to prove that these two do not invert simultaneously.

Similar dynamic behavior was reported[75] for isomerization about the pentacoordinate tin atoms in [$CH_3Sn(CH_2CH_2CH_2)_2NCH_3]_2$. The ^{119}Sn 2D EXSY spectrum displays three signals along the diagonal. The major, central signal was assigned to a symmetric isomer, **10** (Scheme 9), and the two less intense flanking signals were assigned to the inequivalent diastereotopic tin atoms of an isomer, **11**, present to 30%. (This structure is reasonable, but a four-coordinate tin cannot be excluded.) At 248 K exchange between these two isomers is indicated by cross-peaks, but there is no cross-peak between the two tin signals of the minor

SCHEME 9. Stereoisomerization in a Pentacoordinate Ditin Complex

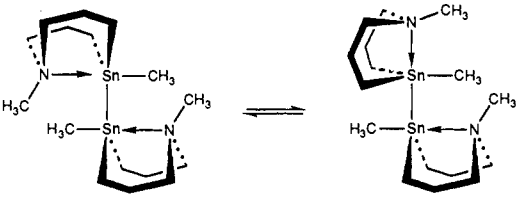

10 11

SCHEME 10. Diastereomerization of η^3-Allylpalladium Chloride Complexes

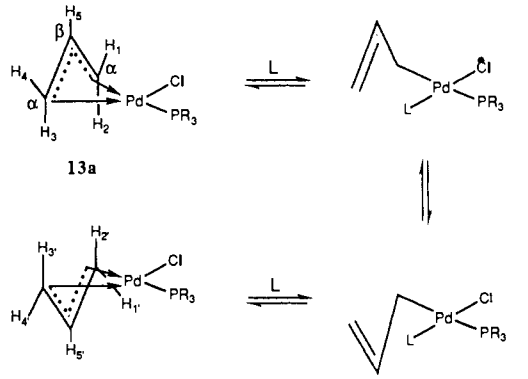

13a 13b

isomer. Therefore, exchange occurs by isomerization at tin, but the two tin atoms of the minor isomer do not interchange simultaneously.

The dynamics of metal–π-allyl complexes[76] have been studied extensively by 2D EXSY. The binuclear species tetra-η^3-allyldichromium, $(\eta^3\text{-}C_3H_5)_4Cr_2$, has one allyl group π-bonded to each chromium, as well as bridging allyl groups trans to each other. The complex occurs as a nearly 1:1 mixture of two diastereomers, one where the nonbridging allyls are cis to each other (**12a**) and the other where they are trans (**12b**). ^{13}C 2D EXSY

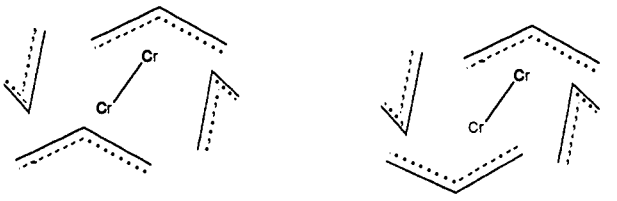

12a 12b

shows that there are two independent stereoisomerizations.[77] One is a topomerization of the cis diastereomer, wherein the inequivalent bridging allyls interchange by a 180° rotation of both of them. The other process is a diastereomerization, interconverting the two diastereomers by a 180° rotation of a nonbridging allyl.

η^3-Allylpalladium chlorides with a chiral phosphine ligand occur as a 1:1 mixture of interconverting diastereomers (Scheme 10). Maintenance of ^{13}C–^{31}P coupling shows that the interconversion of **13a** and **13b** is intramolecular. When the phosphine is *cis*-2,3-diphenyl-1,3-oxaphosphorinane, the proton 2D EXSY spectrum at 298 K shows cross-peaks only between H_1 and $H_{1'}$, H_2 and $H_{2'}$, H_3 and $H_{4'}$, $H_{3'}$ and H_4, and H_5 and $H_{5'}$.[78] These observations can be explained by a $\eta^3 \rightarrow \eta^1$ conversion (assisted by coordination to solvent or to a chloride bridging to another Pd center), followed by rotations about the Pd–C_γ bond and the C_β–C_γ single

bond of the allyl group, and finally an $\eta^1 \rightarrow \eta^3$ conversion. Other processes would not account for the syn/anti isomerization that occurs about C_β–C_γ but does not occur about C_α–C_β. At 330 K many additional cross-peaks appear, as a second process intrudes. For example, H_3 also exchanges with H_1, $H_{1'}$, H_2, $H_{2'}$, $H_{3'}$ (presumed but not resolvable), H_4, and $H_{4'}$, and H_1 exchanges with H_3, $H_{3'}$, H_4, and $H_{4'}$, but not with $H_{1'}$, H_2, or $H_{2'}$. This process is viewed as a topomerization initiated by an $\eta^3 \rightarrow \eta^1$ conversion, which permutes the hydrogens in the sequence ($H_1H_4H_2H_3$) or ($H_{1'}H_{4'}H_{2'}H_{3'}$). However, this mechanism is indistinguishable from cis/trans isomerization via pseudorotation in a five-coordinate intermediate (14, L = solvent

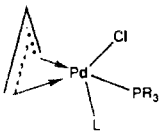

14

or bridging chloride), which exchanges H_1 with H_4, and H_2 with H_3 (or $H_{1'}$ with $H_{4'}$, and $H_{2'}$ with $H_{3'}$). Quantitative 2D EXSY would be useful to establish firmly the pattern of atom interconversions and to evaluate the relative rates of the two processes and how they respond to the size of the phosphine. Qualitatively, complexes with less bulky phosphines, which permit solvent (or bridging chloride) coordination at palladium, do undergo both these stereoisomerizations more rapidly, as judged from the length of the mixing time required to give similar cross-peak patterns. This is consistent with coordination-assisted $\eta^3 \rightarrow \eta^1$ conversion. However, if the high-temperature process involves a five-coordinate intermediate, it should be even more sensitive to steric hindrance.

A remarkable example of the power of 2D EXSY to clarify exchanging systems is its application to $[\eta^2$-$(MeS)_2CHCH(SMe)_2]Cr(CO)_4$.[79] At 20 °C this is present as a 26:74 mixture of cis (**15a**) and trans (**15b**) forms. At −50 °C inversion at sulfur is slow, so that

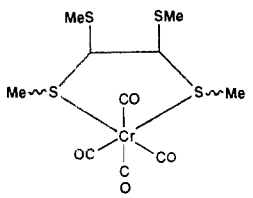

15a

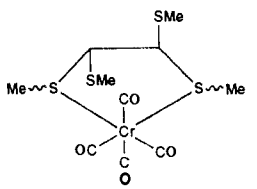

15b

each form is a mixture of invertomers, differing in the stereochemistry at the coordinated *S*-methyls. There are eight *S*-methyl peaks in the ^1H NMR spectrum. A ninth peak shows no cross-peaks in the 2D EXSY spectrum and could be assigned to free ligand present in the sample. The other eight peaks show 2D EXSY cross-peaks due to exchange among the invertomers. From the pattern of cross-peaks and from an estimate of the relative stabilities of the various stereoisomers, it was possible to recognize the exchange pathways and to assign all eight peaks to coordinated or uncoordinated *S*-methyls of four of the six possible stereoisomers. The rate constants for sulfur inversion in each of these were then evaluated by line-shape analysis of the variable-temperature 1D spectrum.

The modes of rearrangement of phenylbis(benzoylacetonato)tin chloride (**16**: R_1, R_2; R_3, R_4 = CH_3, Ph)[20] have been studied by 2D EXSY. The proton 2D

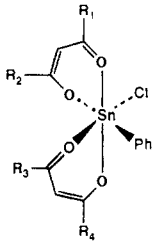

16

spectrum of the methyl region of **16** at 283 K in $CDCl_3$ shows eight signals along the diagonal. These correspond to the methyl groups of the four enantiomeric pairs of diastereomers of **16**. Each methyl shows cross-peaks with three other methyls, although some of these are of poor quality or invisible and only required by the others for the sake of completeness. Each cross-peak corresponds either to a topomerization, which transforms that methyl into the other methyl of that same stereoisomer (or its enantiomer), or to a stereoisomerization that transforms that methyl into one of the two methyls of one of the other three diastereomers. Therefore, there must be exactly three mechanisms operative. From the topological connectivity of the cross-peaks, and from a permutational analysis of possible modes of stereoisomerization,[80] it was concluded that these three mechanisms are three of the four possible Bailar twists (120° rotation of one triangular face of a regular octahedron relative to the opposite face, via a triangular prism), and other alternatives were rejected. This is a fine example of the power of 2D EXSY in chemical kinetics, since the mechanistic conclusions were obtained without the necessity of assigning peaks. Yet this qualitative study cannot guarantee that one cross-peak in each set of three cross-peaks does not arise indirectly. Quantitative 2D EXSY would test this, would provide the relative rates of each of the mechanisms, and would test whether two of the rate constants are identical, as required by the non-self-inverse nature of two of the mechanisms. A chiral probe would also be useful, to verify that the apparent topomerization is actually an enantiomerization.

The chromium complex $Cr(CO)_2(CS)[P(OCH_3)_3]_3$ exists as a mixture of one *fac* and two *mer* stereoisomers. The two *mer* isomers interconvert, as shown in Scheme 11. The ^{31}P NMR spectrum shows a doublet and a triplet for each isomer. The 2D EXSY spectrum at 61 °C shows cross-peaks between all pairs of *mer* peaks, although some involving one of the triplets are too weak to see.[81] This result excludes a mechanism whereby CS and CO ligands interchange by twisting relative to the other four ligands, since that would produce cross-peaks only between doublet and doublet and between triplet and triplet. It was concluded that the mechanism involves a Bailar twist of one triangular face of the octahedron relative to the opposite face. Although this is a reasonable mechanism, the 2D EXSY spectrum is complicated by scalar coupling and possible NOE. These produce cross-peaks between singlets and doublets of the same isomer, and analysis of peak intensities could verify that the cross-peaks between

SCHEME 11. Isomerization in $Cr(CO)_2(CS)[P(OCH_3)_3]_3$

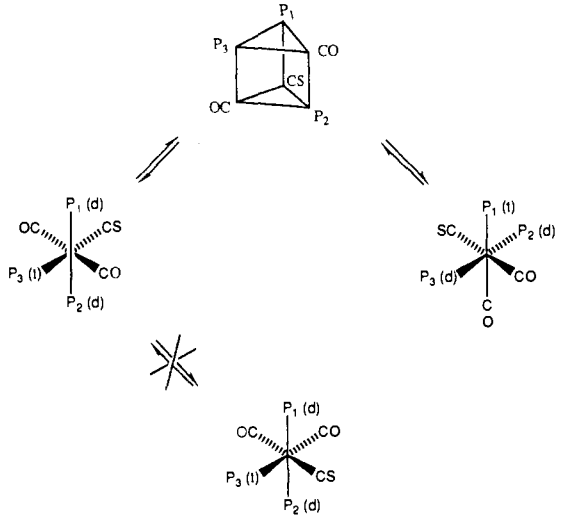

SCHEME 12. Dynamic Equilibria between Dimeric and Monomeric Trichlorostannate–Platinum(II) Complexes

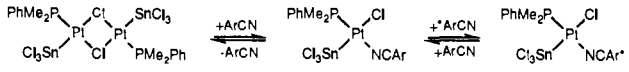

17 18

doublets and triplets of different isomers do not arise indirectly.

The lability of trichlorostannate–platinum(II) complexes useful as hydroformylation catalysts has been investigated by a combination of ^{31}P and ^{19}F 2D NMR.[82] ^{31}P 2D EXSY revealed reaction between the dimeric complex **17** and *p*-fluorobenzonitrile (or benzonitrile) to yield the monomeric complex **18** (Scheme 12). No cross-peaks are seen between ^{195}Pt satellites and the main band of ^{31}P bound to NMR-inactive Pt, eliminating the possibility that the phosphine ligand dissociates from the Pt center during the exchange process. The ^{19}F 2D EXSY spectrum displays a single cross-peak correlating exchange between *p*-fluorobenzonitrile free and coordinated in **18**. This represents evidence for the second exchange process in Scheme 12, although the qualitative data do not exclude indirect exchange, via **17**.

Dissociation of the tin ligand was shown to play a more active role in the exchange resulting from reaction of *cis*- and *trans*-$(R_3P)_2PtCl_2$ (R = *p*-$CH_3C_6H_4$) with $SnCl_2$ (Scheme 13). At 20 °C the proton-decoupled ^{31}P 2D EXSY spectrum shows cross-peaks between the signals of the cis isomer (**19**) and both signals of **20**, but none involving the trans adduct (**21**). Further, the absence of cross-peaks between platinum satellite signals precludes dissociation of the PR_3 ligand as a pathway of exchange. Rather, a direct exchange as shown in Scheme 13 is more likely. In the presence of excess $SnCl_2$ the signal due to **19** is absent and a new signal, assigned as **22**, appears. The 2D spectrum of this solution now reveals cross-peaks indicating exchange between **21** and **22** (Scheme 13), analogous to that between **19** and **20**, plus intramolecular exchange in **20**. This latter is probably due to dissociation of $SnCl_2$, with **19** as intermediate, or else to addition of $SnCl_2$, as in eq 50.

$$cis\text{-}(R_3P)_2PtCl(SnCl_3) + SnCl_2 \rightleftarrows \underset{\mathbf{20}}{} cis\text{-}(R_3P)_2Pt(SnCl_3)_2 \quad (50)$$

SCHEME 13. Exchange Equilibria Involving *cis*- and *trans*-$(R_3P)_2PtCl_2$ (R = *p*-$CH_3C_6H_4$)

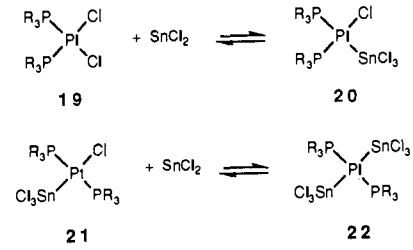

19 20

21 22

The ^1H NMR spectrum of $Pt[\eta^3\text{-}CH_2C(CH_3)CH_2](SnCl_3)(PhCH{=}CH_2)$ (**23**) is complicated by low symmetry and the presence of ^{195}Pt, ^{117}Sn, and ^{119}Sn isotopomers and of two diastereomers. The two diastereomers differ according to which face of $PhCH{=}CH_2$ is coordinated to the Pt. All the peaks could be assigned by various 2D methods. Interconversions of the diastereomers can be detected by 2D EXSY cross-peaks of the π-methallyl methyl and methylene signals.[83] Further cross-peaks are seen between the methyls of each diastereomer and a methyl assigned to $Pt[\eta^3\text{-}CH_2C(CH_3)CH_2](SnCl_3)_3^{2-}$ (**24**). In support of this assignment, the same signal could be enhanced by adding excess $SnCl_3^-$, and the presence of three $SnCl_3$ ligands could be recognized from the relative intensities of the $^{117,119}Sn$ satellites. (This result does not rule out the alternative possibility that the active intermediate under the 2D EXSY condition is $Pt[\eta^3\text{-}CH_2C(CH_3)CH_2](SnCl_3)_2^-$.) Further cross-peaks are seen between the α-CH signals of coordinated $PhCH{=}CH_2$ and free $PhCH{=}CH_2$, either present in trace amounts or added in excess. No cross-peaks are seen between H_1 of **23** and $H_{2'}$ of its diastereomer, between H_3 and $H_{4'}$, or between the corresponding hydrogens of **24**, so that an $\eta^3 \rightarrow \eta^1$ isomerization of the methallyl group, combined with rotation about the $CH_2{=}C(CH_3){-}CH_2Pt$ single bond, is not responsible for the stereoisomerization. Therefore, interchange of the two diastereomers occurs by an intermolecular mechanism (eq 51).

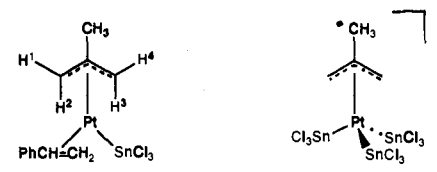

23 24

$$Pt[\eta^3\text{-}CH_2C(CH_3)CH_2](SnCl_3)(PhCH{=}CH_2) + \underset{\mathbf{23}}{} nSnCl_3^- \rightleftarrows Pt[\eta^3\text{-}CH_2C(CH_3)CH_2](SnCl_3)_{n+1}^{n-} + PhCH{=}CH_2 \quad (51)$$

The general applicabilty of 2D EXSY to distinguish intramolecular from intermolecular exchange mechanisms has been demonstrated.[64] The method requires the often encountered situation of an abundant nucleus coupled to another nucleus of low natural abundance. Proton-decoupled ^{31}P 2D NMR was used to confirm the intramolecular ligand exchange in square-planar $(R_3P)_2PtH(SiR'_3)$ (R = cyclohexyl, R' = *p*-$CF_3C_6H_4$) (Scheme 14). The ^{31}P 2D EXSY spectrum of **25** at 298 K displays cross-peaks between the two inequivalent phosphorus nuclei bound to an NMR-inactive platinum.

SCHEME 14. Intramolecular Ligand Exchange in $(R_3P)_2PtH(SiR'_3)$ (R = Cyclohexyl, R' = p-$CF_3C_6H_4$)

25

Additional cross-peaks arise between the phosphorus peaks in the ^{195}Pt isotopomer. The exchange must be intramolecular, since no cross-peaks are seen between ^{31}P resonances of NMR-active and NMR-inactive platinum isotopomers. (Further cross-peaks between doublet components were attributed to chemical exchange, but they are due instead to the complication of ^{195}Pt relaxation.) Similarly, the ethylene exchange process shown in eq 52 leads to 2D EXSY exchange

$$\underset{\mathbf{26}}{(R_3P)_2Pt(\eta^2\text{-}C_2H_4)} \rightleftharpoons \underset{\mathbf{27}}{(R_3P)_2Pt} + C_2H_4 \qquad (52)$$

cross-peaks between ^{31}P resonances of **26** and **27**, but not between resonances of ^{31}P bonded to ^{195}Pt and to an NMR-inactive Pt. (The cross-peaks between the ^{195}Pt isotopomers of **26** and **27** that are visible in the published 2D spectrum correspond to exchange plus ^{195}Pt relaxation, or else the $^1J_{Pt-P}$ coupling constants are of opposite sign in **26** and **27**.) This result suggests direct incorporation and dissociation of ethylene, rather than exchange of ^{31}P between **26** and **27** catalyzed by a trace of R_3P. In contrast, purely intermolecular exchange is seen with $(R_3P)_2HgCl_2$ (R = m-$CH_3C_6H_4$). The ^{31}P 2D EXSY spectrum reveals the dissociation of a phosphine ligand, as indicated by cross-peaks between the ^{31}P signals of phosphines bonded to NMR-inactive mercury and to ^{199}Hg. Although the ^{199}Hg satellites are too weak to be seen in the 2D spectrum, cross-peaks of reasonable intensity are observed as a result of chemical exchange. This example provides an additional application of 2D EXSY, namely, for detecting exchange with a "silent" partner, present only in low concentrations or hidden under other resonances.

C. Biochemical Systems

Exchange networks in some biologically important systems can be traced qualitatively by 2D EXSY. Proton exchange in glutathione (**28**)[85] has been monitored in aqueous solution with suppression of the water signal. At 45 °C, both the cysteine NH and glycine NH

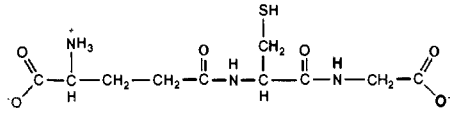

28

exchange, as indicated by ^1H 2D cross-peaks connecting these with H_2O. The 2D intensity ratios, calculated by eq 24 from rate constants determined by saturation-transfer measurements, compare favorably with the experimental ratios. However, no attempt was made to evaluate the rate constants directly from the 2D data.

The study of rotation about amide C–N bonds, as in *N,N*-dimethylacetamide above, has been extended to peptides. Cis/trans isomerization about the peptide bond in aqueous glycylsarcosine (Scheme 15)[86] is evidenced by the ^1H 2D NMR method with spin-locking. This 2D experiment is an extension of a previously described[87] 1D technique. Each peak shows cross-peaks

SCHEME 15. Rotation about the Peptide Bond in Glycylsarcosine

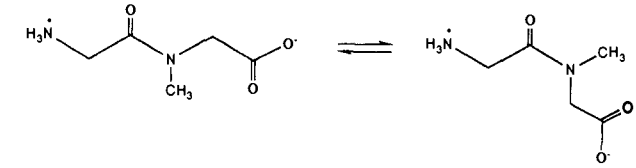

SCHEME 16. Conformational Equilibrium between Boat and Crown Forms of *cyclo*[Pro-NBGly$_2$]

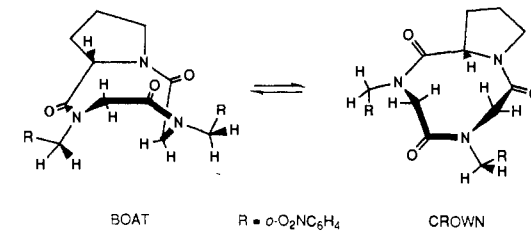

with the corresponding peak of the stereoisomer.

Cis/trans isomerization about the Gly–Pro peptide bond of the pentapeptide *cyclo*([^{15}N]Gly-D-Pro-Gly-[^{15}N]-L-Ala-D-Pro) has been evidenced by ^{15}N 2D NMR.[88] Chemical exchange resulting from interconversion of the minor (cis) and major (trans) [^{15}N]Gly-Pro conformers is indicated by cross-peaks connecting the two glycinamide nitrogen resonances.

The pentapeptide (carbobenzyloxy)glycyl-L-prolyl-L-leucyl-L-alanyl-L-proline can exist as four isomeric forms owing to cis and trans configurations with respect to the Gly–Pro and Ala–Pro peptide bonds. ^{13}C chemical shift measurements are consistent with the assignments of the major isomer as trans,trans and a second isomer as cis,trans (with the terminal proline trans). Interconversion between these two isomers was detected by ^1H 2D EXSY.[89] In the NH region of the spectrum, which is relatively free of overlap, cross-peaks are observed that connect NH resonances of like amino acids in the different isomers.

Interconversion between two conformational isomers of the cyclic tripeptide *cyclo*[Pro-NBGly$_2$] (Scheme 16), where NBGly = *N*-(*o*-nitrobenzyl)glycyl, was detected by ^1H 2D SECSY.[90] The 1D spectrum in $CDCl_3$ solution is quite complex with many overlapping signals due to boat and crown conformers in ratio 20:80. The ring-inversion process that interconverts the two conformers was observed in the 2D exchange spectrum at 58 °C. Cross-peaks are seen between the proline α-hydrogens of the two conformers, between each set of diastereotopic α-hydrogens and the corresponding α-hydrogen of the other conformer, and between each of the four diastereotopic benzyl hydrogens and the corresponding hydrogen of the other conformer. It is readily seen that the low-field hydrogen of each AB system exchanges with the high-field hydrogen of the AB system of the other conformer.

Proton-detected heteronuclear correlation spectroscopy has been applied to the reorientation process that interchanges the ϵ_1 and ϵ_2 protons of the Tyr-35 side chain of basic pancreatic trypsin inhibitor (BPTI, **29**).[53] The method involves a complicated pulse sequence that requires a weakly coupled two-spin system. In this case the spins were the aromatic ^1H–^{13}C of the tyrosine ring. Two pulse sequences were developed, depending on whether both spins undergo exchange or only one does. Either pulse sequence produces direct peaks as well as

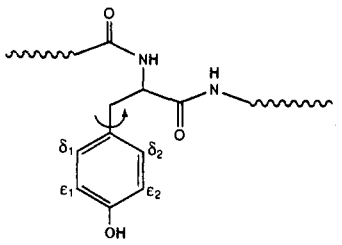

29

exchange cross-peaks associated with phenyl rotation during the mixing time.

The exchange of sodium ions across a membrane has been detected with ^{23}Na 2D NMR.[91] The 2D spectra were obtained with use of aqueous NaCl in a suspension of vesicles, with dysprosium ion to shift the resonance of extravesicular Na^+. In the absence of the ion channel monensin, the ^{23}Na spectrum shows only diagonal peaks corresponding to intra- and extravesicular Na^+. When a micromolar amount of monensin was added to the sample, the 2D spectrum displayed cross-peaks between the internal and external Na^+ signals, showing that monensin permits Na^+ exchange across the membrane. Rate constants for exchange were evaluated by magnetization transfer, and it was suggested that the 2D method could also be used for quantitative kinetics.

A particularly unusual example is the creatine phosphokinase catalyzed transfer of a phosphate group from ATP to creatine (eq 53) in perfused rat heart.[92] The observation of only one pair of cross-peaks in the ^{31}P 2D spectrum indicates exchange between phosphocreatine and ATP.

$$\text{ATP} + \text{creatine} \rightleftarrows \text{ADP} + \text{P-creatine} \quad (53)$$

Exchange in a multisite system has been mapped out with 2D accordion spectroscopy.[31] The adenylate kinase catalyzed exchange of phosphate among the nucleotides AMP, ADP, and ATP was observed via ^{31}P 2D EXSY.[93] Cross-peaks were seen among AMP, αADP, and αATP and among βATP, βATP, and γATP, although those between AMP and αATP and between βATP and γATP are indirect.

Use of 2D EXSY has been made in assigning signals of biological macromolecules, such as the reduced and oxidized forms of cytochrome *c*. The Fe(III) form is paramagnetic, with a well-dispersed ^1H NMR spectrum, much of which can be assigned. Intermolecular electron transfer between the Fe(III) and Fe(II) forms is fast enough to be detected by 2D EXSY, especially at high ionic strength, where it dominates any contribution from cross-relaxation. The cross-peaks then allowed cross-correlation of methyl peaks of leucines and isoleucines of the Fe(II) form.[5] This approach is also applicable to cytochrome c_3.[94] There are four hemes per molecule, and it is possible to prepare a sample at an intermediate level of oxidation. Within each cytochrome c_3, electron transfer is fast and intermolecular exchange leads to cross-peaks between Fe^{III}_2,Fe^{II}_2 and Fe^{III}_3,Fe^{II} species or between Fe^{III}_3,Fe^{II} and Fe^{III}_4 species. These cross-peaks, in the 15–30 ppm region, were used to cross-correlate the assignments of heme methyls.

IV. Quantitative Applications

We next consider the quantitative applications of 2D EXSY. All early examples had been qualitative, using the existence of cross-peaks to map out exchange pathways. More recently quantitative treatment has been possible. The emphasis of this review is on the quantitative applications. In obtaining a 2D NMR spectrum, it is not that much more difficult to obtain meaningful intensities and convert them into rate constants. Certainly the quantitative approach guards against the risk of mistaking indirect cross-peaks for direct exchange pathways.

TABLE 3. Rate Constants (s^{-1}) for Acid-Catalyzed Proton Exchange in Acrylamide and Thioacetamide at 22 °C

	acrylamide[a]		thioacetamide[b]
	2D NMR	saturation transfer	2D NMR
k_{EZ}	2.5	2.5 ± 0.5	<0.14
k_{ZE}	2.2	2.5 ± 0.5	<0.15
k_{ZS}	2.5	3.1 ± 0.5	0.55
k_{ES}	4.9	4.6 ± 0.5	0.54
k_{SE}	0.51	0.43 ± 0.05	0.038
k_{SZ}	0.39	0.34 ± 0.05	0.038

[a] In ethylene glycol. [b] In glycerol–DMSO-d_6.

A. Organic Systems

Proton transfers offer particularly interesting examples of reactions that are amenable to study by 2D EXSY. Proton exchange in amides has been studied extensively by 1D NMR techniques.[95] The acid-catalyzed NH proton exchange in amides occurs by two possible pathways: The N-protonation mechanism (eq 54) proceeds via the high-energy intermediate

$$\text{RCONHR}' + \text{H}^+ \rightleftarrows \text{RCONH}_2^+\text{R}' \quad (54)$$

$RCONH_2^+R'$, in which deprotonation is competitive with rotation about the C–N single bond.[96] The second possible pathway for acid-catalyzed exchange proceeds via O-protonation and the imidic acid (eq 55). In

$$\text{RCONHR}' + \text{H}^+ \rightleftarrows \text{RC(OH)=NHR}'^+ \rightleftarrows \text{RC(OH)=NR}' + \text{H}^+ \quad (55)$$

primary amides (**30**) these two mechanisms can be

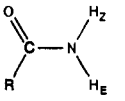

30

distinguished because the N-protonation mechanism requires that intramolecular exchange (H_E with H_Z) occur along with intermolecular exchange (H_E or H_Z with H_2O), whereas no intramolecular exchange is possible via the imidic acid. Such a distinction necessitates site to site rate constants and is not possible by line-shape analysis.

The applicability of quantitative 2D EXSY methods to obtain mechanistic information from multisite kinetics was demonstrated in the investigation of proton exchange in primary amides.[19] This was the first use of pure absorption mode spectra to obtain reliable 2D intensities for kinetics. Figure 8 shows the 2D EXSY spectrum of acrylamide in ethylene glycol solvent under conditions of acid catalysis. The results are shown in Table 3. The exchange rates obtained for acrylamide by ^1H 2D EXSY agree nicely with those previously determined by saturation transfer.[95g] These rate con-

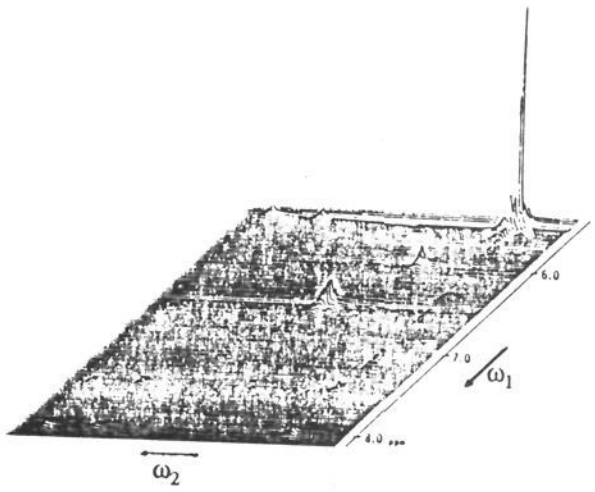

Figure 8. ^{1}H 2D pure absorption phase spectrum of acrylamide in ethylene glycol at measured pH 1.75. The peaks along the diagonal, from bottom left to top right, are H_E, H_Z, CH (vinylics), CH (vinylic), and H_S (OH of solvent); CH_2 of solvent is off-scale. Reprinted from ref 19. Copyright 1984 American Chemical Society.

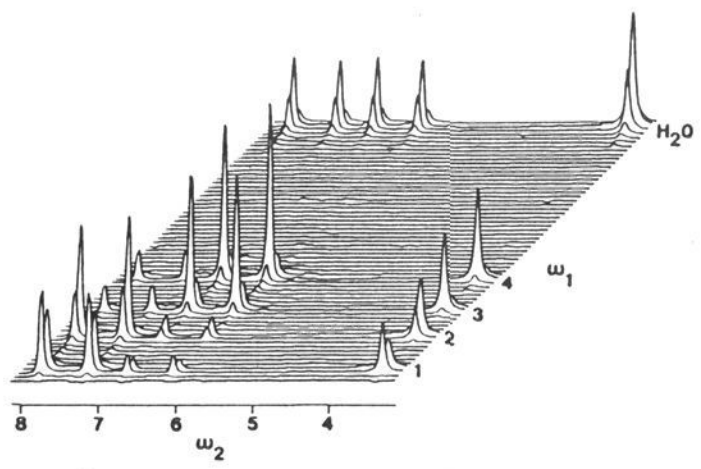

Figure 9. ^{1}H 2D EXSY spectrum of [^{15}N]acetamide in acidified aqueous DMSO-d_6. The sites labeled 1, 3 and 2, 4 correspond to H_E and H_Z, respectively, split by coupling to ^{15}N. Reprinted from ref 97. Copyright 1986 Academic Press.

stants show that within experimental error $k_{ZS} = k_{ZE}$ and $k_{ZS} < k_{ES}$. These results confirm the N-protonation mechanism for acid-catalyzed exchange in acrylamide, and they are inconsistent with the imidic acid mechanism. Further, the faster exchange of H_E shows that $RCONH_3^+$ is so strong an acid that it does not live long enough to achieve rotational equilibrium about the C–N single bond.

The acid-catalyzed exchange rates of thioacetamide (**31**) were also obtained by 2D NMR.[19] This is a system that could not be studied by saturation transfer, since

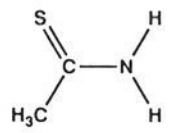

31

the NH peaks are too close to each other. The absence of EZ and ZE cross-peaks suggested that there is no intramolecular exchange, but it was necessary to be quantitative. It is clear from the data in Table 3 that the intramolecular rate constants k_{EZ} and k_{ZE} are indeed significantly less than the intermolecular rate constant k_{ZS} (or k_{ES}). This result is strong evident for the imidic acid mechanism and is inconsistent with N-protonation.

The proton-exchange kinetics of [^{15}N]acetamide in wet DMSO-d_6 were reinvestigated[97] by the 2D EXSY method, with the TPPI technique to obtain pure absorption mode spectra. The ^{1}H 2D spectrum (Figure 9) shows five diagonal peaks, one for water and four for ^{15}N-coupled doublets of both H_E and H_Z, plus cross-

TABLE 4. Rate Constants (s^{-1}) for Acid-Catalyzed Proton Exchange in [^{15}N]Acetamide and 2,4,6-Trimethylbenzamide by 2D NMR

	[^{15}N]acetamide	2,4,6-trimethylbenzamide
k_{EZ}	2.73[a]	0
k_{ZE}	2.80[a]	0
k_{EZ}	0.86	0.6
k_{SE}	0.65	
k_{ZS}	0.66	1.2
k_{SZ}	0.38	

[a] Includes uncatalyzed exchange with $k = 2.1$ s^{-1}.

TABLE 5. Rate constants (s^{-1}) for Proton Exchange in the 1-Cyclohexyluracil (U)–9-Ethyladenine (A)–Water (W) System

ij	k_{ij}	ij	k_{ij}	ij	k_{ij}
UA	1.26	AU	0.49	WU	1.77
UW	4.72	AW	0.30	WA	0.18

TABLE 6. Rate Constants (s^{-1}) for Hindered Rotation in $CF_3CONCH_3(CH_2C_5H_5)$ by 2D NMR

T, K	k	T, K	k
308.2	0.27	333.2	4.5
313.2	0.47	343.2	17.2
323.2	1.0		

peaks between all pairs. Use of eq 26 shows that some of these arise from ^{15}N relaxation and from indirect exchange. Table 4 lists the rate constants, which agree nicely with those determined previously by saturation transfer and line broadening.[95g] By the same reasoning as above, these rate constants show that acid-catalyzed exchange in [^{15}N]acetamide proceeds via the N-protonation mechanism. The mechanism of proton exchange in 2,4,6-trimethylbenzamide was also reinvestigated.[97] The rate constants for acid-catalyzed exchange are included in Table 4. The absence of intramolecular exchange is again evidence for the imidic acid mechanism, via 2,4,6-$(CH_3)_3C_6H_2C(OH)$=NH, rather than the N-protonation mechanism that had been proposed.[98] The further observation that H_Z exchanges with solvent faster than does H_E is also in agreement with the imidic acid mechanism.

Direct exchange between the imino proton of 1-cyclohexyluracil (**32**, R = cyclohexyl) and the amino proton of 9-ethyladenine (**33**), as well as exchange of each NH with water (in wet DMSO-d_6 solution) was measured by ^{1}H 2D EXSY.[37] Exchange among all sites

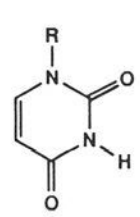

32

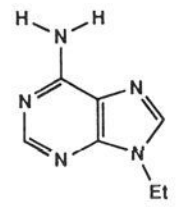

33

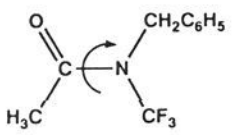

34

was evident by the observation of all possible cross-peaks connecting the uracil NH, adenine NH_2, and water OH signals. The rate constants obtained by analysis of the spectral intensities are presented in Table 5 and agree with those evaluated by 1D methods. A reasonable mechanism for the direct NH exchange involves double proton transfer catalyzed by unstable tautomers of the substrates.

Additional kinetic processes that lend themselves to study by quantitative 2D EXSY are hindered rotation and inversion. Rate constants for the rotation about

TABLE 7. Rate Constants (s^{-1}) for Ring Inversion in *cis*-Decalin by Accordion Spectroscopy

T, K	k	T, K	k
210	0.2	230	4
220	0.9	240	13

TABLE 8. Rate Constants (s^{-1}) for Degenerate Rearrangement of the 2-Methyl-2-norbornyl Cation by 2D NMR

T, K	k	T, K	k
200	2.05	210	4.50
205	3.05	215	8.3

the amide C–N bond in *N*-benzyl-*N*-(trifluoromethyl)acetamide (**34**) were determined by ^{19}F 2D NMR.[99] These rate constants, given in Table 6, were found to compare favorably with values determined by both ^{1}H and ^{19}F line-shape and saturation-transfer methods. A value of $\Delta G^{\ddagger} = 103.2 \pm 8.5$ kJ/mol was obtained for the barrier to hindered rotation in **34**.

Ring-inversion rates for decalin (a mixture of **35a** (cis) + **35b** (trans)) have been measured[31] by ^{13}C accordion spectroscopy. Cross-peaks are seen only for peaks assigned to *cis*-decalin, since *trans*-decalin is stereochemically rigid. The rate constant for ring inversion in

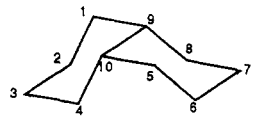

35a

35b

cis-decalin was obtained from the line widths of sums and differences of 2D peaks. The temperature dependence of the rates is displayed in Table 7.

A study of the interconversion of acetaldehyde, CH_3CHO, and its hydrate, $CH_3CH(OH)_2$, by quantitative ^{1}H 2D EXSY[26] gave rate constants in good agreement with those obtained by inversion transfer. At 37 °C in pH 7.4 0.1 M phosphate buffer k(hydration) = 0.38 ± 0.05 s^{-1} and k(dehydration) = 0.28 ± 0.05 s^{-1}.

Although the 2-methyl-2-norbornyl cation had been thought to be static, deuterium labeling shows exchange between $H_{3,exo}$ and $H_{3,endo}$. The proposed mechanism is shown in Scheme 17.[100] The ^{13}C 2D spectrum clearly shows exchange between C_1 and C_6 as well as between C_5 and C_7, but none involving C_2 or C_3. The cross-peak information provided conclusive support for the proposed mechanism. Further, rate constants were extracted from the 2D spectrum. The rate data are given in Table 8. Inexplicably, the values obtained by 2D EXSY are systematically ca. 30% lower than those determined by 1D magnetization transfer.

Stereoisomerization in 1,3-bridged cyclooctatetraenes can proceed via ring inversion or a bond-shifting mechanism. The dynamics of these rapid processes have been probed and quantitated by ^{1}H and ^{13}C 2D EXSY.[101] A series of (1,3)cyclooctatetraenophanes (**36**)

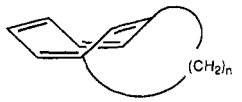

36a n=7
b n=8
c n=9

were prepared and studied. Scheme 18 presents the two pathways. It is apparent that the allylic protons can

SCHEME 17. Rearrangement of the 2-Methyl-2-norbornyl Cation

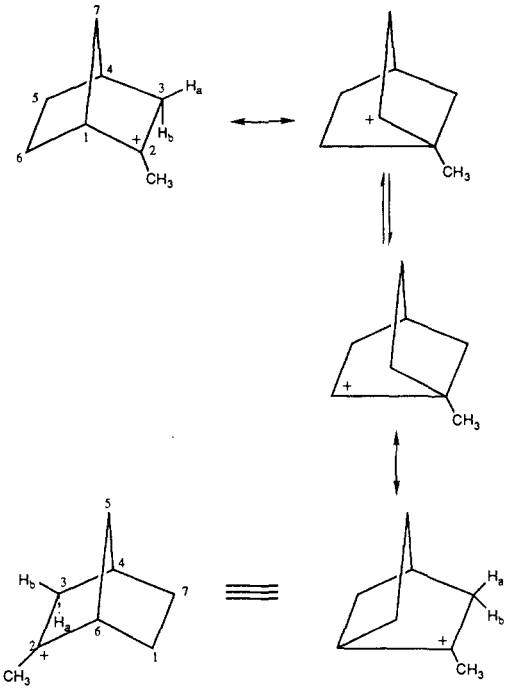

SCHEME 18. Bond Shifting and Ring Inversion Pathways in (1,3)Cyclooctatetraenophane

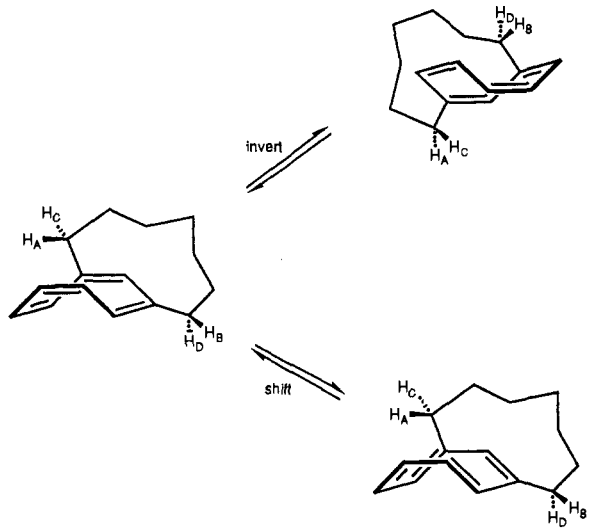

be used to distinguish between the two possible routes by NMR. Ring inversion exchanges geminal protons H_A with H_C and H_B with H_D. In contrast, bond shifting results simply in an exchange of environments of the methylene protons or carbons. For annulene (**36a**) the NMR spectrum contains four diagonal signals corresponding to each of the four allylic protons. To suppress cross-peaks due to scalar coupling, an additional 180° pulse was inserted at random during the mixing time. The 2D EXSY spectra of **36a** at various temperatures are shown in Figure 10. Below 310 K cross-peaks arise only between individual pairs of allylic proton signals, indicating that only ring inversion occurs in this temperature range. The higher temperature spectrum, at 315 K, displays cross-peaks connecting all methylene proton sites. This result implies that both ring inversion and bond shifting are operative. Integration of the ^{1}H 2D spectra allowed rate constants for ring inversion to be extracted, while those for bond

TABLE 9. Activation Parameters for Ring Inversion and Bond Shifting in 36a, 36b, and 36c

	ring inversion[a]			bond shifting[b]		
	36a	36b	36c	36a	36b	36c
E_a, kcal mol^{-1}	12.5	16.2	19.3	16.7	16.2	22.7
$\Delta H^{\ddagger}$, kcal mol^{-1}	12.0 ± 0.7	15.7 ± 0.5	18.7 ± 0.4	15.9 ± 0.8	15.7 ± 0.9	22.0 ± 0.4
$\Delta S^{\ddagger}$, eu	−14.0 ± 2.5	2.2 ± 1.7	1.9 ± 1.4	−6.7 ± 2.4	−9.4 ± 2.9	7.7 ± 1.4
ΔG_{298}, kcal mol^{-1}	16.22 ± 0.11	16.35 ± 0.05	18.09 ± 0.03	17.87 ± 0.05	18.40 ± 0.07	19.76 ± 0.03

[a] ^{1}H 2D EXSY in CD_2Cl_2 solution. [b] ^{13}C 2D EXSY in toluene-d_8 solution.

TABLE 10. Rate Constants (s^{-1}) for the Nitrosobenzene Monomer–Dimer Exchange

T, °C	cis dimer → monomer	trans dimer → monomer	trans → cis dimer
−10	0.14 ± 0.01	0.02 ± 0.02	0.001 ± 0.02
0	0.61 ± 0.04	0.08 ± 0.05	0.08 ± 0.07
10	2.67 ± 0.25	0.40 ± 0.18	0.1 ± 0.2
20	9.6 ± 1	1.9 ± 1.0	−0.2 ± 1.5

shifting were evaluated with the ^{13}C 2D spectra of the allylic carbon atoms. Similar analyses were performed for **36b** and **36c**. The rate data are shown in Table 9.

Nitrosobenzene represents an interesting three-site system.[102] Quantitative ^{13}C 2D EXSY was used to measure the rates of exchange among the monomer (**37a**) and cis and trans dimers (**37b**, **37c**). The 2D ^{13}C

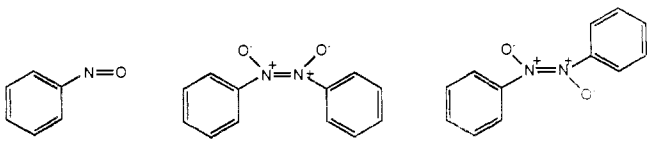

37a **37b** **37c**

spectrum in $CDCl_3$ at 10 °C shows all the aromatic signals for monomer and both dimer species. In the region of the ortho carbon resonances, exchange is manifested by the presence of cross-peaks between all pairs of species. However, it is necessary to analyze the signal intensities quantitatively with eq 24 in order to evaluate the site to site rate constants. These rate constants are presented in Table 10. The rate constant for direct cis/trans interconversion is zero, within experimental uncertainty. Therefore, the cross-peaks between cis and trans dimers arise only indirectly, via the monomer. This result is reasonable, as it implies the absence of any internal rotation about the N–N double bond in the dimers. Rather, the result indicates that cis/trans interconversion proceeds exclusively via dissociation to the monomer.

B. Inorganic and Organometallic Systems

In a detailed study of proton exchange in the ammonium ion, quantitative 2D EXSY was used.[63] The major pathway of base-catalyzed exchange involves the conjugate base ammonia (eq 56).[103] The 2D EXSY

$$NH_4^+ + N'H_3 \rightleftharpoons NH_3 + N'H_4^+ \qquad (56)$$

investigation was carried out with ^{15}N-labeled ammonium nitrate in an optimized solvent mixture of D_2O and H_2O. In this mixture the ammonium ion exists as the five isotopomers $^{15}NH_4^+$, $^{15}NH_3D^+$, $^{15}NH_2D_2^+$, $^{15}NHD_3^+$, and $^{15}ND_4^+$, four of which are distinguishable by proton NMR with deuterium decoupling. Base-catalyzed exchange is observed even near pH 1, and exchange among all isotopomer sites is detected as cross-peaks connecting each pair of species. Exchange with water also occurs and is detected as cross-peaks connecting each ammonium ion species with the water signal. Figure 11 shows the NH region of the pure absorption mode 2D spectrum. The peak heights for each of the 56 cross-peaks, along with the relative site populations, were symmetrized and analyzed by eq 26. The resulting rate and relaxation matrix **R** is displayed in Table 11. The second-order rate constant for NH_3-catalyzed exchange was determined using the individual NH_mD_{3-m} concentrations and the 44 pseudo-first-order rate constants more than once removed from the diagonal. A value of 1.65×10^8 M^{-1} s^{-1}/proton was obtained. The six pairs of rate constants that lie adjacent to the diagonal of **R** contain kinetic information from both NH_3- and H_2O-catalyzed exchange, as affected by any kinetic isotope effects resulting from the difference between deuterium and hydrogen. From 12 independent estimates of the isotope effect a value of $k_H/k_D = 1.56 \pm 0.09$ was calculated for the reaction of eq 56. This is the first example of a kinetic isotope effect for an exchange reaction determined directly in the isotopic mixture, and it is possible only through 2D EXSY.

A wide range of probe nuclei has been used to acquire 2D EXSY spectra. A particularly powerful application of quantitative 2D EXSY extends the scope of nuclei to include ^{119}Sn.[22b] Equimolar amounts of tin(IV) tetrachloride and tin(IV) tetrabromide were mixed in order to measure the rates of intermolecular halide

TABLE 11. Rate and Relaxation Matrix Containing Site to Site Rate Constants for Exchange in $^{15}NH_4^+$

$$NH_nD_{4-n}^+ \rightarrow NH_mD_{4-m}^+$$

	n								
m	1	2	3	4	1	2	3	4	H_2O
1	6.14	0.871	0.105	0.100	0.129	0.028	0.051	0.005	0.025
2	2.239	6.28	1.785	0.346	0.143	0.175	0.146	0.210	0.077
3	0.301	1.983	6.30	2.466	0.280	0.151	0.130	0.300	0.080
4	0.129	0.173	1.110	6.48	0.00	0.121	0.144	0.060	0.028
1	0.129	0.056	0.098	0.00	6.32	0.912	0.205	0.00	0.025
2	0.072	0.175	0.136	0.243	2.345	6.21	1.639	0.593	0.077
3	0.146	0.162	0.130	0.321	0.585	1.821	5.92	2.862	0.080
4	0.006	0.094	0.120	0.051	0.00	0.263	1.145	6.77	0.028
H_2O	0.70	0.70	0.70	0.70	0.70	0.70	0.70	0.70	

TABLE 12. Rate Constants (s^{-1}) for Intermolecular Halide Scrambling in a 1:1 Mixture of $SnCl_4$ and $SnBr_4$

A	B	k_{AB}	k_{BA}
$SnCl_4$	$SnCl_3Br$	39	10
$SnCl_3Br$	$SnCl_2Br_2$	12	9
$SnCl_2Br_2$	$SnClBr_3$	4	6
$SnClBr_3$	$SnBr_4$	1	6

SCHEME 19. Intermolecular Halide Exchange in $SnCl_4Br_{4-n}$

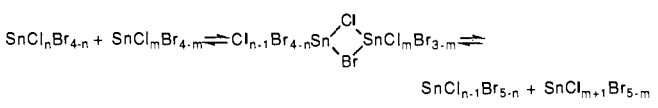

scrambling among five distinguishable $SnCl_nBr_{4-n}$ species. Figure 12 shows the 2D EXSY spectrum for a 1:1 mixture of $SnCl_4$ plus $SnBr_4$. Although there are cross-peaks between all pairs of signals, some arise indirectly. This can be recognized by an induction period in the buildup of cross-peak intensity. The site to site rate constants could be evaluated by fitting the t_m dependence of cross-peak volumes to eq 25. It was found that only one halide is exchanged per step, and there is no direct exchange between $SnCl_nBr_{4-n}$ and $SnCl_{n\pm2}Br_{4-n\mp2}$, etc. Table 12 shows the forward and reverse rate constants for exchange. The data are consistent with a mechanism whereby transfer proceeds in a concerted fashion via a symmetrical, four-center transition state (Scheme 19). From the data in Table 12 it is apparent that the rate constants for reaction of $SnClBr_3 \rightarrow SnBr_4$ are significantly lower than those for $SnCl_4 \rightarrow SnCl_3Br$. These results are rationalized in terms of steric retardation by the bulkier bromine atoms. One alternative mechanism that was not addressed in the original account, yet cannot be ruled out on the basis of the data presented, is catalysis by X^- (eq 57).

$$SnCl_nBr_{4-n} + Cl^- \rightleftarrows SnCl_{n+1}Br_{4-n}^- \rightleftarrows SnCl_{n+1}Br_{3-n} + Br^- \quad (57)$$

Two-dimensional ^{29}Si EXSY has been used to reveal silicate anion exchange pathways in ^{29}Si-enriched potassium silicate solutions.[104] Peaks could be assigned to monomer (Q^0), dimer (Q_2^1), cyclic trimer (Q_3^2), linear trimer ($Q_2^1Q^2$), cyclic tetramer (Q_4^2), and prismatic hexamer (Q_6^3), where the superscript designates the number of attached siloxy groups. At 22 °C and 0.5 M 2:1 (K:Si) potassium silicate, the ^{29}Si 2D EXSY spectrum displays four sets of crosspeaks between Q^0 and Q_2^1, between Q_3^2 and the Q^1 end groups of $Q_2^1Q^2$, between Q_3^2 and the central Q^2 of $Q_2^1Q^2$, and between Q^1 end groups and the central Q^2 of $Q_2^1Q^2$. The first set is due to dimerization of the monomer and dissociation of the dimer. The next two are due to cyclization of the linear trimer and ring opening of the cyclic trimer. The fourth set of cross-peaks is probably not due to direct exchange. Although the expected dependence on mixing time was not verified, no one-step mechanism is reasonable. Instead this may be attributed to an indirect two-step cyclization of the linear trimer followed by reopening at a different Si–Si linkage. There is one additional weak cross-peak between Q^0 and the Q^1 end groups of an otherwise undetectable species, and this may represent addition of monomer to some reactive oligomer. With a mixing time of 0.5 s no cross-peaks involving Q_1^2 or Q_6^3 were seen, so these species are inert on this time scale. The 2D EXSY spectrum provided the first unequivocal evidence that the cyclic trimer is indeed a key intermediate in the silicate anion-exchange process.

SCHEME 20. Rotational Isomerization in $[Mo(CO)(HC{\equiv}CR)_2(Cp)]^+$

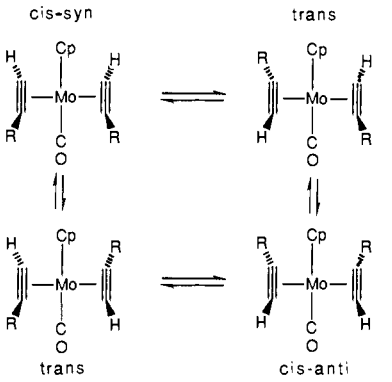

TABLE 13. Rate Constants (s^{-1}) for Stereoisomerization in $[Mo(CO)(HC{=}CR)_2(Cp)]^+$

R	T, K	k(trans → cis-syn)	k(trans → cis-anti)	k(cis-syn → trans)	k(cis-anti → trans)
Ph	323	13.6 ± 0.8		16.8 ± 2.4	
CO_2Me	300		1.1		1.6
	313		3.4		4.2
Me	333	5.1 ± 0.9	2.3 ± 1.2	6.2 ± 1.3	4.3 ± 3.4

A second ^{29}Si 2D EXSY spectrum was acquired on a 1.5 M 1:1 (K:Si) potassium silicate solution at 22 °C. The lower pH in this sample accelerates silicate anion interconversions and increases the degree of polymerization. These effects were manifested in the 2D EXSY spectrum by the appearance of more numerous crosspeaks and by broadening of the resonances.[104] Besides the processes described above, additional processes that could be recognized were formation and dissociation of the linear trimer, addition of monomer to one of the vertices of the cyclic trimer, formation and dissociation of the linear tetramer, and reactions of a bicyclic pentamer.

The rates of stereoisomerization in pseudotetrahedral $[Mo(CO)(HC{\equiv}CR)_2(Cp)]^+$ (R = tBu, Ph, CO_2Me, Me) were measured[105] by quantitative ^1H 2D EXSY. These are present as two cis isomers and a *dl* pair of trans isomers (Scheme 20). There is no cross-peak between the two cis isomers or between the diastereotopic hydrogens of the trans isomer, so that the mechanism involves independent rotations of the two alkynes. The site to site rate constants obtained in this study were converted to macroscopic rate constants for isomerization. Table 13 presents these values and the associated errors. The equilibrium constant derived from the rate data is in fair agreement with that obtained by direct integration of the 1D spectrum.

The solution dynamics of a series of lanthanide(III) complexes of diethylenetriaminepentaacetate (DTPA, $^-O_2CCH_2N[CH_2CH_2N(CH_2CO_2^-)_2]_2$) in D_2O were investigated by ^1H 2D EXSY methods.[106] The structure of these complexes is a capped square antiprism, illustrated in Scheme 21. The 1D spectrum shows 18 peaks spread over ca. 100 ppm by the paramagnetic lanthanide shift. At higher temperature these coalesce to nine peaks. Signals were assigned by partial deuteration, by COSY spectroscopy, and by comparison of

SCHEME 21. Conformational Rearrangement in the Square Antiprism Ln(DPTA)$^{2-}$ [a]

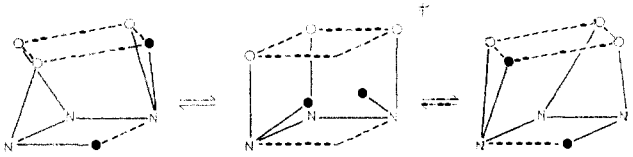

[a] Solid lines designate two-atom links. The metal and one water molecule at the top have been omitted.

SCHEME 22. Interconversion between Meso and *dl* Forms of $Me_3PtX(MeSCH_2CH_2SMe)$

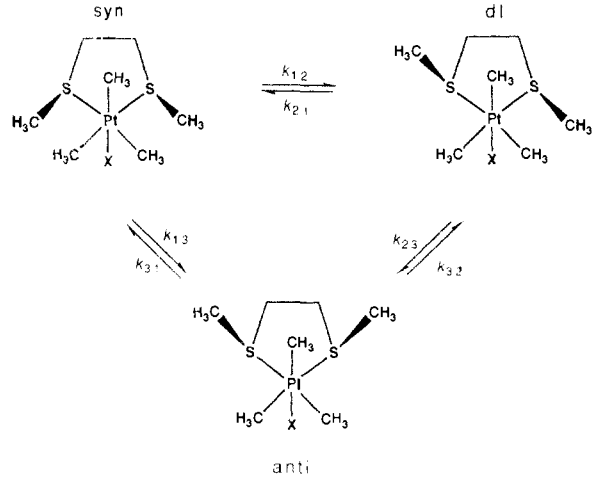

chemical shifts with those calculated from the crystal structure of NdDTPA. The 2D spectrum shows up to nine pairs of cross-peaks. The dynamic process is an enantiomerization (Scheme 21), which replaces a carboxylate in the base of the square antiprism with one from the opposite end of the ligand, thereby interchanging CH_2 groups (and interchanging the diastereotopic hydrogens of the CH_2 of the central $CH_2CO_2^-$ with each other). A short mixing time around 1 ms was used, since T_1 is quite short for these paramagnetic species; the temperature was adjusted to keep the rate constant greater than T_1^{-1}. Pure absorption mode spectra were obtained, and peak volumes were approximated by the volume of a frustum of a cone cut by two contour levels. For $PrDTPA^{2-}$ at 5 °C the rate constant is 265 s^{-1}. At higher temperatures the rate constants were evaluated from the coalescence behavior in 1D spectra. This 1D method was also used for $EuDTPA^{2-}$ and $YbDTPA^{2-}$, where the shorter T_1 precludes clear resolution of all nine 2D cross-peaks. However, the 2D method was quite useful for correlating the exchanging peaks in this system where the coalescence temperature varies widely. For each complex all rate constants fit on a single Eyring plot, so that only one stereochemical process is operative. Moreover, this process involves the central $CH_2CO_2^-$, which had been suggested as uncoordinated.

Low-temperature ^{195}Pt studies[107] show that octahedral complex $Me_3PtX(MeSCH_2CH_2SMe)$ exists as two meso forms (syn, anti) and a *dl* pair (Scheme 22). All are of *fac* stereochemistry, with three heteroatoms mutually cis. The observed rate data for the interconversions are given in Table 14.[25] Although cross-peaks are seen between the two meso forms, these arise only indirectly, and the rate constant k_{13} or k_{31} for double sulfur inversion is zero, within experimental error.

TABLE 14. Rate Constants (s^{-1}) for Sulfur Inversion in $Me_3PtX(MeSCH_2CH_2SMe)$

T, K	k_{12}	k_{23}	10^3k_{13}
	X = I		
233	0.036 ± 0.008	0.032 ± 0.005	4 ± 5
243	0.13 ± 0.01	0.12 ± 0.01	16 ± 27
253	0.52 ± 0.03	0.50 ± 0.03	4 ± 40
263	1.46 ± 0.10	1.47 ± 0.12	−50 ± 100
273	4.3 ± 0.27	4.2 ± 0.38	100 ± 300
283	11.3 ± 1.2	9.9 ± 2.0	50 ± 1200
	X = Cl		
243	0.11 ± 0.02	0.21 ± 0.60	12 ± 70
253	0.39 ± 0.04	0.54 ± 0.35	64 ± 100

TABLE 15. Activation Parameters Derived from the ^{195}Pt 2D EXSY Spectrum of $[Me_3PtI(MeSCH_2CH_2SEt)]$

parameter	cis-syn → trans-anti	cis-anti → trans-syn	cis-syn → trans-syn	trans-anti → cis-anti
$\Delta G^{\ddagger}$(25 °C), kJ mol^{-1}	61.1	58.2	64.4	65.4
$\Delta H^{\ddagger}$, kJ mol^{-1}	63.0	64.3	65.8	57.9
$\Delta S^{\ddagger}$, J K^{-1} mol^{-1}	6.4	20.3	4.8	−24.9

SCHEME 23. Sulfur Inversion Processes among Invertomers of $Me_3PtI(MeSCH_2CH_2SEt)$

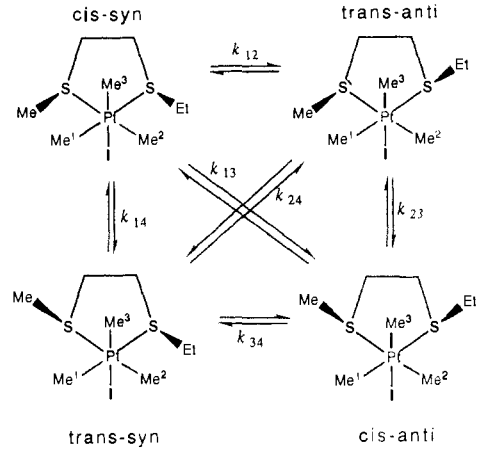

Similar studies of sulfur inversion were performed on the complex $[Mo(CO)_4(CH_3SCH_2CH_2SCH_3)]$.[108]

This method was extended to the dynamics of sulfur inversion in $Me_3PtI(MeSCH_2CH_2SEt)$.[109] Conventional 1D NMR methods were incapable of delineating the kinetic processes and extracting all four rate constants by this system. By ^{195}Pt NMR the four invertomers shown in Scheme 23 could be distinguished and their relative populations measured. Between 233 and 288 K these interconvert, as evidenced by cross-peaks in the 2D spectrum. The activation parameters derived from the rate constants are given in Table 15. At all temperatures the rate constants k_{13} and k_{24} remain zero, within experimental error. Even though there are detectable cross-peaks between cis-syn and cis-anti and between trans-anti and trans-syn, evaluation of rate constants from the 2D intensities shows that these arise only indirectly. This result implies that single-site sulfur inversion occurs at rates measurable by NMR whereas double sulfur inversion is too slow to measure. Only the quantitative 2D EXSY approach could allow such a definitive exclusion. A second feature of the kinetics is the lower $\Delta G^{\ddagger}$ for inversion of the bulkier *S*-ethyl group relative to *S*-methyl. This direct comparison, in the same molecule, would not have been

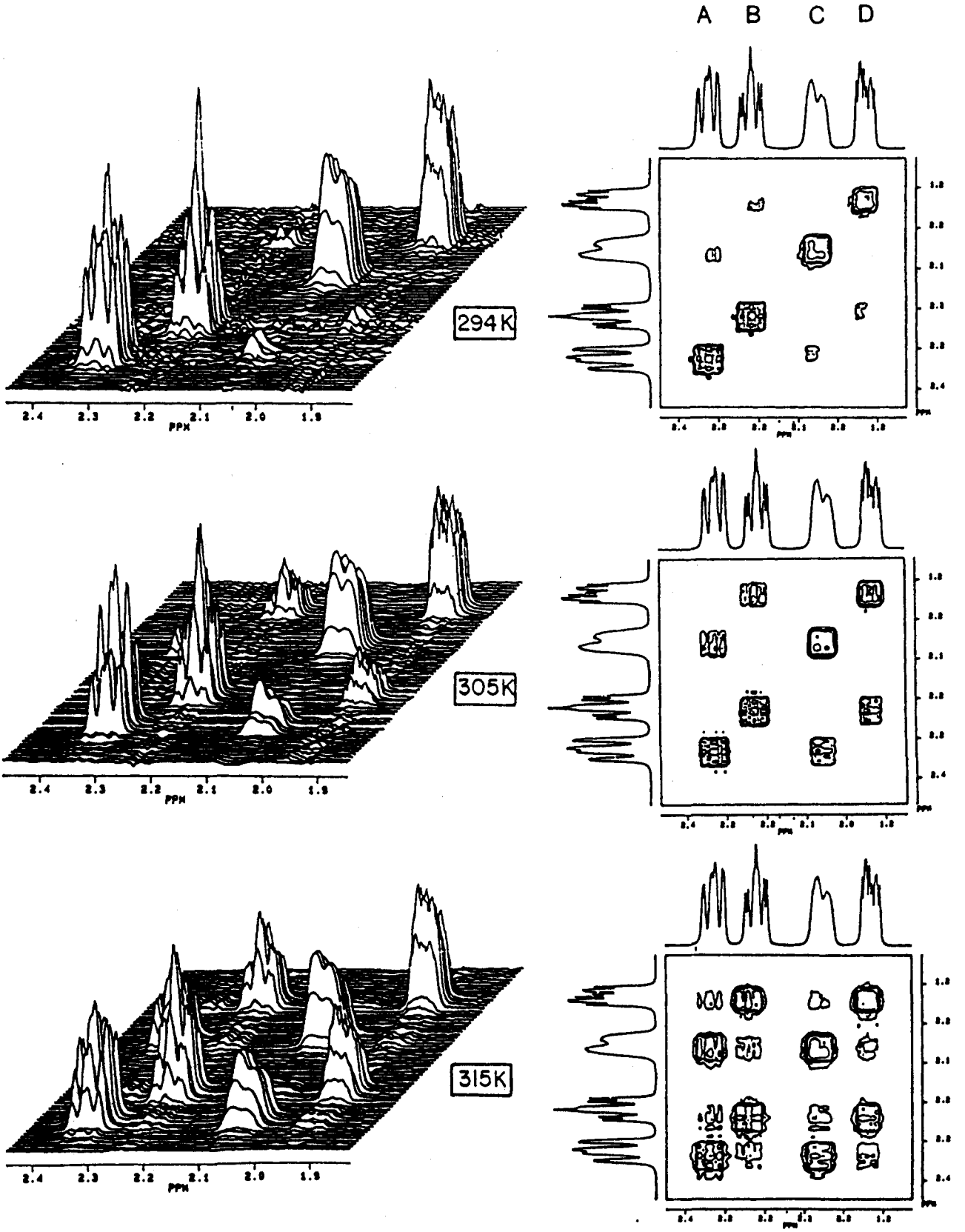

Figure 10. 500-MHz ^1H 2D EXSY spectra of (1,3)cyclooctatetraenophane (**36a**) in CD_2Cl_2 solution at the indicated temperatures. Reprinted from ref 101. Copyright 1990 American Chemical Society.

possible by line-shape methods.

Another aspect of this kinetic study involves a ^1H 2D EXSY investigation of the Pt–methyl region of the spectrum of $Me_3PtI(MeSCH_2CH_2SEt)$. In the temperature range 333–378 K fluxional behavior of the $PtMe_3$ moiety with respect to the other ligands was observed as cross-peaks among all three Pt–methyl resonances. From the intensities all three rate constants for exchange among the axial and two equatorial positions were calculated. Activation parameters derived from the exchange rate constants are given in Table 16. The remarkable result is that the rates of the three types of methyl–methyl exchange are different, with the rate of equatorial–equatorial interchange being signif-

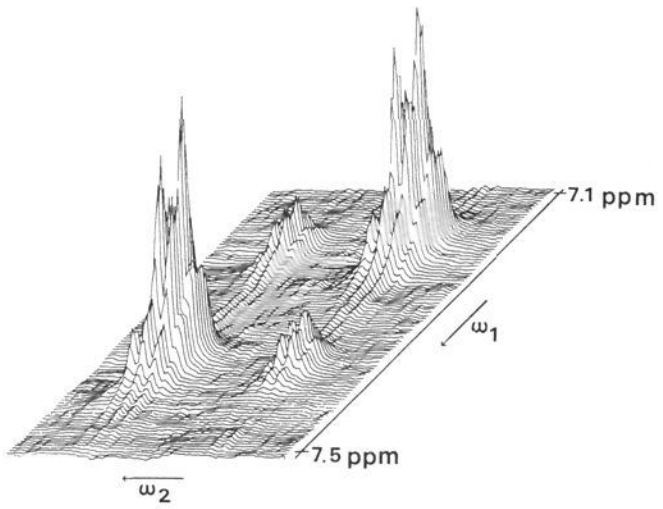

Figure 11. NH region of the ^1H 2D exchange spectrum of $^{15}NH_4^+$ in a D_2O/H_2O solvent mixture near pH 1.0. Along the diagonal, from bottom left to top right, are peaks corresponding to the isotopomers NHD_3^+, $NH_2D_2^+$, NH_3D^+, and NH_4^+ for each of the two ^{15}N spin states. Reprinted from ref 63.

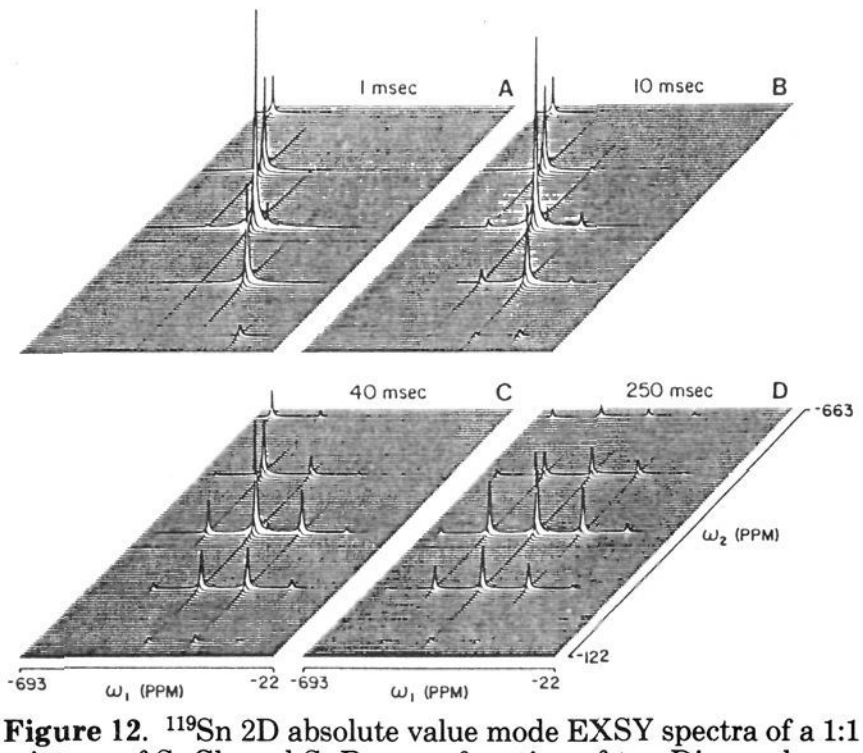

Figure 12. ^{119}Sn 2D absolute value mode EXSY spectra of a 1:1 mixture of $SnCl_4$ and $SnBr_4$ as a function of t_m. Diagonal runs from top left to bottom right. Reprinted from ref 22b. Copyright 1985 Academic Press.

TABLE 16. Activation Parameters for Methyl Interchange in $Me_3PtI(MeSCH_2CH_2SEt)$

parameter	e1–e2	a–e1	a–e2
$\Delta G^{\ddagger}$(25 °C), kJ mol^{-1}	97.7	92.6	90.9
$\Delta H^{\ddagger}$, kJ mol^{-1}	123	111	109
$\Delta S^{\ddagger}$, J K^{-1} mol^{-1}	85.0	62.2	60.7

icantly lower than the rates of axial–equatorial interchange. This behavior is inconsistent with a Bailar twist, rotating the three methyls 120° relative to the other three ligands. The kinetic data were interpreted as evidence for rotation of the disulfide ligand simultaneous with rotation of the Pt–methyls. An uncorrelated combination of these processes would result in an equatorial–equatorial exchange rate greater than axial–equatorial exchange. A 180° disulfide ligand rotation correlated with a 120° $PtMe_3$ rotation was suggested as the most probable fluxional mechanism. This would not interchange the two equatorial methyls, so it was necessary to assume an additional mechanism to account for that interchange. However, it seems unlikely that two different mechanisms would be so similar in rate, and it is difficult to envision the transition state for the correlated rotation. Instead we propose that methyl interchanges proceed via trigonal-bipyramid

SCHEME 24. Proposed Dissociative Mechanism for Ligand Exchange in $Me_3PtI(MeSCH_2CH_2SEt)$

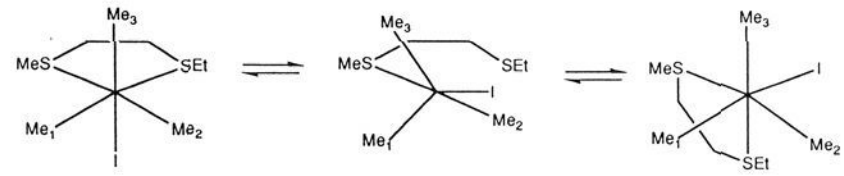

SCHEME 25. Dynamic Interconversion in $(MeS)_2CHCH(SMe)_2$ Complexes of Trimethylplatinum(IV) Halides

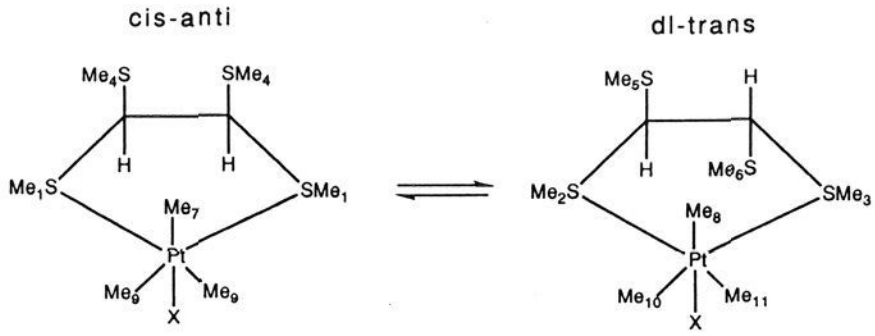

intermediates. Scheme 24 shows such a mechanism for interchanging one equatorial methyl with the axial. Cleavage of the other Pt–S bond would exchange the other equatorial methyl. If the bound sulfur were equatorial rather than apical in the trigonal bipyramid, or if the intermediate undergoes two pseudorotations, the two equatorial methyls would interchange, but this could be a slightly slower process. The large positive activation entropy is consistent with this dissociative mechanism.

Similar studies were performed on the complexes $Me_3PtX(MeSCH_2CH_2SEt)$ (X = Cl, Br) and $Me_3PtX(MeSCH_2CH_2StBu)$ (X=Cl, I).[110] At 243 K, the invertomers interconvert by sulfur inversion (Schemes 22 and 23) and the rate constants could be measured by ^{195}Pt 2D EXSY. Although populations are halide-dependent, the rate constants are essentially independent of halogen. The 2D EXSY analysis of $Me_3PtX(MeSCH_2CH_2StBu)$ was not necessary, since inversion of the S-tBu is so much faster than inversion of the S–Me that the two processes could be treated independently by 1D NMR techniques. However, the rate of S–Me inversion is an average over the two possible S–tBu configurations, which are rapidly interconverting. The general conclusion from these quantitative studies is that the sulfur inversion barriers decrease with steric bulk of the alkyl group: S–Me (64 kJ mol^{-1}) > S–Et (60 kJ mol^{-1}) ≫ S–tBu (45 kJ mol^{-1}).

At higher temperature there is again exchange among the three methyls in the complexes $Me_3PtCl(MeSCH_2CH_2SEt)$ and $Me_3PtI(MeSCH_2CH_2StBu)$, studied by ^1H 2D NMR. For the former, the behavior is quite similar to that of the chloro analogue, described above, but 3–4-fold faster. For the latter, the two axial–equatorial interchange processes occur at significantly different rates, reflecting the differing Pt–SMe and Pt–StBu bond strengths. It is not clear how this difference manifests itself in the correlated rotation mechanism that was proposed, but it is quite consistent with the dissociative mechanism (Scheme 24).

The latest in this extensive investigation of sulfur inversion and fluxional processes in thioether complexes of trimethylplatinum(IV) halide involves the 1,1,2,2-tetrakis(methylthio)ethane derivatives (Scheme 25; X = Cl, Br, I).[111] This has the further complication of two additional chiral centers, so that the two uncomplexed

TABLE 17. Activation Energies, $\Delta G^{\ddagger}$ (Kilojoules per Mole, 363 K), for High-Temperature Fluxions in $Me_3PtX[(MeS)_2CHCH(SMe)_2]$ (X = Cl, Br, I)

X	cis-anti → *dl*-trans	Pt–Me exch
Cl	90.6	90.6
Br	91.2	90.1
I	90.6	89.9

methylthio substituents can be cis-syn, cis-anti, or trans. Only the latter two are seen, although molecular models suggest that the steric repulsions in the cis-syn are not so large. The trans form appears as four stereoisomers, interconverting by sulfur inversion. One of the three possible stereoisomers of the cis-anti form is destabilized sterically and not seen, but the other two interconvert by sulfur inversion. These interconversions can be seen in ^{195}Pt 2D EXSY spectra, but all the rate constants could be obtained simply by ^1H line-shape analysis of the CH groups.

More interesting is the high-temperature dynamic behavior, whose elucidation required 2D EXSY. At 363 K sulfur inversion is rapid, so that it is necessary to consider only the cis-anti and *dl*-trans forms. As shown in Scheme 25, there are six different methylthio environments and five different methylplatinum environments. The 2D spectrum shows all 30 cross-peaks between all pairs of methylthio signals and all 20 (somewhat overlapping) cross-peaks between all pairs of methylplatinum signals. Therefore, three processes are occurring simultaneously: cis/trans interconversion, exchange of coordinated and uncoordinated sulfurs, and exchange of platinum methyls. Rather than solve for all 50 site to site rate constants, the problem was reduced to two two-site interchanges, one between coordinated (Me_{1-3}) and uncoordinated (Me_{4-6}) thiomethyls and the other between axial ($Me_{7,8}$) and equatorial (Me_{9-11}) methylplatinums. The rate constants obtained were converted into the $\Delta G^{\ddagger}$(363 K) values shown in Table 17. A comparison of the $\Delta G^{\ddagger}$ values obtained for Me_3Pt exchange with those derived for SMe exchange shows that they are very similar. It was therefore concluded that the 1,3 metal pivot of the $(MeS)_2CHCH(SMe)_2$ ligand and the Pt–methyl exchange processes are concerted. This was viewed as a mechanism wherein an uncoordinated sulfur becomes coordinated to the platinum, to produce a seven-coordinate intermediate whose nonrigidity permits exchange of methyls on Pt. However, this is a 20-electron intermediate, and extension of the dissociative process proposed above (Scheme 24) would account for the simultaneity of all these processes.

Scrambling reactions of metal carbonyls lend themselves to investigation by dynamic techniques.[112] The exchange kinetics of the three inequivalent carbon monoxide ligands bound to each of the two terminal ruthenium atoms in **38** have been investigated by ^{13}C

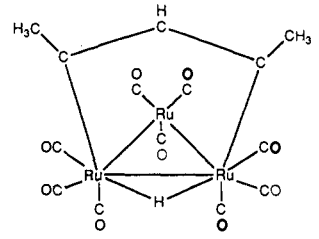

38

SCHEME 26. Metal Migration Pathways in $M(CO)_3(\eta^6\text{-}C_8H_8)$

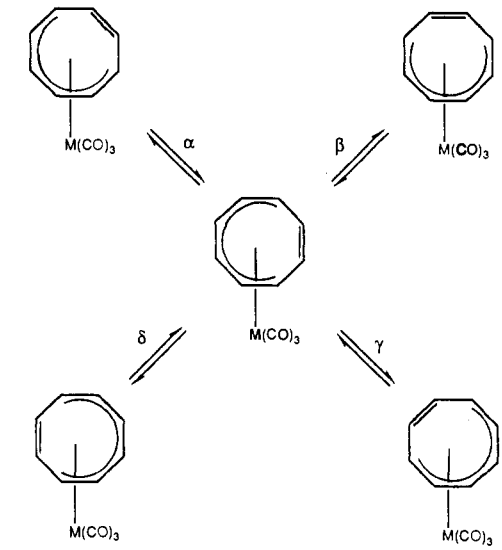

2D EXSY.[22c] (The carbon monoxides on the bridging ruthenium exchange rapidly.) All three pairs of carbon monoxide ligands interchange with equal rates (ca. 4 s^{-1}) within experimental error. This suggests that the exchange is concerted, rather than pairwise. There was no evidence for exchange of the CO ligands between bridging and terminal ruthenium atoms.

Another system in which carbon monoxide ligand exchange was observed is the osmium cluster **39**.[113] The use of 75% ^{13}C-enriched CO led to ^{13}C–^{13}C scalar coupling. The combined COSY–EXSY method called

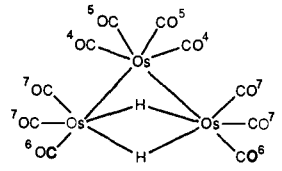

39

COCONOSY was used to assign peaks and to analyze the exchange kinetics. By fitting the t_m dependence of the peak intensities, the rate constant $k_{67} + k_{76}$ could be evaluated as 1.2 s^{-1}.

^1H and ^{13}C 2D EXSY experiments were performed on four η^1-$LW(CO)_5$ complexes, with L = $PhCH_2SSCH_2Ph$, $MeSCH_2SMe$, *cyclo*(SCHMeSCHMeSCHMe), and *cyclo*($SCMe_2SCH_2CH_2$).[114] Each of these undergoes 1,2 or 1,3 metallotropic shifts near ambient temperature. Rate constants could be measured by ^1H 2D EXSY. However, the carbonyl region of the ^{13}C 2D spectrum showed no cross-peaks and hence no evidence of axial–equatorial CO exchange. Thus, the $W(CO)_5$ group remains rigidly bonded during the metallotropic shifts.

Metal migration reactions in (η^6-cyclooctatetraene)-tungsten and -chromium tricarbonyls have been investigated by both ^1H and ^{13}C 2D EXSY.[115] The 2D EXSY spectrum of $W(CO)_3(\eta^6\text{-}C_8H_8)$ or $Cr(CO)_3(\eta^6\text{-}C_8H_8)$ shows significant cross-peak intensity between cyclooctatetraene sites. The four possible metal migrations in $M(CO)_3(\eta^6\text{-}C_8H_8)$ are shown in Scheme 26. The possible 1,2, 1,3, 1,4, and 1,5 metal shifts are denoted α, β, γ, and δ, respectively. The site to site rate

TABLE 18. Rate Constants (s^{-1}) for Metal Migrations in $M(CO)_3(\eta^6\text{-}C_8H_8)$

T, °C	k_{12} ($\alpha + \beta$)	k_{13} ($\beta + \gamma$)	k_{14} ($\gamma + \delta$)	k_{23} ($\alpha + \delta$)	k_{24} ($\beta + \gamma$)	k_{34} ($\alpha + \beta$)	α	β
				M = W				
0	0.038	0.011	0.0045	0.013	0.027	0.022	0.012	0.011
10	0.27	0.14	0.028	0.12	0.14	0.28	0.13	0.15
10[a]	0.26	0.15	−0.0005	0.12	0.15	0.27	0.12	0.15
15	0.50	0.53[b]	0.014	0.20	0.27	0.51	0.22	0.29
20	1.11	0.96[b]	0.04	0.47	0.63	1.08	0.47	0.63
				M = Cr				
−10	0.35	0.43[b]	−0.0014	0.12	0.31	0.34	0.078	0.27
0	2.00	1.83[b]	0.053	0.45	1.36	1.57	0.44	1.35

[a] From ^{13}C 2D exchange experiment. [b] Errors in these values are larger owing to peak overlap.

TABLE 19. 2D ^{13}C EXSY Derived Rate Constants (s^{-1}) for Rearrangement of $[Re_3(\mu\text{-}H)_4(CO)_9NCMe]^-$

	284 K	278 K	271 K
k_{AD}	1.34	0.84	0.39
k_{AC}	1.14	0.77	0.34
k_{DC}	1.24	0.83	0.34
k_{EB}	2.49	1.60	0.81

constants derived from analysis of the 2D intensities are given in Table 18. Rate constants obtained by ^{13}C 2D NMR agree very well with those obtained by ^1H 2D NMR, which requires less time. Also included in Table 18 is the correspondence between the site to site rate constants and the migrations in Scheme 26. Since k_{14} is zero, within experimental error, the 1,4 and 1,5 shifts (migrations γ and δ, respectively) occur at negligibly low rates. The nonzero rate constants then provide an overdetermined set of equations for fitting the rate constants for 1,2 and 1,3 shifts (migrations α and β, respectively). These rate constants are also included in Table 18. The data indicate that both 1,2 and 1,3 metal shifts are equally likely for the tungsten complex. For the chromium complex, exchange is faster and the 1,3 metal shift occurs approximately 3 times as fast as the 1,2 shift. These results exclude an η^8-cyclooctatetraene intermediate, whose symmetry would require random shifts. Although the authors proposed an η^6-bicyclo[4.2.0]octatriene intermediate, the results are more simply consistent with an η^4-cyclooctatetraene intermediate (40).

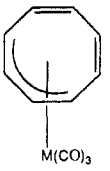

40

Ligand rearrangement in the complex $[Re_3(\mu\text{-}H)_4(CO)_9N{\equiv}CMe]^-$ (41) has been investigated with ^{13}C 2D EXSY.[116] The 2D spectrum of 20% ^{13}C-enriched 41 shows cross-peaks among CO groups labeled A, C, and D and also between those labeled B and E but none connecting these two sets. Analysis of the spectral intensities yielded the kinetic data shown in Table 19. The mechanism given in Scheme 27 was proposed. Loss of the acetonitrile from 41 leads to the coordinatively unsaturated intermediate 42. Bridging of hydrogen H_b to all three rhenium atoms yields a symmetrical intermediate 43, although an alternative is that H_b simply migrates to the adjacent Re–Re bond. This mechanism preserves the distinction between the two sets of CO

SCHEME 27. Intramolecular Rearrangement of $[Re_3(\mu\text{-}H)_4(CO)_9NCMe]^-$

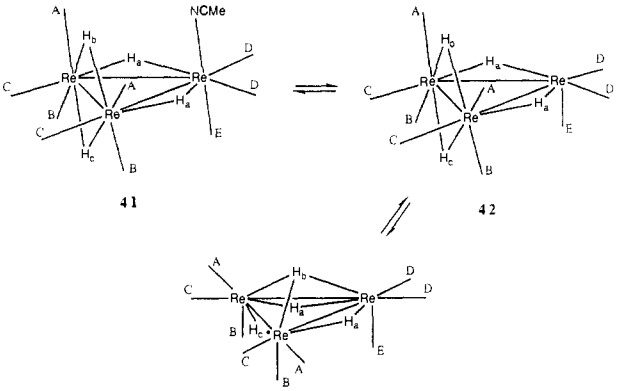

ligands, and it also accounts for the statistical factor of 2 in k_{EB}.

C. Biochemical Systems

The applicability of quantitative 2D EXSY to the study of biologically important systems is only beginning to be realized. It is especially useful since it is noninvasive and can be used to monitor the dynamics of metabolic processes not only in vitro but also in vivo. A few examples exist that demonstrate its unique potential.

In mapping out the structure and dynamics of proteins and enzyme active sites, the motional freedom of a probe group can be a useful tool. Such a group is the bis(4-fluorophenyl)amide moiety of [bis(4-fluorophenyl)carbamoyl]-α-chymotrypsin (44). X-ray crys-

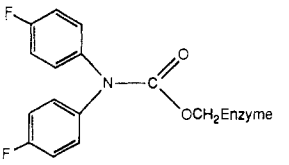

44

tallographic studies[117] suggest that one phenyl group is situated inside the enzyme while the other is directed toward the protein surface. By ^{19}F 2D EXSY the rate constant for interchange of the two 4-fluorophenyl groups is found to be 12 ± 4 s^{-1} at 5 °C.[118] Since the protein structure has so little influence on the rotation of the diphenylcarbamoyl group, it was concluded that the rotation occurs in a conformation of the enzyme that is locally unfolded.

A spin-locking technique has been used to obtain the ^{13}C 2D EXSY spectrum of the protein bovine pancreatic

TABLE 20. Rate Constants (s^{-1}) for Proton Exchange in Viomycin

proton	k	proton	k	proton	k
2	0.39	6	0.52	9	0.13
3	1.45	7	1.21	10	0.75
5	1.18	8	0.44		

trypsin inhibitor (**29**).[119] Rotation about the C_β–C_γ bond of the tyrosine-35 residue interconverts positions ϵ_1 with ϵ_2 and δ_1 with δ_2. From the 2D intensities the exchange rate constant was found to be 8.5 ± 0.5 s^{-1}, with an activation energy of 15.3 ± 0.8 kcal/mol.

Exchange of the NH protons of the antibiotic viomycin (**45**) at pH 4 has been quantitated by ^1H 2D EXSY.[120] Pure absorption mode spectra with solvent suppression displayed 2D cross-peaks between most NH sites and the water resonance. Analysis of the plots

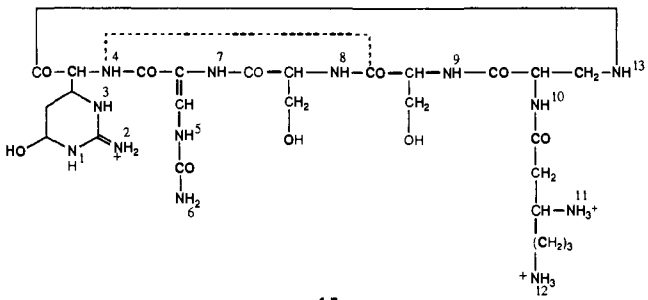

45

of cross-peak height versus mixing times yielded first-order rate constants for exchange. Results for those NH protons exchanging at suitable rates are given in Table 20. Exchange of the intramolecularly hydrogen bonded H_4 is too slow to measure.

Enzyme-catalyzed reactions of biological importance are amenable to study by quantitative 2D EXSY. Phosphoglyceromutase is an enzyme that converts 3-phosphoglycerol (3-PG) into 2-phosphoglycerol (2-PG) (eq 58). The dynamics of the reaction are evidenced

$$HOCH_2CH(OH)CH_2OPO_2^-OH \rightleftarrows (HOCH_2)_2CHOPO_2^-OH \quad (58)$$

by the observation of ^{31}P NMR cross-peaks connecting the 2-PG and 3-PG signals.[121] From the 2D NMR intensities the rate constants were obtained: k_1 = 0.19 ± 0.03 s^{-1}, k_{-1} = 1.58 ± 0.20 s^{-1}. These values agree nicely with those obtained by biochemical analysis.

The enzyme phosphoglucose isomerase catalyzes the interconversion of glucose 6-phosphate (Glc-6-P) and fructose 6-phosphate (Fru-6-P). This isomerization, along with the anomerization between α-Glc-6-P and β-Glc-6-P, was studied[122] by ^{31}P 2D EXSY. Along the diagonal of the spectrum lie three signals corresponding to β-Glc-6-P, α-Glc-6-P, and α- plus β-Fru-6-P, the latter two anomers being coalesced into a single peak. A 2D spectrum showed cross-peaks between all pairs of species, indicating the occurrence of both isomerization and anomerization. The rate constants were obtained by the initial rate approximation. For the nonenzymatic anomerization of α-Glc-6-P and β-Glc-6-P at 37 °C, the rate constants obtained by 2D EXSY agree with the values determined by optical rotation measurements. Table 21 shows the rate constants for the isomerization and anomerization reactions at 25 °C. A comparison of the anomerization rates in the presence and absence of phosphoglucose isomerase demonstrates that this process is indeed enzyme-catalyzed. Further,

TABLE 21. Rate Constants (s^{-1}) for the Interconversion of Glucose 6-Phosphate and Fructose 6-Phosphate at 25 °C

	+enzyme	-enzyme
α-Glc-6-P → β-Glc-6-P	0.29	0.06
β-Glc-6-P → α-Glc-6-P	0.15	0.036
Fru-6-P → α-Glc-6-P	3.4	
α-Glc-6-P → Fru-6-P	2.5	
Fru-6-P → β-Glc-6-P	<0.04	
β-Glc-6-P → Fru-6-P	<0.04	

SCHEME 28. Anomerization Pathways in D-Talose

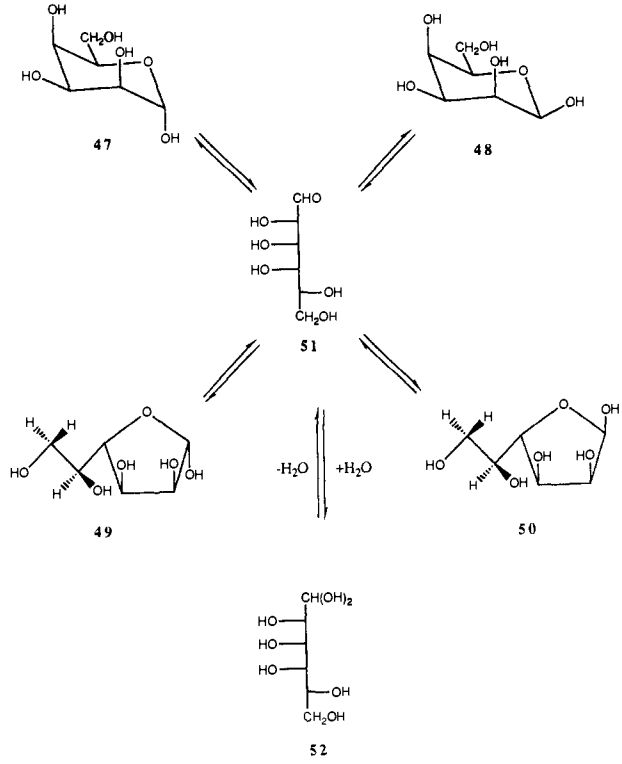

the data show that the enzyme does not produce β-Glc-6-P directly from Fru-6-P, but rather it is first converted by the enzyme to α-Glc-6-P.

Rate constants for anomerization of two monosaccharides have been determined[123] by ^{13}C 2D EXSY. In both cases the sugars were enriched in ^{13}C at the anomeric carbon. Exchange between the two cyclic furanose forms of D-erythrose (**46**) in aqueous solution

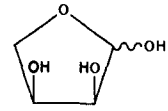

46

was detected as a pair of cross-peaks between the two sites. Analysis of the 2D intensities yielded rate constants $k_{\alpha\beta}$ = 0.11 s^{-1} and $k_{\beta\alpha}$ = 0.045 s^{-1}, in excellent agreement with those obtained by the saturation-transfer method. The second system of study was aqueous D-talose, which is present as nearly equal amounts of two pyranose (**47**, **48**) and two furanose (**49**, **50**) forms, as well as small amounts of the open aldehyde **51** and hydrate **52** (Scheme 28). Interconversion between each of the cyclic species was evidenced in the ^{13}C 2D NMR spectrum. Since tautomerization proceeds via the open aldehyde form **51**, each interconversion is strictly a three-site exchange process. However, analysis of the 2D spectrum was carried out assuming only two-site exchange processes, which is valid since the

TABLE 22. Rate Constants (s^{-1}) for the Anomerization of D-Talose at 64 °C

reaction	10^3k	reaction	10^3k
$\alpha f \rightarrow \beta f$	110	$\beta f \rightarrow \alpha f$	190
$\alpha f \rightarrow \alpha p$	45	$\alpha p \rightarrow \alpha f$	24
$\alpha f \rightarrow \beta p$	16	$\beta p \rightarrow \alpha f$	11
$\beta f \rightarrow \alpha p$	51	$\alpha p \rightarrow \beta f$	15
$\beta f \rightarrow \beta p$	24	$\beta p \rightarrow \beta f$	9
$\alpha p \rightarrow \beta p$	*a*	$\beta p \rightarrow \alpha p$	*a*

[a] These rate constants were too small to be measured by 2D EXSY.

equilibrium concentration of 51 is small. The 10 rate constants derived via eq 26 are given in Table 22. These rate constants agree with those determined by saturation transfer, which could also be used to calculate correctly the time dependence of the concentrations of the four anomeric species undergoing equilibrium at lower temperature.

The in vivo phosphorylation of creatine by adenosine triphosphate (ATP), catalyzed by creatine phosphokinase, was studied by 2D EXSY.[124] The sample was the head (brain) or leg of an anesthetized rat. In the ^{31}P spectra the only cross-peaks detected were between phosphocreatine (CrP) and the γ-phosphate of ATP. Other reactions, such as the adenylate kinase reaction and exchange between inorganic phosphate and ATP, are too slow to be detected under these conditions. The rate constants for phosphoryl transfer were obtained by evaluation of the mixing time dependence of the cross-peak volumes. From the initial slope of this plot, and from known CrP concentrations, the flux rates are $v_{leg} = 13$ μmol/s per g of weight and $v_{brain} = 2$ μmol/s per g of weight. These are similar to those calculated based on bulk concentrations and creatine phosphokinase kinetic data measured in vitro.

This reaction has also been studied more extensively in vitro.[125] The ^{13}P 2D EXSY spectrum of a reaction mixture with 124 mM CrP, 44 mM Cr, 44 mM ATP, and 65 mg/mL of enzyme at pH 7.2 and 37 °C shows only a single pair of cross-peaks between CrP and the γ-phosphate of ATP. Since the adenosine diphosphate (ADP) concentration was too low to detect, additional cross-peaks between ATP and ADP were not seen. From an initial rate approximation the rate constant for phosphoryl transfer from ATP to CrP was determined as 0.29 s^{-1}. From the equilibrium CrP to ATP ratio the reverse rate constant equals 0.10 s^{-1}. The rate constants are properly linear in enzyme concentration. Also, they are independent of substrate concentration, so they correspond to v_{max}. The insensitivity of NMR requires a substrate concentration above the Michaelis constant of the enzyme, and this is likely to be a general limitation.

In another study of this same reaction[93] but with 8 mg/mL enzyme and ca. 10 mM substrate at 304 K and with phase-sensitive ^{31}P accordion spectroscopy[31] quantitative evaluation of the cross-peak intensity yielded a rate constant of 0.33 s^{-1}. This is in quite good agreement with the rate constant of 0.30 s^{-1} obtained by saturation transfer under these conditions.

Even in a field as new as quantitative 2D EXSY, controversy can be sparked. Such is the case for the adenylate kinase (AK) catalyzed reaction of adenosine mono-, di-, and triphosphates (eq 59). Two separate

$$2ADP \rightleftharpoons ATP + AMP \quad (59)$$

groups have undertaken study of this reaction by ^{31}P 2D EXSY, Kantor, Ferretti, and Balaban[125] in 1984 and Mendz, Robinson, and Kuchel[121] in 1986. Despite the slightly different conditions used by each, their spectra are qualitatively the same. Four pairs of cross-peaks are detected, signifying the occurrence of the following processes

$$\alpha ADP \rightleftharpoons \alpha ATP$$

$$\alpha ADP \rightleftharpoons AMP$$

$$\beta ADP \rightleftharpoons \beta ATP$$

$$\beta ADP \rightleftharpoons \gamma ATP$$

plus a fifth pair of cross-peaks between AMP and αATP, due to indirect exchange, via ADP. The puzzling result is that both groups observe βATP–βADP cross-peaks that are smaller than the AMP–αADP cross-peaks.

Kantor et al. suggested that this difference in intensities implies that the former interchange occurs at a lower rate. This led them to invoke a two-step reaction mechanism (eqs 60 and 61) with a kinetically significant

$$2ADP + \text{enzyme} \underset{k_2}{\overset{k_1}{\rightleftharpoons}} \text{ATP–enzyme} + AMP \quad (60)$$

$$\text{ATP–enzyme} \underset{k_4}{\overset{k_3}{\rightleftharpoons}} ATP + \text{enzyme} \quad (61)$$

enzyme–substrate complex. Analysis of the t_m dependence of cross-peak intensities gave the pseudo-first-order rate constants $k_1[E] = 1.2$ s^{-1}, $k_2[E\text{–ATP}] = 1.2$ s^{-1}, $k_3 = 14$ s^{-1}, and $k_4[E] = 50$ s^{-1}. However, since $[E\text{–ATP}]/[ATP] = k_4[E]/k_3$, these rate constants require that 78% of the ATP be present as E–ATP, even though enzyme is present in far less than stoichiometric amounts.

Mendz et al. favor an interpretation of the cross-peak intensity difference that does not explicitly include an enzyme–substrate complex. Instead, they suggest that short spin–spin relaxation times (T_2) can account for the smaller βADP–βATP cross-peaks. In support they present data for the six phosphorus nuclei, both with and without enzyme. They find that T_2 of βATP is much shorter than T_2 of the other species. They also find that the βATP diagonal peak is less intense than the other ATP diagonal peaks. They therefore conclude that the short T_2 accounts for the lower intensities of both diagonal peaks and cross-peaks. However, both of these groups used peak volumes for their intensity values, and peak volumes ought to be independent of T_2. In eq 23 T_2 has already been taken into account, and it is clear that the effect of T_2 is only to broaden peaks. Regardless, Mendz et al. conclude that the AK-catalyzed reaction occurs simply as in eq 62, with

$$2ADP \underset{k_r}{\overset{k_f}{\rightleftharpoons}} AMP + ATP \quad (62)$$

the rate constants $k_f = 0.72 \pm 0.05$ s^{-1} and $k_r = 0.92 \pm 0.06$ s^{-1}. Unfortunately, it is not possible to derive these values from the data given, and the **R** matrix that was published does not correspond to any mechanism.

We have recalculated[126] the rate constants from the Mendz intensities and obtained four independent estimates for $k_f[ADP]$ of 0.75, 0.88, 0.83, and 0.49 s^{-1}. For the alternative two-step mechanism (eqs 60 and 61) these values correspond to $k_1[ADP][E]$ and to three

independent estimates of $k_1[ADP][E]/r$, respectively, where $r = 1 + k_2[AMP]/k_3$. The last value, corresponding to βADP → βATP, is certainly lower than the others, but the one corresponding to αADP → αATP is not lower, even though the αADP–αATP cross-peak intensity is nearly as low as that of βADP–βATP. It may be that the reduced intensity of the βATP diagonal peaks and cross-peaks is an artifact from integrating broad peaks in absolute value mode. The βATP peak is clearly the broadest, since it is split by two adjacent ^{31}P nuclei. If so, then the βADP–βATP exchange rate is not really lower than the others. Moreover, although the two-step mechanism requires the value of $k_1[ADP][E]$ to be greater than $k_1[ADP][E]/r$, the difference is not significant, so there seems to be no kinetic evidence that requires an enzyme–substrate complex. It is clear that this is a reaction that would benefit from further study.

D. Future Opportunities

Many multisite exchange reactions that were studied by older DNMR methods might be worth reinvestigating and extending by 2D EXSY. Among these are NH proton exchange in aqueous solutions of peptides and proteins[85,120,127] and in porphyrins,[128] stereoisomerization of metal tris(β-diketonates),[129] rearrangement of barbaryl cations,[130] the *N*-methyl interchanges of $(Me_2N)_2C{=}CXY$,[131] the rearrangements of tropylium azide,[132] and the ring rotation in tetra-*tert*-butyluranocene.[133]

2D EXSY is widely applicable to multisite exchange kinetics, and many applications will be forthcoming. As with any DNMR technique, it is limited to exchange reactions. In practical terms, this means that the reaction must be reversible, with detectable amounts of both reactants and products. A significant advantage is that the method is applicable to degenerate rearrangements (identity reactions), where there is no net reaction. A further requirement is that the rate must be on the time scale of DNMR methods. Often these requirements may be met by suitable modification of the reaction or reaction conditions.

The time requirements of 2D EXSY may be daunting. The variants described in section II.D.4 may offer some simplification if there are few sites. However, the increasing automation of NMR experiments is making overnight 2D experiments quite feasible.

V. Summary

It has been shown that 2D NMR offers a unique, effective, and powerful means of studying and quantitating the dynamics of a wide variety of chemical systems of organic, inorganic, and biochemical nature. The information extracted from a 2D exchange spectrum can provide substantial insight into mechanisms for reactions of interest.

Often qualitative results are sufficient. The 2D spectrum shows which peaks exchange with which others, and this information may clarify the mechanism or permit rejection of mechanisms. Further, this information may be used to support kinetic analysis of 1D spectra by lineshape analysis.

Little additional effort is now required to obtain quantitative data from 2D EXSY spectra. An attractive feature of quantitative 2D NMR is that it allows one to evaluate the rate constants of several kinetic processes occurring simultaneously in a given sample. Further, the rate information obtained is in the form of site to site rate constants for each individual process.

An essential factor in using quantitative 2D NMR properly is obtaining pure absorption mode spectra. Most of the studies detailed above were carried out with absolute value spectra instead. The reason for this may be instrumental limitations in performing the necessary phase cycling and/or data handling. The interpretation of absolute value spectra is risky since the peak intensities obtained by this method may not accurately reflect the rate information. Fortunately, it is now quite easy to obtain pure absorption mode spectra.

Finally, in many instances quantitative 2D NMR offers a significant savings in experimental time for studying multisite kinetics. In contrast to performing a series of magnetization-transfer and relaxation time determinations, which can be quite time consuming, a single pure absorption mode 2D NMR spectrum allows all rate processes in a system to be observed concurrently, and analysis of this spectrum provides all the site to site rate constants for the system.

Acknowledgments. This work was supported by the National Science Foundation (Grant CHE87-14451). We are grateful to Dr. Keith G. Orrell for providing us with manuscripts in press and to the reviewers for helpful comments.

References

(1) (a) Johnson, C. S. *Adv. Magn. Reson.* **1965**, *1*, 33. (b) Binsch, G. *Top. Stereochem.* **1968**, *3*, 97. (c) Jackman, L. M.; Cotton, F. A. *Dynamic Nuclear Magnetic Resonance Spectroscopy*; Academic: New York, 1975. (d) Sandström, J. *Dynamic NMR Spectroscopy*; Academic: London, 1982. (e) Kaplan, J. I.; Fraenkel, G. *NMR of Chemically Exchanging Systems*; Academic: New York, 1980. (f) Oki, M. *Applications of Dynamic NMR Spectroscopy to Organic Chemistry*; VCH: Deerfield Beach, FL, 1985.

(2) Gutowsky, H. S.; Saika, A. *J. Chem. Phys.* **1953**, *21*, 1688. Gutowsky, H. S.; McCall, D. W.; Slichter, C. P. *Ibid.* **1953**, *21*, 279. Gutowsky, H. S.; Holm, C. H. *Ibid.* **1956**, *25*, 1228. Takeda, M.; Stejskal, E. O. *J. Am. Chem. Soc.* **1960**, *82*, 25. Rogers, M. T.; Woodbrey, J. C. *J. Phys. Chem.* **1962**, *66*, 540. Allerhand, A.; Gutowsky, H. S.; Jonas, J.; Meinzer, R. A. *J. Am. Chem. Soc.* **1966**, *88*, 3185. Perrin, C. L. *Magn. Reson. Chem.* **1988**, *26*, 224.

(3) (a) Forsen, S.; Hoffman, R. A. *J. Chem. Phys.* **1963**, *39*, 2892. (b) Campbell, I. D.; Dobson, C. M.; Ratcliffe, R. G.; Williams, R. J. P.; *J. Magn. Reson.* **1978**, *29*, 397. (c) Perrin, C. L.; Johnston, E. R. *J. Magn. Reson.* **1979**, *33*, 619.

(4) Reviews: Hoffman, R. A.; Forsen, S. *Prog. Nucl. Magn. Reson. Spectrosc.* **1966**, *1*, 15. Noggle, J.; Schirmer, R. *The Nuclear Overhauser Effect*; Academic: New York, 1971. Mann, B. E. *Prog. Nucl. Magn. Reson. Spectrosc.* **1977**, *11*, 95. Alger, J. R.; Shulman, R. G. *Q. Rev. Biophys.* **1984**, *17*, 83.

(5) Boyd, J.; Moore, G.; Williams, G. *J. Magn. Reson.* **1984**, *58*, 511.

(6) Wynants, C.; Van Binst, G.; Mügge, C.; Jurkschat, K.; Tzschach, A.; Pepermans, H.; Gielen, M.; Willem, R. *Organometallics* **1985**, *4*, 1906.

(7) Derome, A. *Modern NMR Techniques for Chemistry Research*; Pergamon: New York, 1987.

(8) Sanders, J. K. M.; Hunter, B. K. *Modern NMR Spectroscopy*; Oxford University: Oxford, 1987.

(9) Ernst, R. R.; Bodenhausen, G.; Wokaun, A. *Principles of Nuclear Magnetic Resonance in One and Two Dimensions*; Oxford University: Oxford, 1987.

(10) Croasmun, W. R.; Carlson, R. M. K. *Two-Dimensional NMR Spectroscopy: Applications for Chemists and Biochemists*; VCH: New York, 1987.

(11) Benn, R.; Gunther, H. *Angew. Chem., Int. Ed. Engl.* **1983**, *22*, 350.

(12) Bax, A.; Lerner, L. *Science* **1986**, *232*, 960.

(13) Kessler, H.; Gehrke, M.; Griesinger, C. *Angew. Chem., Int. Ed. Engl.* **1988**, *27*, 490.
(14) Orrell, K. G.; Sik, V. *Annu. Rep. NMR Spectrosc.* **1987**, *19*.
(15) Willem, R. *Prog. Nucl. Magn. Reson. Spectrosc.* **1987**, *20*, 1.
(16) Jeener, J.; Meier, B. H.; Bachmann, P.; Ernst, R. R. *J. Chem. Phys.* **1979**, *71*, 4546.
(17) Nagayama, K.; Kumar, A.; Wüthrich, K.; Ernst, R. R. *J. Magn. Reson.* **1980**, *40*, 321.
(18) Macura, S.; Ernst, R. R. *Mol. Phys.* **1980**, *41*, 95.
(19) Perrin, C. L.; Gipe, R. K. *J. Am. Chem. Soc.* **1984**, *106*, 4036.
(20) Willem, R.; Gielen, M.; Pepermans, H.; Hallenga, K.; Recca, A.; Finocchiaro, P. *J. Am. Chem. Soc.* **1985**, *107*, 1153.
(21) Kumar, A.; Wagner, G.; Ernst, R. R.; Wüthrich, K. *J. Am. Chem. Soc.* **1981**, *103*, 3654.
(22) (a) Oschkinat, H.; Pastore, A.; Bodenhausen, G. *J. Am. Chem. Soc.* **1987**, *109*, 4110. (b) Ramachandran, R.; Knight, C. T. G.; Kirkpatrick, R. J.; Oldfield, E. *J. Magn. Reson.* **1985**, *65*, 136. (c) Hawkes, G. E.; Lian, L.-Y.; Randall, E. W.; Sales, K.; Aime, S. *Ibid.* **1985**, *65*, 173. (d) Bronnimann, C. E.; Szeverenyi, N. M.; Maciel, G. E. *J. Chem. Phys.* **1983**, *79*, 3694.
(23) Keepers, J. W.; James, T. L. *J. Magn. Reson.* **1984**, *57*, 404.
(24) (a) Bremer, J.; Mendz, G. L.; Moore, W. J. *J. Am. Chem. Soc.* **1984**, *106*, 4691. (b) Olejniczak, E. T.; Gampe, R. T., Jr.; Fesik, S. W. *J. Magn. Reson.* **1986**, *67*, 28.
(25) Abel, E. W.; Coston, T. P. J.; Orrell, K.; Sik, V.; Stephenson, D. *J. Magn. Reson.* **1986**, *70*, 34.
(26) Kuchel, P. W.; Bulliman, B. T.; Chapman, B. E.; Mendz, G. L. *J. Magn. Reson.* **1988**, *76*, 136.
(27) States, D. J.; Haberkorn, R. A.; Ruben, D. J. *J. Magn. Reson.* **1982**, *48*, 286.
(28) (a) Redfield, A. G.; Kunz, S. *J. Magn. Reson.* **1975**, *19*, 250. (b) Marion, D.; Wüthrich, K. *Biochem. Biophys. Res. Commun.* **1983**, *113*, 967. (c) Nagayama, K. *J. Magn. Reson.* **1986**, *66*, 240.
(29) Marion, D.; Ikura, M.; Tschudin, R.; Bax, A. *J. Magn. Reson.* **1989**, *85*, 393.
(30) Perrin, C. L. *J. Magn. Reson.* **1989**, *82*, 619.
(31) Bodenhausen, G.; Ernst, R. R. *J. Am. Chem. Soc.* **1982**, *104*, 1304.
(32) Bodenhausen, G.; Ernst, R. R. *J. Magn. Reson.* **1981**, *45*, 367.
(33) Morris, G. A.; Freeman, R. A. *J. Magn. Reson.* **1978**, *29*, 433.
(34) Malloy, C. R.; Sherry, A. D.; Nunnally, R. L. *J. Magn. Reson.* **1985**, *64*, 243.
(35) Gesmar, H.; Led, J. J. *J. Magn. Reson.* **1986**, *68*, 95.
(36) Grassi, M.; Mann, B. E.; Pickup, B. T.; Spencer, C. M. *J. Magn. Reson.* **1986**, *69*, 92.
(37) Bellon, S. F.; Chen, D.; Johnston, E. R. *J. Magn. Reson.* **1987**, *73*, 168.
(38) Perrin, C. L.; Engler, R. E. *J. Magn. Reson.*, in press.
(39) Engler, R. E.; Johnston, E. R.; Wade, C. G. *J. Magn. Reson.* **1988**, *77*, 377.
(40) Martin, G. E.; Zektzer, A. S. *Two-Dimensional NMR Methods for Establishing Molecular Connectivity*; VCH: New York, 1988. Schraml, J.; Bellama, J. M. *Two-Dimensional NMR Spectroscopy*; Wiley: New York, 1988.
(41) Brocas, J.; Gielen, M.; Willem, R. *The Permutational Approach to Dynamic Stereochemistry*; McGraw-Hill: New York, 1983.
(42) Perrin, C. L.; Johnston, E. R.; Ramirez, J. L. *J. Am. Chem. Soc.* **1980**, *102*, 6299.
(43) Carpenter, B. K. *Determination of Organic Reaction Mechanisms*; Wiley: New York, 1984.
(44) Burwell, R. L., Jr.; Pearson, R. G. *J. Phys. Chem.* **1968**, *70*, 300.
(45) Klemperer, W. G. *J. Am. Chem. Soc.* **1972**, *94*, 6940.
(46) Macura, S.; Huang, Y.; Suter, D.; Ernst, R. R. *J. Magn. Reson.* **1981**, *43*, 259.
(47) Macura, S.; Wüthrich, K.; Ernst, R. R. *J. Magn. Reson.* **1982**, *46*, 269.
(48) Mirau, P.; Bovey, F. *J. Am. Chem. Soc.* **1986**, *108*, 5130.
(49) Scarsdale, J. N.; Yu, R. K.; Prestegard, J. H. *J. Am. Chem. Soc.* **1986**, *108*, 6778. Fesik, S. W.; O'Donnell, T. J.; Gampe, R. T., Jr.; Olejniczak, E. T. *Ibid.* **1986**, *108*, 3165. Bovey, F. A.; Mirau, P. A. *Acc. Chem. Res.* **1988**, *21*, 37.
(50) Bothner-By, A. A.; Stephens, R. L.; Lee, J.; Warren, C. D.; Jeanloz, R. W. *J. Am. Chem. Soc.* **1984**, *106*, 811.
(51) Bax, A.; Davis, D. G. *J. Magn. Reson.* **1985**, *63*, 207. Davis, D. G.; Bax, A. *J. Am. Chem. Soc.* **1985**, *107*, 2820.
(52) Wagner, G.; Bodenhausen, G.; Muller, N.; Rance, M.; Sorensen, O.; Ernst, R. R.; Wüthrich, K. *J. Am. Chem. Soc.* **1985**, *107*, 6440.
(53) Montelione, G. T.; Wagner, G. *J. Am. Chem. Soc.* **1989**, *111*, 3096.
(54) Hore, P. J. *J. Magn. Reson.* **1983**, *55*, 283. Morris, G. A.; Smith, K. I.; Waterton, J. C. *Ibid.* **1986**, *68*, 526. Zuiderweg, E. R. P.; Hallenga, K.; Olejniczak, E. T. *Ibid.* **1986**, *70*, 336. Brown, S. C.; Weber, P. L.; Mueller, L. *Ibid.* **1988**, *77*, 166.
(55) Yannoni, C. S. *Acc. Chem. Res.* **1982**, *15*, 201. Lyerla, J. R.; Yannoni, C. S.; Fyfe, C. A. *Ibid.* **1982**, *15*, 208.
(56) Haasnoot, C. A. G.; Van de Ven, F. J. M.; Hilbers, C. W. *J. Magn. Reson.* **1984**, *56*, 343. Gurevich, A. Z.; Barsukov, I. L.; Arseniev, A. S.; Bystrov, V. F. *Ibid.* 471.
(57) Meier, B. H.; Ernst, R. R. *J. Am. Chem. Soc.* **1979**, *101*, 6441.
(58) Huang, Y.; Macura, S.; Ernst, R. R. *J. Am. Chem. Soc.* **1981**, *103*, 5327.
(59) Biali, S.; Rappoport, Z. *J. Org. Chem.* **1986**, *51*, 2245.
(60) Willem, R.; Jans, A.; Hoogzand, C.; Gielen, M.; Van Binst, G.; Pepermans, H. *J. Am. Chem. Soc.* **1985**, *107*, 28.
(61) Kemmink, J.; Vuister, G. W.; Boelens, R.; Dijkstra, K.; Kaptein, R. *J. Am. Chem. Soc.* **1986**, *108*, 5631.
(62) Bodenhausen, G.; Ernst, R. R. *Mol. Phys.* **1982**, *47*, 319.
(63) Dwyer, T. J. Ph.D. Thesis, University of California at San Diego, 1988. Perrin, C. L.; Dwyer, T. J. Manuscript in preparation.
(64) Szeverenyi, N.; Sullivan, M.; Maciel, G. *J. Magn. Reson.* **1982**, *47*, 462. Szeverenyi, N.; Bax, A.; Maciel, G. *J. Am. Chem. Soc.* **1983**, *105*, 2579.
(65) Rossetti, R.; Brus, L. E. *J. Chem. Phys.* **1980**, *73*, 1546.
(66) Meier, B.; Storm, C.; Earl, W. *J. Am. Chem. Soc.* **1986**, *108*, 6072.
(67) Schmidt, C.; Blümich, B.; Spiess, H. W. *J. Magn. Reson.* **1988**, *79*, 269.
(68) Kentgens, A. P. M.; De Jong, A. F.; De Boer, E.; Veeman, W. S. *Macromolecules* **1985**, *18*, 1045.
(69) Harbison, G.; Raleigh, D.; Herzfeld, J.; Griffin, R. *J. Magn. Reson.* **1985**, *64*, 284.
(70) Boeffel, C.; Luz, Z.; Poupko, R.; Vega, A. J. *Isr. J. Chem.* **1988**, *28*, 283.
(71) Benn, R.; Cibura, K.; Hofmann, P.; Jonas, K.; Rufinska, R. *Organometallics* **1985**, *4*, 2214.
(72) Anklin, G.; Pregosin, P. *Magn. Reson. Chem.* **1985**, *23*, 671.
(73) Coffindaffer, T. W.; Westler, W. M.; Rothwell, I. P. *Inorg. Chem.* **1985**, *24*, 4565.
(74) Bauer, W.; Feigel, M.; Muller, G.; Schleyer, P. v. R. *J. Am. Chem. Soc.* **1988**, *110*, 6033.
(75) Jurkschat, K.; Tzschach, A.; Mugge, C.; Piret-Meunier, J.; Van Meerssche, M.; Van Binst, G.; Wynants, C.; Gielen, M.; Willem, R. *Organometallics* **1988**, *7*, 593.
(76) Vrieze, K. In Reference 1c, p 441.
(77) Benn, R. *Angew. Chem., Int. Ed. Engl.* **1982**, *21*, 626.
(78) Meyer, H.; Zschunke, A. *J. Organomet. Chem.* **1984**, *269*, 209. Zschunke, A.; Nehls, I.; Meyer, H. *Ibid.* **1981**, *222*, 353.
(79) Abel, E. W.; Higgins, K.; Orrell, K.; Sik, V.; Curzon, E.; Howarth, O. *J. Chem. Soc., Dalton Trans.* **1985**, 2195.
(80) Willem, R.; Gielen, M.; Pepermans, H.; Brocas, J.; Fastenakel, D.; Finocchiaro, P. *J. Am. Chem. Soc.* **1985**, *107*, 1146.
(81) Ismail, A. A.; Sauriol, F.; Sedman, J.; Butler, I. S. *Organometallics* **1985**, *4*, 1914.
(82) Ruegger, H.; Pregosin, P. S. *Inorg. Chem.* **1987**, *26*, 2912.
(83) Ammann, C.; Pregosin, P. S.; Ruegger, H.; Grassi, M.; Musco, A. *Magn. Reson. Chem.* **1989**, *27*, 355.
(84) Hampden-Smith, M. J.; Ruegger, H. *Magn. Reson. Chem.* **1989**, *27*, 1107.
(85) Cutnell, J. D. *J. Am. Chem. Soc.* **1982**, *104*, 362. Schwartz, A. L.; Cutnell, J. D. *J. Magn. Reson.* **1983**, *53*, 398.
(86) Bleich, H.; Wilde, J. *J. Magn. Reson.* **1984**, *56*, 149.
(87) Hennig, J.; Limbach, H. H. *J. Magn. Reson.* **1982**, *49*, 322.
(88) Schiksnis, R. A.; Rockwell, A. L.; Gierasch, L. M.; Opella, S. J. *J. Magn. Reson.* **1988**, *79*, 318.
(89) Gray, G. A. *Org. Magn. Reson.* **1983**, *21*, 111.
(90) Kessler, H.; Schuck, R.; Siegmeier, R. *J. Am. Chem. Soc.* **1982**, *104*, 4486.
(91) Shungu, D. C.; Briggs, R. W. *J. Magn. Reson.* **1988**, *77*, 491.
(92) Garlick, P.; Turner, C. *J. Magn. Reson.* **1983**, *51*, 536.
(93) Boyd, J.; Brindle, K. M.; Campbell, I. D.; Radda, G. K. *J. Magn. Reson.* **1984**, *60*, 149.
(94) Santos, H.; Turner, D. L.; Xavier, A. V.; Le Gall, J. *J. Magn. Reson.* **1984**, *59*, 177.
(95) (a) Berger, A.; Loewenstein, A.; Meiboom, S. *J. Am. Chem. Soc.* **1959**, *81*, 62. (b) Stewart, W. E.; Siddall, T. H., III. *Chem. Rev.* **1970**, *70*, 517. (c) Molday, R. S.; Kallen, R. G. *J. Am. Chem. Soc.* **1972**, *94*, 6739. (d) Yavari, I.; Roberts, J. D. *Ibid.* **1978**, *100*, 5217. (e) Redfield, A. G.; Waelder, S. *Ibid.* **1979**, *101*, 6151. (f) Perrin, C. L.; Johnston, E. R.; Lollo, C. P.; Kobrin, P. A. *Ibid.* **1981**, *103*, 4691. (g) Perrin, C. L.; Johnston, E. R. *Ibid.* **1981**, *103*, 4697.
(96) Perrin, C. L. *J. Am. Chem. Soc.* **1974**, *96*, 5628.
(97) Johnston, E. R.; Dellwo, M.; Hendrix, J. *J. Magn. Reson.* **1986**, *66*, 399.
(98) McClelland, R. A.; Reynolds, W. F. *Can. J. Chem.* **1979**, *57*, 2896.
(99) Baine, P. *Magn. Reson. Chem.* **1986**, *24*, 304.
(100) Baine, P.; Domenick, R. L.; Servis, K. L. *Magn. Reson. Chem.* **1987**, *25*, 1035.
(101) Paquette, L. A.; Wang, T.-Z.; Luo, J.; Cottrell, C. E.; Clough, A. E.; Anderson, L. B. *J. Am. Chem. Soc.* **1990**, *112*, 239.

(102) Orrell, K. G.; Sik, V.; Stephenson, D. *Magn. Reson. Chem.* **1987**, *25*, 1007.
(103) Grunwald, E.; Loewenstein, A.; Meiboom, S. *J. Chem. Phys.* **1956**, *25*, 382; **1957**, *27*, 630. Loewenstein, A.; Meiboom, S. *Ibid.* **1957**, *27*, 1067. Meiboom, S.; Loewenstein, A.; Alexander, S. *Ibid.* **1958**, *29*, 969. Emerson, M. T.; Grunwald, E.; Kromhout, R. A. *Ibid.* **1960**, *33*, 547.
(104) Knight, C. T. G.; Kirkpatrick, R. J.; Oldfield, E. *J. Magn. Reson.* **1988**, *78*, 31.
(105) Kook, A.; Nicklas, P.; Selegue, J.; Smith, S. *Organometallics* **1984**, *3*, 499.
(106) Jenkins, B. G.; Lauffer, R. B. *J. Magn. Reson.* **1988**, *80*, 328. Jenkins, B. G.; Lauffer, R. B. *Inorg. Chem.* **1988**, *27*, 4730.
(107) Abel, E. W.; Khan, A. R.; Kite, K.; Orrell, K.; Sik, V. *J. Chem. Soc., Dalton Trans.* **1980**, 1175.
(108) Abel, E. W.; Budgen, D. E.; Moss, I.; Orrell, K. G.; Sik, V. *J. Organomet. Chem.* **1989**, *362*, 105.
(109) Abel, E. W.; Moss, I.; Orrell, K. G.; Sik, V.; Stephenson, D. *J. Chem. Soc., Dalton Trans.* **1987**, 2695.
(110) Abel, E. W.; Moss, I.; Orrell, K. G.; Sik, V.; Stephenson, D.; Bates, P. A.; Hursthouse, M. B. *J. Chem. Soc., Dalton Trans.* **1988**, 521.
(111) Abel, E. W.; Coston, T. P. J.; Higgins, K. M.; Orrell, K. G.; Sik, V.; Cameron, T. S. *J. Chem. Soc., Dalton Trans.* **1989**, 701. Abel, E. W.; Coston, T. P. J.; Orrell, K. G.; Sik, V. *Ibid.* **1989**, 711.
(112) Aime, S.; Milone, L. *Prog. Nucl. Magn. Reson. Spectrosc.* **1977**, *11*, 183.
(113) Hawkes, G. E.; Lian, L.-Y.; Randall, E. W.; Sales, K. *J. Chem. Soc., Dalton Trans.* **1985**, 225.
(114) Abel, E. W.; Moss, I.; Orrell, K. G.; Qureshi, K. B.; Sik, V.; Stephenson, D. *J. Chem. Soc., Dalton Trans.* **1988**, 1489.
(115) Abel, E. W.; Orrell, K. G.; Qureshi, K. B.; Sik, V.; Stephenson, D. *J. Organomet. Chem.* **1988**, *353*, 337.
(116) Beringhelli, T.; D'Alfonso, G.; Molinari, H.; Hawkes, G. E.; Sales, K. D. *J. Magn. Reson.* **1988**, *80*, 45.
(117) Robillard, G. T.; Powers, J. C.; Wilcox, P. E. *Biochemistry* **1972**, *11*, 1773. Brown, W. E. *Ibid.* **1975**, *14*, 5079.
(118) Cairi, M.; Gerig, J. T. *J. Am. Chem. Soc.* **1983**, *105*, 4793.
(119) Davis, D.; Bax, A. *J. Magn. Reson.* **1985**, *64*, 533.
(120) Dobson, C. M.; Lian, L.-Y.; Redfield, C.; Topping, K. D. *J. Magn. Reson.* **1986**, *69*, 201.
(121) Mendz, G. L.; Robinson, G.; Kuchel, P. W. *J. Am. Chem. Soc.* **1986**, *108*, 169.
(122) Balaban, R. S.; Ferretti, J. A. *Proc. Natl. Acad. Sci. U.S.A.* **1983**, *80*, 1241.
(123) Snyder, J. R.; Johnston, E. R.; Serianni, A. S. *J. Am. Chem. Soc.* **1989**, *111*, 2681.
(124) Balaban, R. S.; Kantor, H.; Ferretti, J. A. *J. Biol. Chem.* **1983**, *258*, 12787.
(125) Kantor, H. L.; Ferretti, J. A.; Balaban, R. S. *Biochim. Biophys. Acta* **1984**, *789*, 128.
(126) Dwyer, T. J.; Perrin, C. L. Unpublished calculations.
(127) Tuchsen, E.; Woodward, C. *J. Mol. Biol.* **1987**, *193*, 793.
(128) Crossley, M. J.; Field, L. D.; Harding, M. M.; Sternhell, S. *J. Am. Chem. Soc.* **1987**, *109*, 2335.
(129) Holm, R. H. In Reference 1c.
(130) Engdahl, C.; Ahlberg, P. *J. Am. Chem. Soc.* **1979**, *101*, 3940.
(131) Wennerbeck, I.; Sandström, J. *Org. Magn. Reson.* **1972**, *4*, 783.
(132) Feigel, M.; Kessler, H.; Leibfritz, D.; Walter, A. *J. Am. Chem. Soc.* **1979**, *101*, 1943.
(133) Luke, W. D.; Streitwieser, A., Jr. *J. Am. Chem. Soc.* **1981**, *103*, 3241.